SHRP-ID/UWP-91-511

SHRP-IDEA

Research Products and Technical Progress

Strategic Highway Research Program
National Research Council

Strategic Highway Research Program Executive Committee

John R. Tabb, Chairman
Mississippi Highway Department

William G. Agnew
General Motors Research (retired)

E. Dean Carlson, Ex Officio
Federal Highway Administration

A. Ray Chamberlain
State of Colorado Department of Highways

Raymond F. Decker
University Science Partners Inc.

Thomas B. Deen, Ex Officio
Transportation Research Board

Thomas M. Downs
New Jersey Department of Transportation

Horace B. Edwards
Kansas Department of Transportation

Tom Espy, Jr.
Alabama Highway Department

Francis B. Francois, Ex Officio
American Association of State Highway and Transportation Officials

Donald N. Geoffroy
New York Department of Transportation

William L. Giles
Ruan Transportation Management Systems

Boris Hryhorczuk, Ex Officio
Manitoba Department of Transportation

Thomas D. Larson, Ex Officio
Federal Highway Administration

Harold L. Michael
Purdue University

Wayne Muri
Missouri Highway and Transportation Department

Henry A. Thomason, Jr.
Texas Department of Highways and Public Transportation

Roger L. Yarbrough
Apcon Corporation

Damian J. Kulash
Executive Director

Edward T. Harrigan
Asphalt Program Manager

Neil F. Hawks
LTPP Program Manager

Don M. Harriott
Concrete and Structures/Highway Operations Program Manager

Harry Jones
Finance and Administration Director

Karen Haas Smith
Organizational Relations Director

K. Thirumalai
SHRP-IDEA Program Manager

SHRP-ID/UWP-91-511

SHRP-IDEA

Research Products and Technical Progress

SHRP-ASCE Meeting
April 8-10, 1991
Denver, CO

Strategic Highway Research Program
National Research Council
Washington, D.C. 1991

SHRP-ID/UWP-91-511
Program Manager: *K. Thirumalai*

Executive Editor: *Karen Haas Smith*
Substantive Editor: *Katharyn Bine Brosseau*
Copyeditor: *Katharyn Bine Brosseau*
Production Editor: *Sarah K. Fox*

April 1991

Strategic Highway Research Program
2101 Constitution Avenue, N.W.
Washington, D.C. 20418

(202) 334-3774

Acknowledgments

The research described herein was supported by the Strategic Highway Research Program (SHRP). SHRP is a unit of the National Research Council that was authorized by section 128 of the Surface Transportation and Uniform Relocation Assistance Act of 1987.

This report was prepared by SHRP-IDEA based on input from the project investigators.

Contents

Reference to SHRP-IDEA Products xi

Quick-Setting Glass Cement 3

Noncontact Laser Inspection of Pavement Surfaces 9

Laboratory Simulator for Pavement Performance 15

Image Processing Algorithms for Cracks 21

Corrosion Detector 25

Rapid Profile Using a Laser Beam 31

Freeze Coring of Fresh Concrete and Air Void Measurement 37

Portable Corrosion Rate Monitor 43

Biological Material for Ice Control 47

Chemical Agents to Control Alkali-Silica Reaction 53

Fiber-Optic Air-Void Meter 59

Low-Cost Carbon-Fiber Concrete 65

Fiber-Optic Weigh-In-Motion System 69

Conducting Polymer Anode for Cathodic Protection 75

Load Measuring Mat 81

Smart Structure Technology 87

Automated Crack Repair System 93

Intelligent and Localized Weather Prediction 99

Electro-Acoustic Modification of Concrete 105

Conversion Residue Binder for Asphalt 111

Automated Asphalt Process Analyzer
Using Nuclear Magnetic Resonance 115

Flexible Stress Cell 121

Silicon Coating Process for Rebars 127

Corrosion Repair Treatment for Marine Structures 133

Dynamic Analysis Procedure
for Falling-Weight Deflectometer Data 139

List of Figures

Figure 1. Scanning Electron Microscope Photographs of a Dense Stratlingite Cement Paste 4

Figure 2. Fly Ash Containing Glass Cement Mortars (Activated) 7

Figure 3. Schematic of General Layout of Laser System for Noncontact Inspection 10

Figure 4. Waveform from Aged Asphalt Sample 13

Figure 5. Diagram of Centrifuge 16

Figure 6. Processed Video Images 22

Figure 7. Corrosion Rates With and Without Cathodic Protection 26

Figure 8. Impedance With and Without Chloride 28

Figure 9. Impedance With Cathodic Protection 29

Figure 10. Schematic Diagram of the Laser-Beam-Carried Microwave-Interferometer 32

Figure 11. Specimen Mold for Freezing Fresh Concrete 38

Figure 12. Schematic of Air Void Measurement by Laser Instrument 40

Figure 13. Typical Impedance Spectrum of Corroding Rebar in Concrete 44

Figure 14. Schematic of AFP Binding to Ice 49

Figure 15. Blocking of Crystal Growth by AFPs. 50

Figure 16. Effect of Chemicals on Solubility of Spratts Aggregate 55

Figure 17. Expansion of Mortar Bars made with 3% Opal Replacement 56

Figure 18. Components of the Fiber-Optic Air Meter 60

Figure 19. Fiber-Optic Air Meter with Laptop Computer 62

Figure 20. Fiber-Optic Air Meter in the Field 63

Figure 21. Schematic Diagram of a Transmission-Based Pressure Sensor 70

Figure 22. Schematic Diagram of a Reflection-Based Pressure Sensor 72

Figure 23. Polypyrrole in a Concrete Specimen 77

Figure 24. Diffusion of Monomer through Concrete 78

Figure 25. Schematic cross section of a Capacitative Strip Wheel Force Sensor Incapsulated in a Polyurethane Tile 83

Figure 26. Photograph of WIMstrip Prototype 84

Figure 27. Eddy Current Assessment of Ferrite Tagged Cement 89

Figure 28. Active Tagging Concept 90

Figure 29. Eddy Current Measurement of Asphalt Concrete Compaction 92

Figure 30. Illustration of a Possible Field System for Filling Cracks 95

Figure 31. Photograph of the Laboratory Demonstration System 96

Figure 32. Modules of Current System Design 102

Figure 33. Schematic of the Experimental Setup Electro-Acoustic Technology . . 107

Figure 34. Effect of Electro-Acoustic Technology on the Electrochemical Impedance of a Concrete Specimen 108

Figure 35. Moisture-Induced Damage 113

Figure 36. Pulse Sequences in Asphalt Samples 117

Figure 37. Block Design of the Proposed Spectrometer 118

Figure 38. Diagram of Flexible Stress Cell 123

Figure 39. Reactor System for Coating Steel Rebars with Silicon 129

Figure 40. Silicide Coatings of Steel Rebars at Different Temperatures 130

Figure 41. Application of Anode on Reinforcing Steel 134

Reference to SHRP-IDEA Products

Asphalt

ID003[1] Laboratory Simulator for Pavement Performance
ID016[1] Smart Structure Technology
ID020 Conversion Residue Binder for Asphalt
ID021 Automated Asphalt Process Analyzer Using Nuclear Magnetic Resonance

Pavement Performance

ID002[1] Noncontact Laser Inspection of Pavement Surfaces
ID003[1] Laboratory Simulator for Pavement Performance
ID004 Image Processing Algorithms for Cracks
ID006 Rapid Profile Using a Laser Beam
ID013 Fiber-Optic Weigh-In-Motion System
ID015 Load Measuring Mat
ID022 Flexible Stress Cell
ID025 Dynamic Analysis Procedure for Falling-Weight Deflectometer Data

Concrete and Structures

Concrete

ID001[1] Quick-Setting Glass Cement
ID007 Freeze Coring of Fresh Concrete and Air-Void Measurement
ID011[2] Fiber-Optic Air-Void Meter
ID012 Low-Cost Carbon-Fiber Concrete
ID016[1] Smart Structure Technology
ID019 Electro-Acoustic Modification of Concrete

---

[1]IDEA projects that have application in more than one SHRP program area

[2]IDEA Phase II projects (prototyping and field evaluation) are currently under way.

Structures

ID002[1] Noncontact Laser Inspection of Pavement Structures
ID005 Corrosion Detector
ID008[2] Portable Corrosion Rate Monitor
ID010 Chemical Agents to Control Alkali-Silica Reaction
ID014 Conducting Polymer Anode for Cathodic Protection
ID023 Silicon Coating Process for Rebars
ID024 Corrosion Repair Treatment For Marine Structures

Highway Operations

Maintenance

ID001[1] Quick-Setting Glass Cement
ID017[2] Automated Crack Repair System

Snow and Ice Control

ID009 Biological Material for Ice Control
ID018[2] Intelligent and Localized Weather Prediction

[1]IDEA projects that have application in more than one SHRP program area

[2]IDEA Phase II projects (prototyping and field evaluation) are currently under way.

The projects under SHRP's Innovations Deserving Exploratory Analysis (IDEA) program focus on new and alternative approaches to solving the technical problems addressed through SHRP's programs in Asphalt, Concrete and Structures, Highway Operations, and Long-Term Pavement Performance.

IDEA projects evaluate and test new and unconventional approaches that have the potential to produce "leapfrog technologies" or significant improvements in the construction and maintenance of highway systems. The projects selected for IDEA are characterized by high risk combined with potential to produce significant technological breakthroughs and result in large payoffs.

The IDEA projects are performed in two phases. The Phase I IDEA project evaluates the conceptual feasibility of innovative products. The Phase I project funding is generally below $100,000, with a typical project duration of less than 12 months. Typically Phase I projects attempt to prove the potential feasibility of innovative technologies using small to bench-scale laboratory tests and analysis procedures.

A selected few of the successful and highly deserving IDEA Phase I projects are undergoing IDEA Phase II project evaluations. The IDEA Phase II projects typically perform the prototyping and testing of proven IDEA concepts. Phase II projects signify the second and important step toward IDEA product application in practice. All IDEA Phase II projects are cost-shared by the users of the products, or by state highway agencies that work in conjunction with the principal investigator. This shared involvement in the IDEA project by project users and practitioners helps to accelerate implementation of IDEA products in highway practice.

A listing of all IDEA products under development are categorized in each SHRP program area. The 25 IDEA projects described in this booklet are in different stages of completion and include all Phase I projects currently under way or completed. The following four IDEA products are currently undergoing Phase II project evaluations and are indicated in the project progress descriptions.

IDEA #ID008	Portable Corrosion Rate Monitor
IDEA #ID011	Fiber-Optic Air-Void Meter
IDEA #ID017	Automated Crack Repair System
IDEA #ID018	Intelligent and Localized Weather Prediction

Only a limited number of successful IDEA Phase I projects were considered for Phase II because of resource limitations and time constraints in producing a fieldworthy product for application to highway practice during the SHRP program.

This booklet is designed to provide comprehensive technical information on all IDEA projects, and presents a collection of emerging innovative technologies and products in SHRP research areas. The booklet highlights specific innovations for each IDEA concept and presents the technical status and summary of progress. Technical issues that require further consideration are also presented for each project.

Quick-Setting Glass Cement

IDEA 001 - Stratlingite-Hydrogarnet Glass Cement

Investigators: J. F. MacDowell, Corning Incorporated, Corning, New York; Roger G. Slutter[1] and T. Huang, Lehigh University, Fritz Engineering Laboratory, Bethlehem, Pennsylvania

IDEA Product

A new type of high-alumina cement that is quick-setting and can be rapidly placed for pothole patching, or as a top course over exposed rebar, is under development. The material has good potential for use as a durable repair material to provide increased repair-rate efficiency, high early strength, and reduced highway "downtime" for repair maintenance.

Innovation

A new family of stratlingite-hydrogarnet glass cements with high early strength and low porosity was discovered and patented by the Corning laboratories. A glass cement study by Corning showed that stratlingite (gehlenite hydrate) could constitute the principal phase of a strong, fast-setting cement. Prior hydration studies by others of $CaO\text{-}Al^2\ 0^3\text{-}SiO^2$ (C-A-S) glasses have concluded that: (l) activators such as Portland cement clinker, gypsum, or lime were required to produce practical rates of hydration; and (2) stratlingite was only a transient phase in the hydration of these glasses. However, Corning scientists formed stable stratlingite cement pastes directly from glass without the use of activators.

Corning found glasses that hydrated to a mixture of stratlingite and hydrogarnet with initial sets of one to two hours, final sets of three to four hours, and achieved up to 10,000 psi compressive strength in four hours. These cement pastes also displayed higher porosities than the slow-curing pure stratlingite cements, but had much lower porosities than Portland or other commercial cements. Figure 1 shows the microstructure topography of stratlingite cement paste with dense granular interlocking and minimal voids.

---

[1]Corning and SHRP acknowledge the leadership and contribution to this project by Dr. Slutter until his untimely death on July 10, 1990.

A. Polished Only

B. Polished and Etched

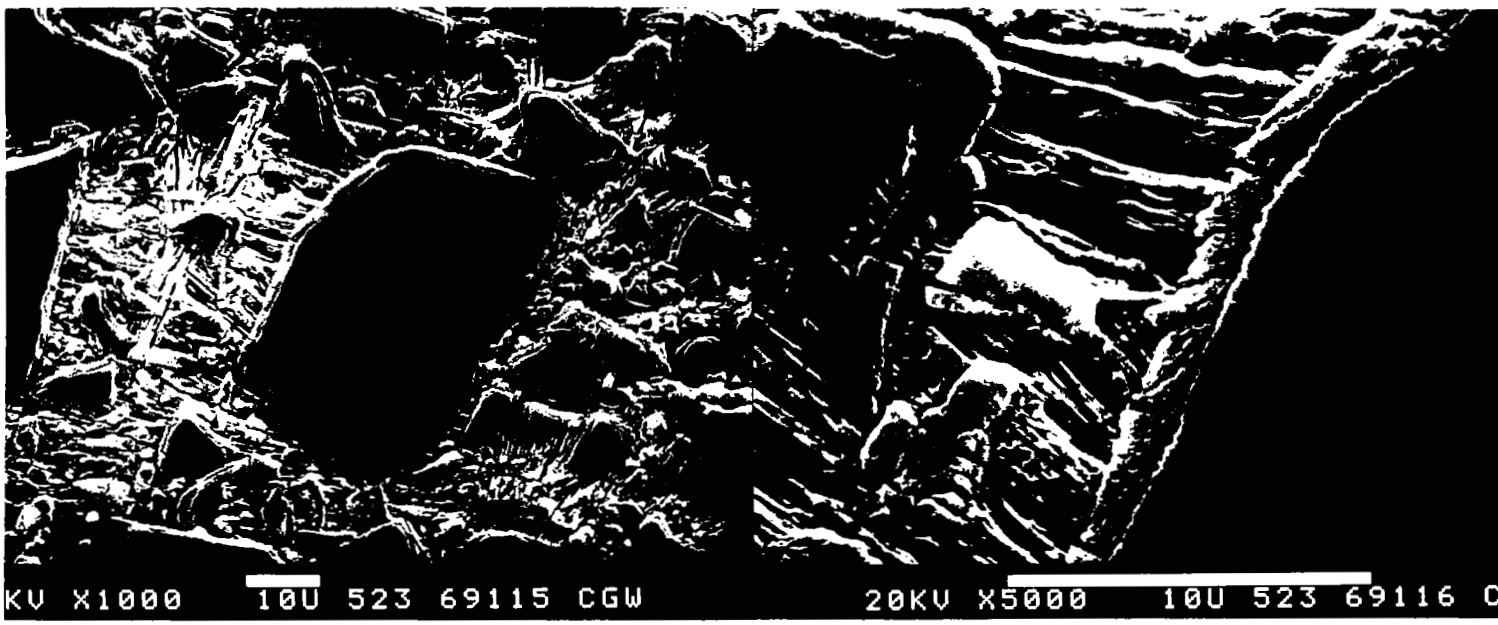

Figure 1. Scanning Electron Microscope Photographs of a Dense Stratlingite Cement Paste

Project Summary and Progress

Five of Corning's new glass cements and mortars that hydrate directly to stratlingite (C^2ASH^8) and hydrogarnet (C^3AH^6) have been evaluated at Lehigh University's Fritz Engineering Laboratory under the SHRP award.

- Compressive strengths over 8,000 psi have been routinely measured on two of the stratlingite-hydrogarnet glass cements (both neat and mortar) three hours after mixing. Although water cement ratio experiments indicate a nearly 25 percent reduction in strength in going from a 0.4 to 0.6 water/cement ratio, three-hour values over 6,000 psi were still obtained at the 0.6 ratio.

- Limited tensile bonding data to Portland concrete (ASTM C190) shows values roughly comparable to Type III Portland mortar.

To follow up this project work, Corning and Master Builders are working together at their own cost to develop a fully characterized rapid repair mix for concrete. They are focusing on the areas of shrinkage, workability, and corrosion testing. Tests are being performed to confirm environmental and strength results and to identify the requirements for high durability and cost-effective design. Tests include:

- compressive strength
- flexural strength
- split tensile strength
- shear bond to cement
- tensile bond to cement
- length change
  - sulfate resistance
  - thermal expansion
- abrasion resistance
- chloride permeability
- freeze thaw
- strength as a function of time and temperature

Initial observations have indicated:

- material dynamics are quite different than Portland cement
- low water-to-cement ratios (.18 to .3)
- rapid chloride test (fly-ash/S-HG cement with activator) - moderate results

- early mixes were overdesigned, and should be optimized for highway repairs
- early results on mortars with fly ash indicate high early strengths using as little as 3 percent Corning cement and 25 percent commercial fly ash (Figure 2).

Technical Issues for Further Consideration

Although Lehigh University's study strongly suggests that new stratlingite-hydrogarnet glass cements can be developed into an excellent high-early-strength patching material, there are a number of additional properties that need to be investigated before commercialization can be considered.

Shrinkage characteristics; properties of these cements in concrete (with a range of aggregates); freeze-thaw behavior; and workability versus strength with and without water reducers, are all of critical importance for many applications. Studies to determine strength as a function of time and temperature also must be conducted. The best way to investigate many of these critical properties is through controlled field testing with potential users of these cements. Working relationships with potential customers are being considered for limited field testing under controlled conditions.

Stratlingite-hydrogarnet glass cements are a promising new family of "hydroceramics" that may have great utility as highway and bridge deck patching or reconstruction materials. Their inherently higher cost (due to the more expensive raw materials and the high-temperature glass-melting step in their manufacture) will narrow the field of application to situations demanding higher early strength and lower porosity than currently available products provide. Other advantages (or disadvantages) of these materials may emerge only through extensive application testing.

MIX	1 CEMENT/8 ASH/23 SAND	1 CEMENT/9 ASH/26 SAND
FLY ASH	NOT SPECIFIED	NOT SPECIFIED
GLASS CEMENT	FORMULA 1	FORMULA 2
SAND	70%	70 %
ACTIVATOR	NOT SPECIFIED	NOT SPECIFIED
W/C	.18	.3
SET TIME	22 MIN.	42 MIN.
WORKABILITY	GOOD	GOOD
COMPRESSIVE STRENGTH		
24 HOURS	4,940 PSI	7,285 PSI
7 DAYS	7,961 PSI	10,400 PSI
28 DAYS	9,920 PSI	-
FLEXURAL	1,104 PSI	>1,000 PSI (EST.)
LENGTH Δ: 7 DAYS WET	(NO SAMPLE)	+.0033%

Figure 2. Fly Ash Containing Glass Cement Mortars (Activated)

Noncontact Laser Inspection of Pavement Structures

IDEA 002 - Evaluation of the Use of Laser-Ultrasonic Inspection of Concrete and Asphalt

Investigators: R.L. Smith, C.G. Tasker, F.K. Brocklehurst and B.C. Moss, Harwell Laboratory/National Nondestructive Testing Center, Oxfordshire, United Kingdom

IDEA Product

A noncontact inspection system, using lasers to generate and detect ultrasonic waves, for inspecting pavements and bridge structures was tested. The system could be mounted on a vehicle or gantry. This product has the potential to provide rapid assessment of the condition of roads and bridges.

Innovation

Laser technology is used to generate and detect ultrasonic waves without any physical contact with the structure. The inspection technique has the potential to provide information on the condition of pavements and structures by locating delaminations, loss of section, voids, and so forth. By quickly identifying problem areas, maintenance programs can be planned more effectively, saving time and money.

Project Summary and Progress

The work conducted has shown that laser generation and detection of ultrasound waves in concrete and asphalt is feasible. The results are comparable with conventional ultrasonic systems. The project results provide the basis for the production of a prototype laser-based system.

The laboratory system set up for this experimental program was a powerful, pulsed Nd-YAG laser which produced ultrasound waves in the concrete or asphalt by ablating the surface of the material with a 75-M.-joules, 20-nanosecond pulse (Figure 3). The effect of this short, sharp impact pulse on the materials was to produce ultrasonic shock waves that were detected by means of a steady state He-Ne laser interferometer of the Michelson type. The monitoring of these modes of vibration in the material can reveal information about the properties and structure of the material itself.

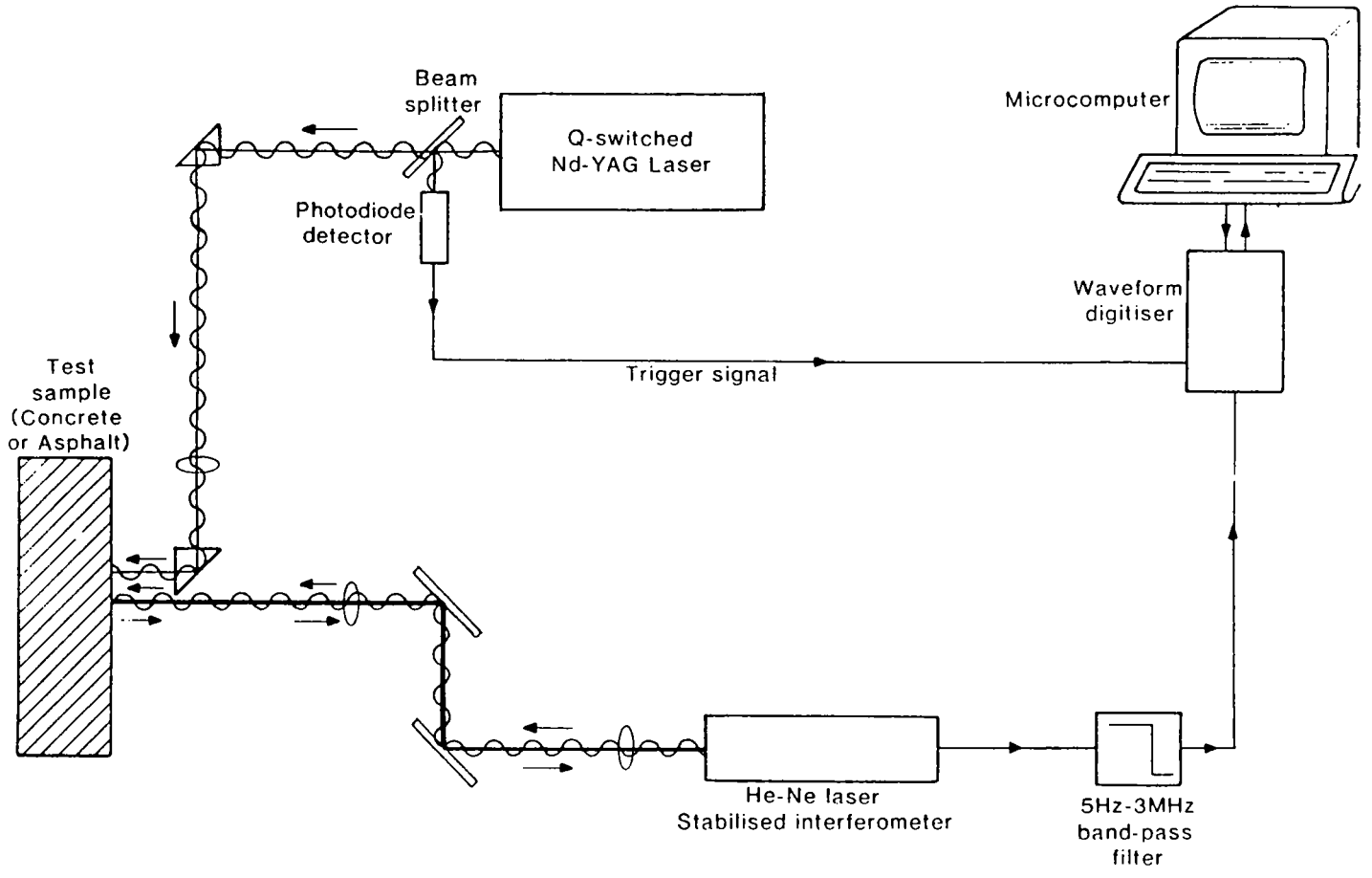

Figure 3. Schematic of General Layout of Laser System for Noncontact Inspection

Initially, tests with the laser system were carried out on concrete slabs 35 mm and 65 mm thick to determine how effectively the laser system would both remotely generate and detect ultrasonic vibrations in thin-section concrete. Further concrete samples were manufactured comprising blocks 100 mm, 150 mm, 200 mm, and 250 mm thick, constructed with 20-mm sieved aggregate. A number of other concrete blocks manufactured contained simulated delaminations, voids and reinforcing mesh.

The significant features which normally characterized the digitized waveforms obtained from the interferometer were the firing pulse from the Nd-YAG laser, the surface wave, the reflected compression wave, the reflected shear wave and the acoustic wave. With known values of the velocity of sound in each concrete sample (measured using standard ultrasonic techniques), and the arrival times of the reflected compression and shear waves obtained from the interferometer waveforms for each sample, values for the thicknesses of concrete or the depth of defect in the concrete could be calculated for these samples. The surface wave position in the waveform also is a useful feature as it provides a check on the velocity of ultrasound in the materials. The acoustic wave is a less desirable feature which can mask other features in the waveform. It derives from the rapid heating of the air at the point of impact of the Nd-YAG laser beam. The acoustic wave's appearance in the waveform is dependent upon the chosen separation distance between the two laser beams. These waveform features (apart from the acoustic wave) are the basis for the calculations of thickness of concrete or the depth of defects or artifacts.

Results obtained from the thin concrete slabs using different wave transmission arrangements proved valuable in establishing a general technique for the rest of the experimental program. Based on preliminary tests a surface separation arrangement was found the most appropriate for the experimental work on further samples. The separation used was usually between 20 mm and 40 mm. Thicker concrete blocks containing the 20-mm sieved aggregate presented no problems in scanning other than the diminution in the size of the peak from the reflected compression wave as thickness increased.

The concrete blocks containing artificial defects gave some encouraging results when subjected to examination by the laser system. The artificial delamination, although not an ideal method of simulating a real delamination, did show up as a broad peak superimposed upon the general background level in the waveform. The simulated void samples gave reasonable results. The large void (150 x 100 x 15 mm) embedded 50 mm below the surface of a concrete block 100 mm thick showed up in the resulting waveforms. The concrete block containing three small voids at different depths showed pronounced multiple peaks in its waveform.

Results obtained from the scanning of asphalt with the laser system were quite variable. It was very difficult to obtain a peak for the compression wave reflected off the bottom surface of fresh, hot-rolled asphalt. Also, because of the rough surface finish (compared to the concrete samples) the surface wave energy was lost very quickly. Some aged asphalt samples had been acquired from a site which had carried traffic for approximately 10 years. These samples had a 50-mm-thick wearing course on top of a 60-mm-thick base course. One of these samples had a very prominent delamination between these two layers. This delamination showed up very well in the waveform obtained. In general, the results from the aged asphalt were far better than those obtained from the fresh, hot-rolled asphalt (Figure 4).

The research that has been carried out with this laser system shows that lasers can be used remotely to generate and detect responses to ultrasound in concrete and asphalt. The ultrasonic responses obtained from the test samples using this laser system compared favorably with the results obtained by inspection using a pair of 50 kHz piezoelectric transducers in transmit/receive mode. By using the techniques developed in this experimental program, not only can compression, wave velocity measurements, and thickness measurements be made without resorting to the physical contact required with conventional transducers, but it is also feasible to detect embedded artifacts and to detect estimate the size of defects within the concrete or asphalt.

Technical Issues for Further Consideration

There are two major issues for further consideration:

1. Development of the full potential of ultrasonics as an inspection technique for concrete and asphalt.

2. Development of a suitable laser system to meet on-site conditions.

Since this contract started, at least one company, ULTRA-OPTEC in Canada, has been set up to design and build laser ultrasonic systems for use in industrial situations. By collaboration with the highway authorities, manufacturing companies, and relevant R&D institutes, a system for on-site use could be developed.

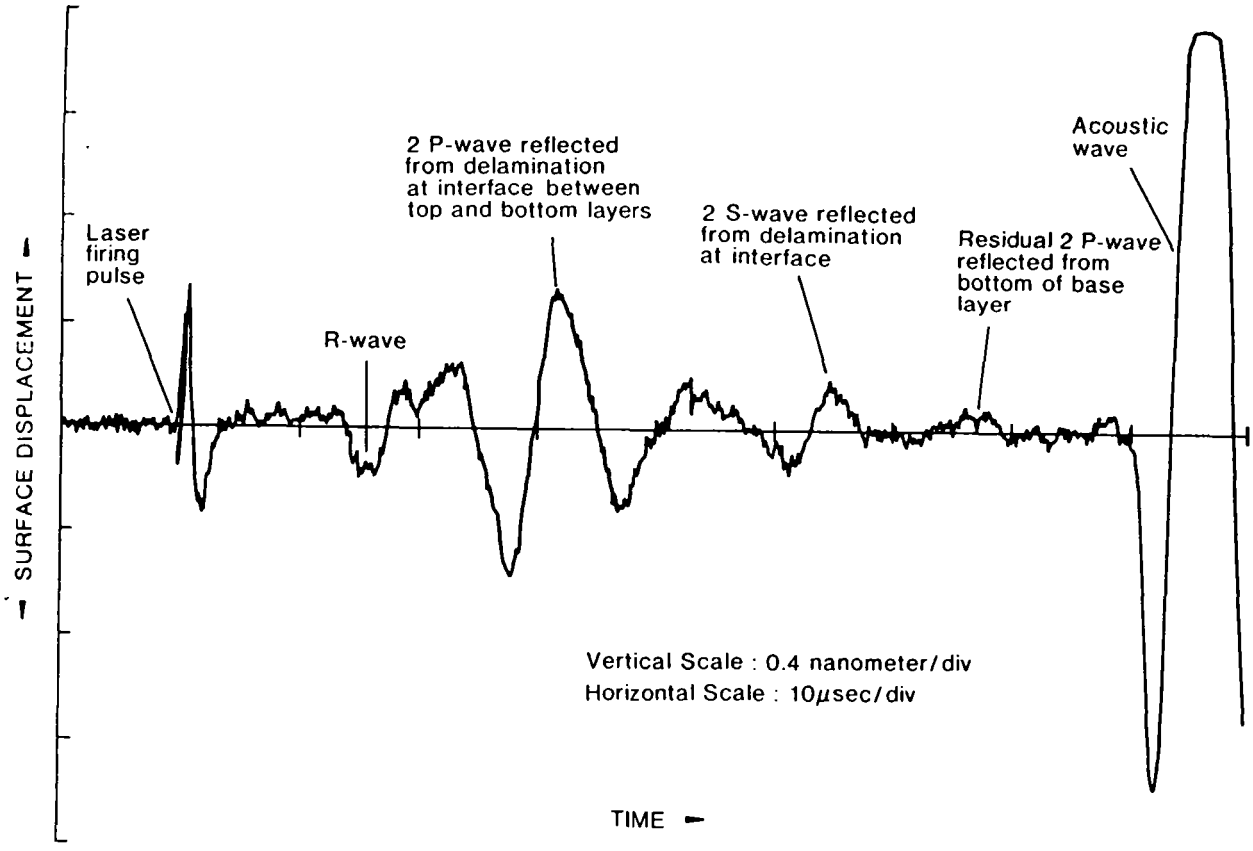

Figure 4. Waveform from Aged Asphalt Sample

Laboratory Simulator for Pavement Performance

IDEA 003 - Centrifuge Tests to Simulate Asphalt Pavement Performance

Investigators: Yang H. Huang, Vincent P. Drnevich, and Hossien Roghani, University of Kentucky, Lexington, Kentucky

IDEA Product

Centrifuge modeling using small-scale pavement models was developed to predict fatigue cracking and rutting of full-depth asphalt pavements. The project has shown that centrifuge testing can be easily implemented for pavement modeling and design analysis.

Innovation

The current method of predicting fatigue cracking and rutting is to test separately the paving materials (such as hot mix asphalt, untreated granular materials, and subgrade soils) separately, then to input their individual properties into a computer model. The centrifuge method tests all paving materials as a unit under loading and boundary conditions similar to those of the prototype pavement. Figure 5 shows the centrifuge tester. The method offers an estimation of the design's durability. It measures directly the parameters affecting fatigue cracking and rutting, taking into account the interactions among all layers. The method, therefore, offers a laboratory test for real pavement distress.

Project Summary and Progress

Small-scale pavement models can save money as well as reduce the tedious tasks of material testing and computer modeling. Static and repeated load tests showed that centrifuge models could be used to predict pavement distress and that the responses obtained from the models correlated with the computer solutions. The work accomplished under this project is preliminary. Further validation of the concept by using a high-capacity centrifuge with a large environmentally controlled capsule is needed.

A knowledge of pavement distress is required to predict the pavement performance of a design. Fatigue cracking and permanent deformation are two types of asphalt pavement

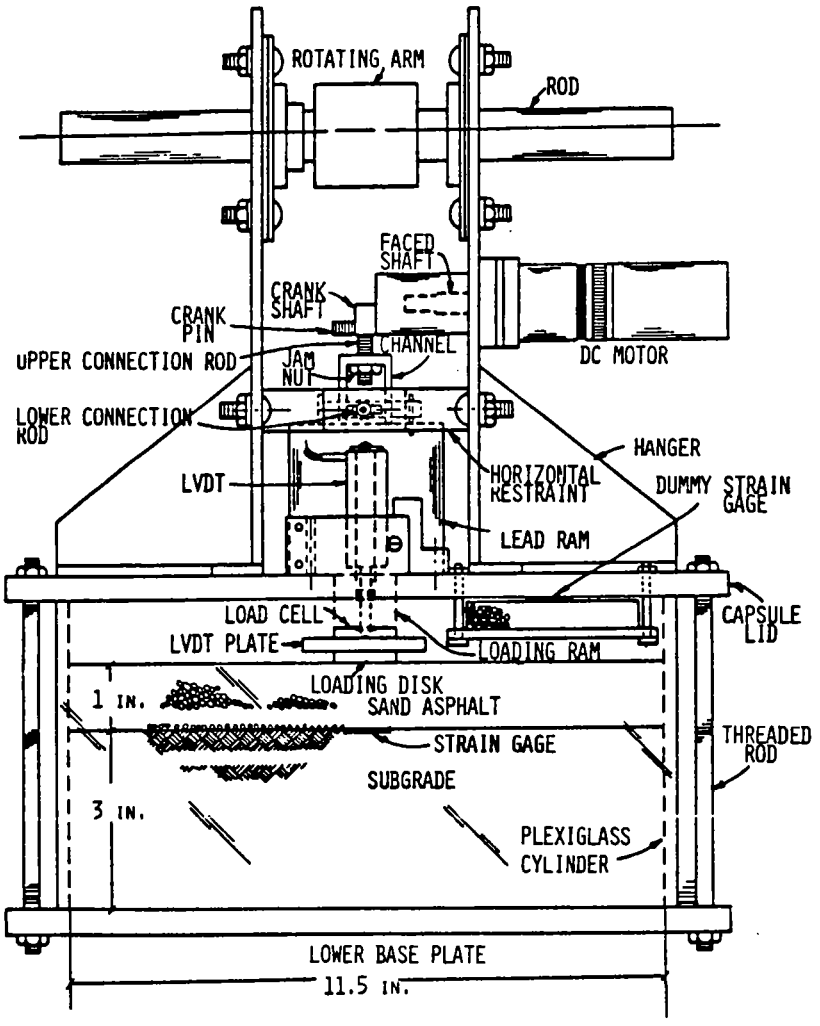

Figure 5. Diagram of Centrifuge

This schematic diagram shows the centrifuge capsule housing the 1:10 pavement model consisting of 1 in of sand asphalt on a sandy subgrade. A small motor was used to lift a 9.1 lb lead ram and drop it on a loading disk 0.5 in in radius. Due to the 10 g centrifugal force, the actual load applied is 91 lb and results in a contact pressure of 80 psi. Thus the testing of the small-scale model is equivalent to testing a 10-in, full-depth asphalt pavement under a 9,000 lb wheel load with a contact radius of 6 in and a contact pressure of 80 psi.

distress. Fatigue cracking is caused by tensile strain at the bottom of the asphalt layer. Rutting is caused by accumulated permanent deformations on the road surface. Both permanent deformation and tensile strain are due to the repeated application of wheel loads. Pavement performance under service conditions is affected by both the characteristics of the materials in the individual layer and the complicated interactions among all layers in the pavement structure.

A small-scale model of a pavement section was constructed. This model was subjected to repeated loading tests in a centrifuge. The model was then removed from the centrifuge to directly measure the resilient tensile strains at the bottom of the asphalt layer and the accumulated permanent deformations near the pavement surface. The centrifuge insured that the stresses and strains due to self-weight were the same in the small-scale model as in the prototype pavement. Tensile strain was measured instead of observing the fatigue cracking directly because of the very long testing time required for fatigue cracking to occur. The models were tested to 10,000 repetitions, but more than one million repetitions may be required to induce fatigue cracking. A static load test also was performed after the repeated load test.

Model pavements in two different scales (1:10 and 1:20) were constructed, using two different asphalt contents and compaction levels. It was found that the resilient deformations and strains measured in the 1:10 models corresponded well with those in the 1:20 models for all test combinations. Although the permanent deformations evinced large variations, the average of the 1:10 models also correlated with that of the 1:20 models.

Comparisons were made between the model responses and computer solutions. The results of both static and repeated load tests indicate that the deformations and strains of the centrifuge models are greater than those of the computer models. Factors other than the difference in contact conditions may contribute to the discrepancy. For example, the computer models assume that each layer is homogeneous with the same elastic modulus throughout the layer, although the modulus of the sand layer should decrease with increasing lateral distances from the load. The resilient modulus of the asphalt layer for the computer models was obtained from tests on cylindrical specimens under a stress of 20 psi (138 kPa), which is small compared to an actual loading of 80 psi (552 kPa). If larger stresses were used in the tests, the resilient modulus of the asphalt layer would decrease and a better match between the centrifuge and computer models could be obtained.

The effect of the centrifuge on model responses was investigated by conducting 1 g tests in which the same repeated load was applied to 1:20 models by dead weights without the 20 g centrifugal force. It was found that the average resilient deformations

of 1 g tests were five times greater than those of 20 g tests, and the resilient strains and permanent deformations were also two to four times larger. The large influence of the centrifuge is not due to the effect of self-weight but rather due to the lack of contact between the prefabricated asphalt layer and the subgrade. This conclusion is supported by the facts that: (1) both the resilient strains and deformations obtained from the 1:10 models are slightly greater than those by the 1:20 models; and that (2) the strains and deformations obtained from both model tests are greater than those from the computer models.

The testing of small-scale models requires the use of small aggregates for the asphalt mix. To be sure that the deformation characteristics of coarse asphalt mixes can be reproduced by this fine-aggregate mix, cylindrical asphalt specimens of fine, medium, coarse and very coarse mixes were fabricated and their properties compared. It was found that the deformation characteristics of the coarser mixes, when designed by the Marshall procedure, did not vary significantly and fell within the range of the fine mix simply by varying the asphalt content and density of the fine mix.

Technical Issues for Further Consideration

The use of small-scale pavement models subjected to centrifugal forces and repeated loads for predicting fatigue cracking and rutting is an untried, innovative concept. The advantage of centrifuge testing is that it directly shows the extent of fatigue cracking and rutting at any given number of load repetitions by considering not only the properties of each component layer but also the interaction between all layers. This exploratory study has indicated the great promise of centrifuge testing for pavement analysis and design. However, the following improvements should be made before the method can be used for routine pavement evaluation.

1. Due to the small size of the centrifuge capsule, the existing model can only test a full-depth sand asphalt on a subgrade of very limited depth with only two scale factors. A larger and longer capsule should be designed and constructed to accommodate thicker layers, larger aggregates for asphalt concrete and granular base, and several different scale factors.

2. Due to wear and tear on the mechanism and limited testing time, only 10,000 repetitions were applied in the repeated load test. No fatigue cracking could be observed. A pneumatic or electrohydraulic loading system should be installed so that various waveforms with repetitions up to one million or more may be applied until the model fails.

3. The capsule can test the small-scale models only at room temperature at present. It is recommended that the capsule be insulated and equipped with a temperature control device, so the responses of the model can be evaluated at different temperatures.

4. Feasibility tests on compacting the asphalt mixture directly on the top of the subgrade have shown that the sample capsule must be prepared carefully to insure that the asphalt layer and the subgrade are in full contact. This necessity may cause difficulties in installing a strain gage on the underside of the asphalt layer and in compacting the thin asphalt layer without disturbing the subgrade. If the centrifuge modeling concept is valid, it is really not necessary to monitor the tensile strains. A direct observation of fatigue cracking is a better approach than the measuring of tensile strains. Additional instrumentation would be necessary to observe and measure the surface cracking within the capsule.

Image Processing Algorithms for Cracks

IDEA 004 - Image Processing for a Pavement Crack Monitor

Investigators: D.S. Mahler, Z.K. Kharoufa, E. Wong, and S. Magnus, KLD Labs, Inc., Huntington Station, New York

IDEA Product

This project developed software for image processing and data reduction algorithms to find and analyze cracks in both asphalt and portland cement concrete (PCC) road surfaces. The software can be incorporated into automated video crack analysis monitoring (AVCAM). Such a system can potentially analyze pavement images and provide an overall condition analysis of a given length of highway in real time.

Innovation

Analysis of highway cracks required the design of innovative algorithms and modification of standard algorithms for use with the system. The software routines are capable of real-time synthesis of crack data on either asphalt or concrete surfaces with minimal user interaction.

Project Summary and Progress

Many images of roadway surfaces possess substantial amounts of aggregate and other textured features that result in image noise. Procedures have been developed to automatically select a threshold value for potential cracks, and to rapidly eliminate most of the remaining image noise caused by undesirable features (Figure 6). In addition to eliminating the image noise, algorithms also have been developed to label each object for further analysis. To date this analysis includes:

1. determination of the overall crack length;

2. determination of the crack direction;

3. determination of the crack width.

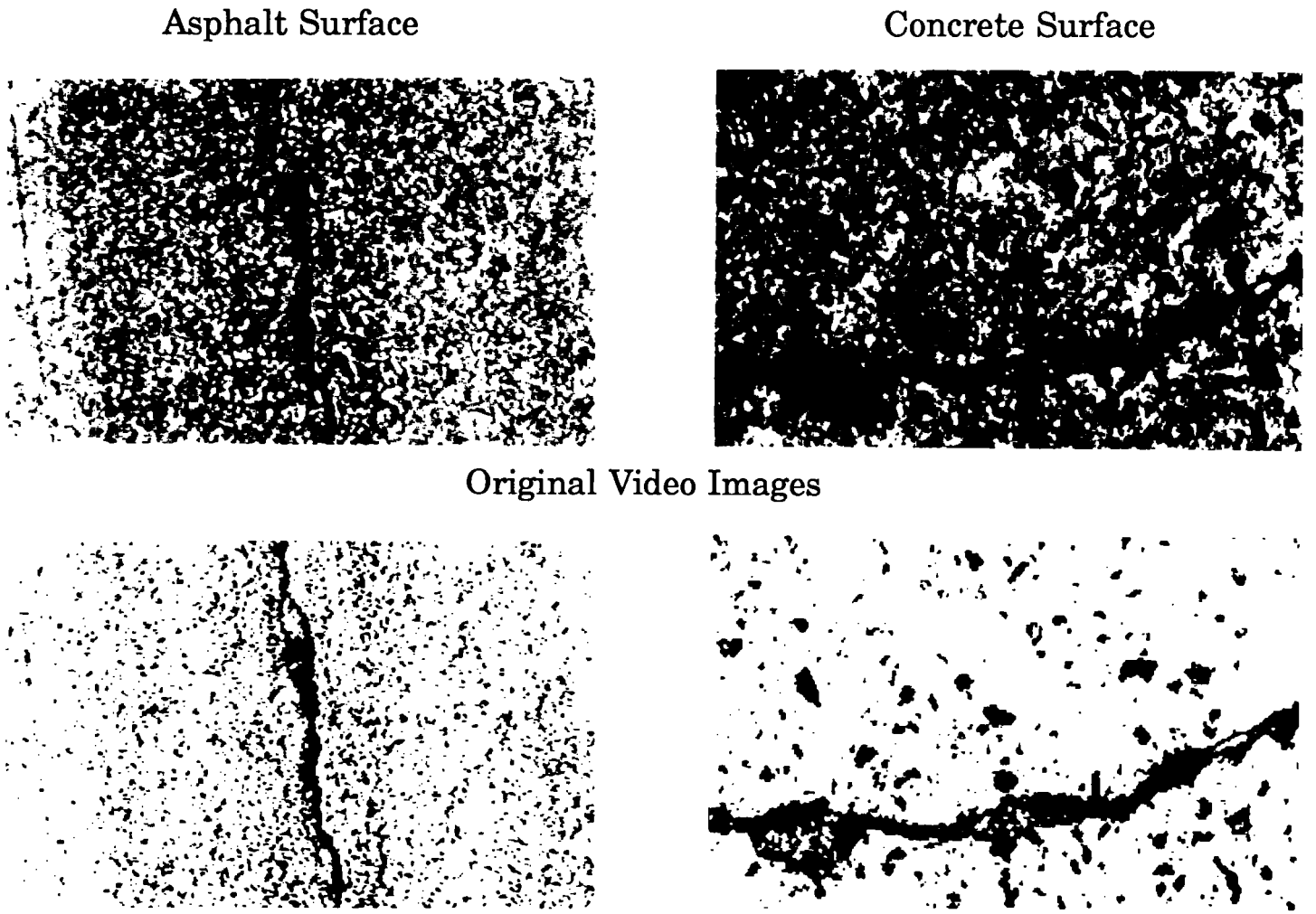

Figure 6. Processed Video Images

The algorithms developed to determine these parameters include:

1. Gradient Histogram Algorithm - To determine the proper intensity threshold value, which initially identifies dark-colored objects, shadows, and potential cracks.

2. Blob Coloring Algorithm - To rapidly eliminate noise features the image and to label remaining crack features which are to be further analyzed to determine pertinent crack parameters.

3. Chain Code and Thinning Algorithms - To determine the crack lengths, to identify side cracks, and (when combined with the output of the Blob Coloring Algorithm) to determine the crack width.

More than 90 images have been investigated using the algorithms developed for the Phase I product. These algorithms have proven suitable for asphalt and concrete pavements. Both asphalt and PCC surfaces have been investigated without the need for operator interaction. This capability implies that the system to be developed can be used by operators with minimal technical backgrounds.

In some cases, the modifications are as simple as repositioning the camera to view a wall or ceiling, or changing a lens to reduce or enlarge the field of view. Some applications, such as dam inspections, might require a different means of traversing a surface.

Technical Issues for Further Consideration

The basic concepts and algorithms developed under these efforts can be applied to new areas of technology. The use of machine vision to automatically recognize and measure cracks in pavement surfaces is not an easy problem to solve. This fact has been stated repeatedly by numerous experts in the field of machine vision. Nevertheless, based on a concerted effort of individuals with varying technical backgrounds, solutions to many of the difficulties have been developed. For those directly involved in the project, an optimistic outlook now exists for the development of a fully automated AVCAM within the next few years based on existing technology.

The algorithms have proven to be useful tools to provide the crack direction, length, and width. The following major aspects of these algorithms need to be further addressed:

1. The overall subjective ratings of the algorithms must be improved.

2. The ability to handle complex cracks (e.g., alligator cracking) must be developed.

Corrosion Detector

IDEA 005 - An Electrochemical Method for Detecting Ongoing Corrosion of Steel in a Concrete Structure with Cathodic Protection Applied

Investigators: N.G. Thompson and K.M. Lawson, Cortest Technologies, Inc., Columbus, Ohio

IDEA Product

Alternating current impedance spectroscopy (ACIS) was used to develop a simple monitoring technique to detect corrosion and evaluate the effectiveness of a cathodic protection (CP) system without complicated criteria or measurement techniques. The method detects ongoing corrosion on a cathodically protected structure, and provides information for cost-effective actions necessary for extending the bridge deck life.

Innovation

The ACIS method can detect ongoing corrosion without interrupting the cathodic protection system. Therefore, it can evaluate the effectiveness of the CP system. The premise for the work was based on the fact that, while corrosion is occurring, the ACIS spectrum is dominated by a Warburg behavior (slope of 1 in the Nyquist plot, Figure 7). In a system with no corrosion, the ACIS spectrum is represented by a single time-constant response.

Product Summary and Progress

The product results indicate that for single reinforcing steel specimens, significant changes in the impedance spectra occur upon going from a corroding condition to extremely low corrosion (passive conditions), or where corrosion is mitigated by cathodic protection. For the conditions examined, the corrosion process for the single reinforcing steel specimens was characterized by a diffusion-controlled reaction sequence and the Nyquist plot was dominated by a Warburg impedance. For passive conditions where the corrosion rate is extremely low, the Nyquist plot exhibited behavior characterized by an extremely large polarization resistance. For the frequency range examined, only the initial portions of the semicircle of a single, time-constant response were observed in the Nyquist plot (the imaginary portion of the impedance was continuing to increase very

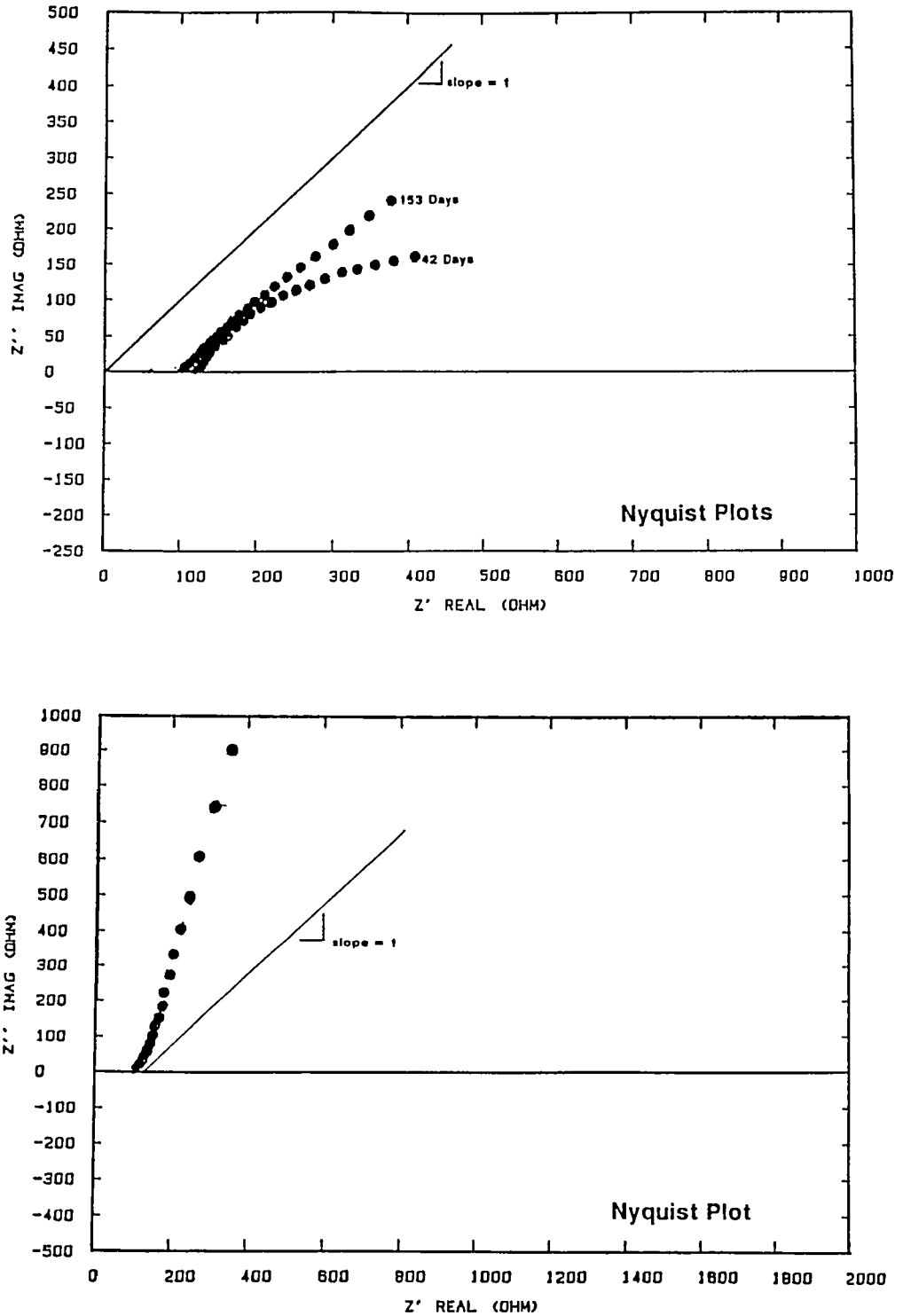

Figure 7. Corrosion Rates With and Without Cathodic Protection

Nyquist plots for single rebar samples in concrete containing 15 lbs/yd^3 chloride. The top figure shows freely corroding conditions with the data fitting a slope of 1 which indicates ongoing corrosion. The bottom figure shows a sample exposed to the same conditions, but cathodically protected. Note that with adequate CP applied, the spectrum no longer fits a slope of 1, and no ongoing corrosion is occurring.

rapidly with decreasing frequency). Upon application of cathodic protection to high Cl conditions which exhibited the Warburg behavior in the Nyquist plot while freely corroding, the impedance spectrum exhibited a single, time-constant response (Figure 8). Visual examination of the reinforcing steel following exposure confirmed that the basic premise of predicting corrosion behavior based on the ACIS spectrum is feasible for short, single lengths of reinforcing steel.

Interpretation of the ACIS data became much more difficult when testing the concept on concrete slabs with varying Cl content and two layers of reinforcing steel mats. The difficulties were caused by the macro-cell corrosion reactions that occurred on the different areas of the reinforcing steel mats exposed to the different Cl concentrations. It was most difficult to interpret the ACIS data when the samples were freely corroding. For the freely corroding conditions, the reinforcing steel exposed to the no-Cl condition exhibited a compressed semicircle, two-time constant behavior with an extremely low polarization resistance. The macro-cell corrosion between the no-Cl condition and the high-Cl conditions established relatively high rates of cathodic reactions on the steel surface in the concrete containing no Cl (cathodic polarization). For the reinforcing steel exposed to the high-Cl conditions, a Warburg impedance no longer dominated the reaction sequence (Figure 9). This is most likely due to the fact that diffusion of oxygen to the corroding area no longer controlled the corrosion rate, but that the corrosion rate is controlled by the macro-cell current coming from an area outside that measured by the ACIS spectrum. It is much more difficult to interpret the difference in the ACIS spectra between noncorroding and corroding conditions in the presence of macro-cells. The cathodic polarization of the slabs to potentials 200 mV more negative than the most negative free-corrosion potential produced some changes to the ACIS spectra, but these changes are much less significant than those observed for the single reinforcing steel specimens.

Technical Issues for Further Consideration

The data described above indicates a very important aspect of measuring corrosion rates under freely corroding conditions. Polarization resistance (PR) techniques are appropriate for mapping the corrosion rate of a concrete structures. The findings in this study indicate that PR values alone cannot map the corrosion rate of a structure which has a varying Cl content and large macro-cell corrosion areas of the couple (little or no corrosion) can have a PR value that is similar to the corrosion current of the anodic areas. The PR technique cannot differentiate between anodic and cathodic currents; it only measures the total electrochemical activity, or current. Therefore, the study indicated that in the vicinity of macro-cell couples, PR provides an overestimate of the corrosion rate of the noncorroding areas. However, it should be noted that at distances far enough away from the macro-cell couples in areas of relatively constant Cl content

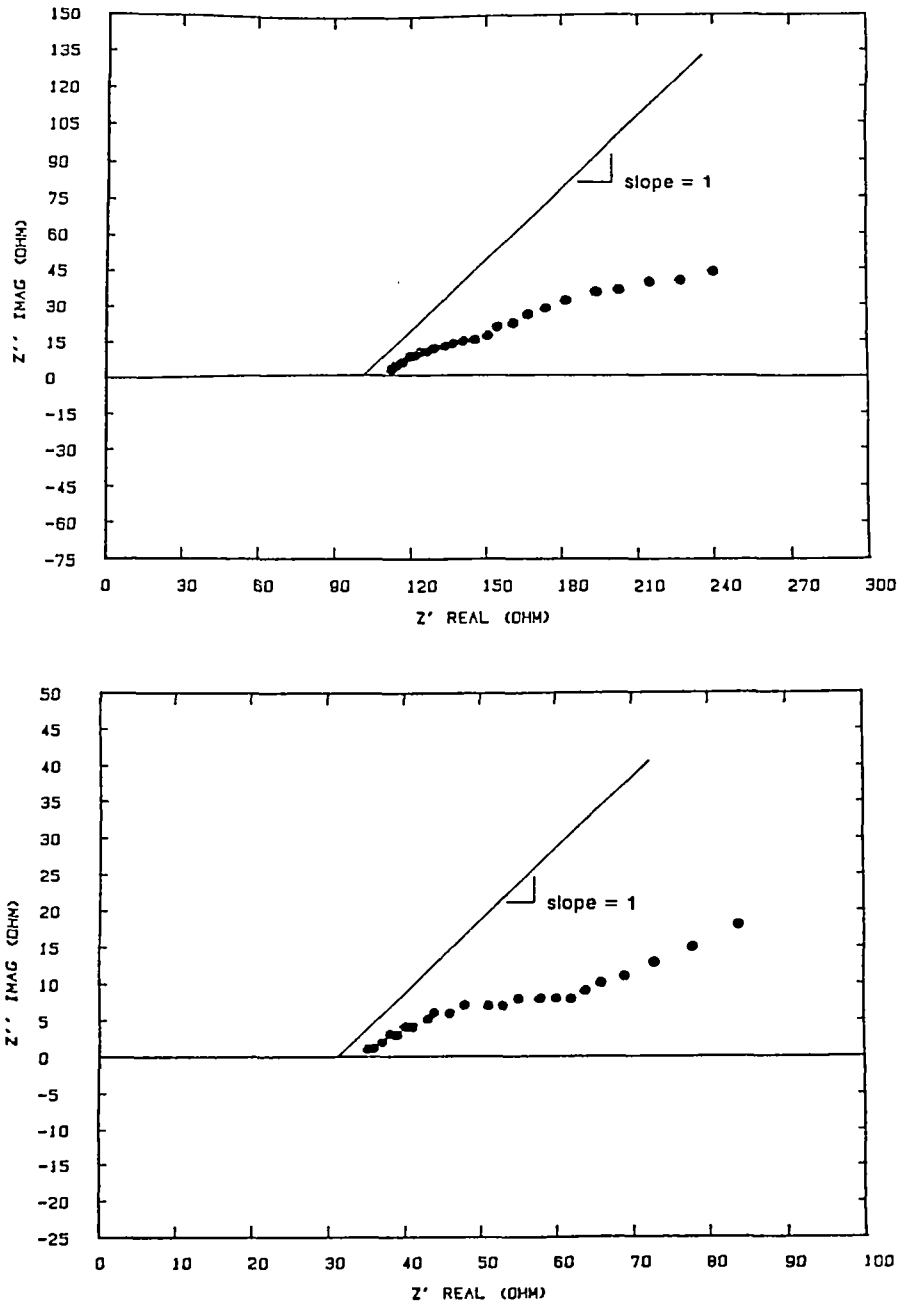

Figure 8. Impedance With and Without Chloride

ACIS spectra for the no-Cl and 45-lbs/yd^3 quadrants of one of the slabs. In the quadrant containing no Cl, a non-Warburg response with a large Rp value was expected. However, a multiple time-constant type response is observed with a relatively low polarization resistance indicated. Examining the 45 lbs/yd^3 Cl quadrant, the impedance values are less than was observed for the no-Cl condition, but the shape of the curves is similar. Based on the data for the single reinforcing steel specimens, the magnitude of the differences between PR values for no-Cl and 45-lbs/yd^3-Cl conditions were expected to be a factor of 10 to 100, not of a factor of 4.

The impedance spectra from isolated rebar sections disconnected from the rest of the reinforced steel mat were significantly different from Figure 7. The ACIS spectrum for the isolated rebar section in the no-Cl condition shows two-time constants with the impedance at low frequencies tending toward ever-increasing values similar to the spectrum shown for the no-Cl condition with the single reinforcing bars.

The high-Cl isolated rebar section shows a Nyquist plot with a similar shape to that shown in Figure 7 (high Cl, continuous reinforcing steel). The impedances are somewhat greater for the isolated rebar section shown in the bottom figure, which is most likely due to a lower corrosion rate for the isolated rebar section since the corrosion is not being driven to higher values (lower impedances) by a macro-cell couple as in the case for a continuous reinforcing steel mat.

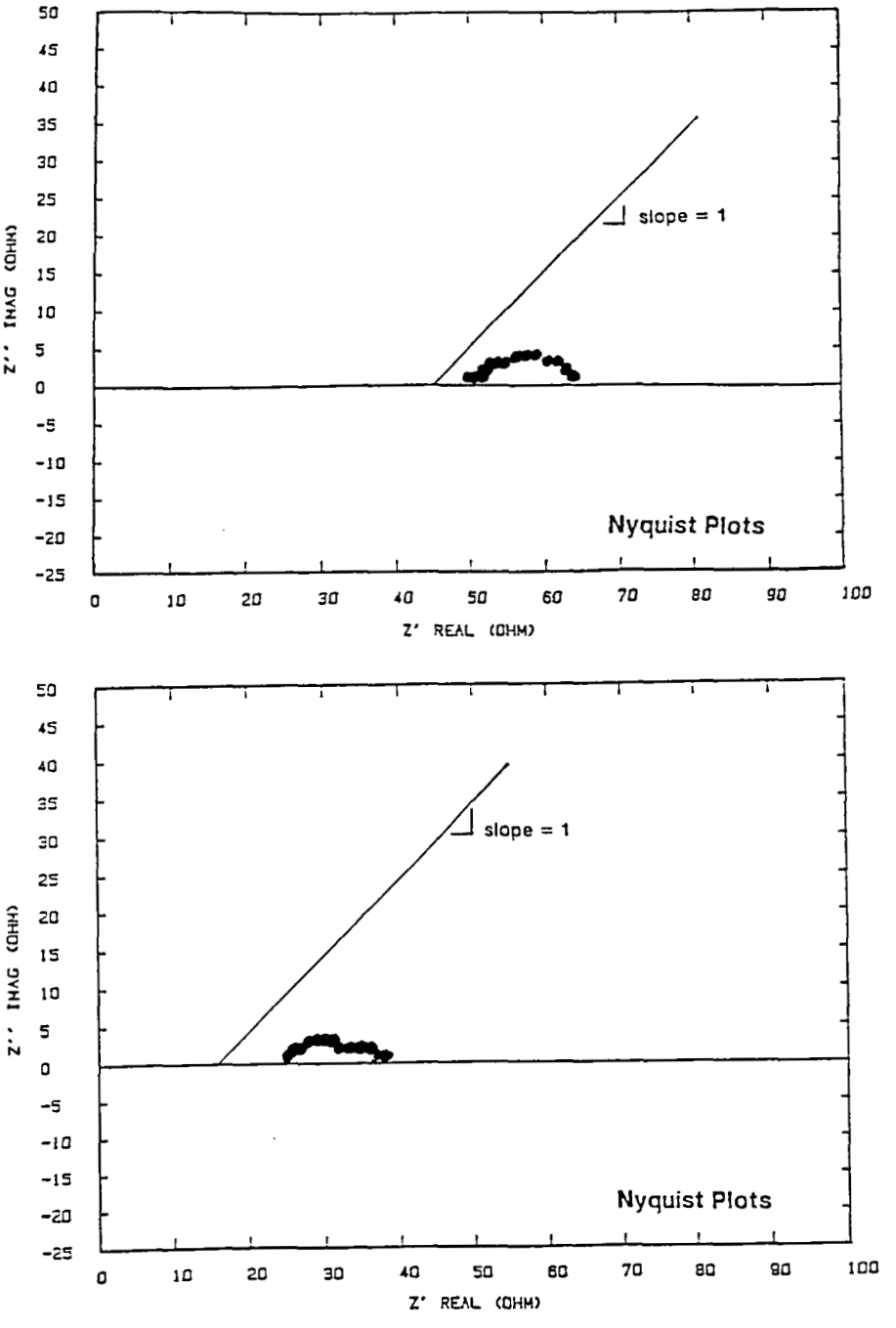

Figure 9. Impedance With Cathodic Protection

ACIS spectra from the test slab polarized 200 mV cathodically. The spectra show a non-Warburg impedance behavior (No slope of 1).

The primary difference in the Nyquist plot between the freely corroding and the cathodically polarized conditions is that for the cathodically polarized conditions, the imaginary component of impedance goes to zero within the frequency examined. Therefore, the application of CP has produced an observable change in the impedance spectra, but the change was much more difficult to characterize for the large slab specimens than it was for the single rebar specimens.

(and constant potential), macro-cell currents may be extremely low. Therefore, in this latter case, the PR values can indicate that careful interpretation is required. A combination of potential and PR mapping can provide an accurate description of the corrosion conditions of a bridge deck when properly interpreted.

Rapid Profile Using a Laser Beam

IDEA 006 - Laser-Beam-Carried Microwave-Interferometer for Rapid Pavement Profiling

Investigators: Dwight D. Egbert and M. Sami Fadali, University of Nevada, Reno, Nevada

IDEA Product

The laser-beam-carried microwave-interferometer (LBCMI) measures pavement topography by rapid scanning of pavement surfaces. Existing methods for measuring pavement topography are still relatively slow, or make measurements only a discrete intervals. Rapid measurement of continuous profiles would give engineers a more accurate picture of roadway topography.

Innovation

The basic concept of the LBCMI system consists of a scanning mirror mounted on a vehicle. This mirror directs a laser beam transversely across the pavement lane as the vehicle proceeds (Figure 10). The laser used is a gallium-aluminum-arsenide solid state laser which can easily be amplitude-modulated at frequencies up to 500 MHz. Modulation frequencies between 400 and 500 MHz result in a wavelength on the order of 75 cm. Thus, with a phase difference resolution on the order of one degree, road surface topography can be obtained with a precision on the order of one mm.

The road surface height measurement is obtained by comparing the phase delay of the modulated wave reflected from the roadway to that of a reference phase obtained at the laser source. The beam splitter mirror extracts a small portion of the beam and sends it to the reference receiver, where it is converted to an electrical reference signal in the 400 to 500 MHz frequency range.

A second small mirror routes the primary laser beam to a scanner mirror that sweeps the laser beam across the region of interest. The second small mirror is directly in front of the main receiver lens at a 45° angle to the lens. This configuration creates simultaneously a scanning transmitter and a scanning receiver. Thus, the instantaneous field-of-view of the main receiver lens is always centered on the same pavement position that the main laser beam is illuminating.

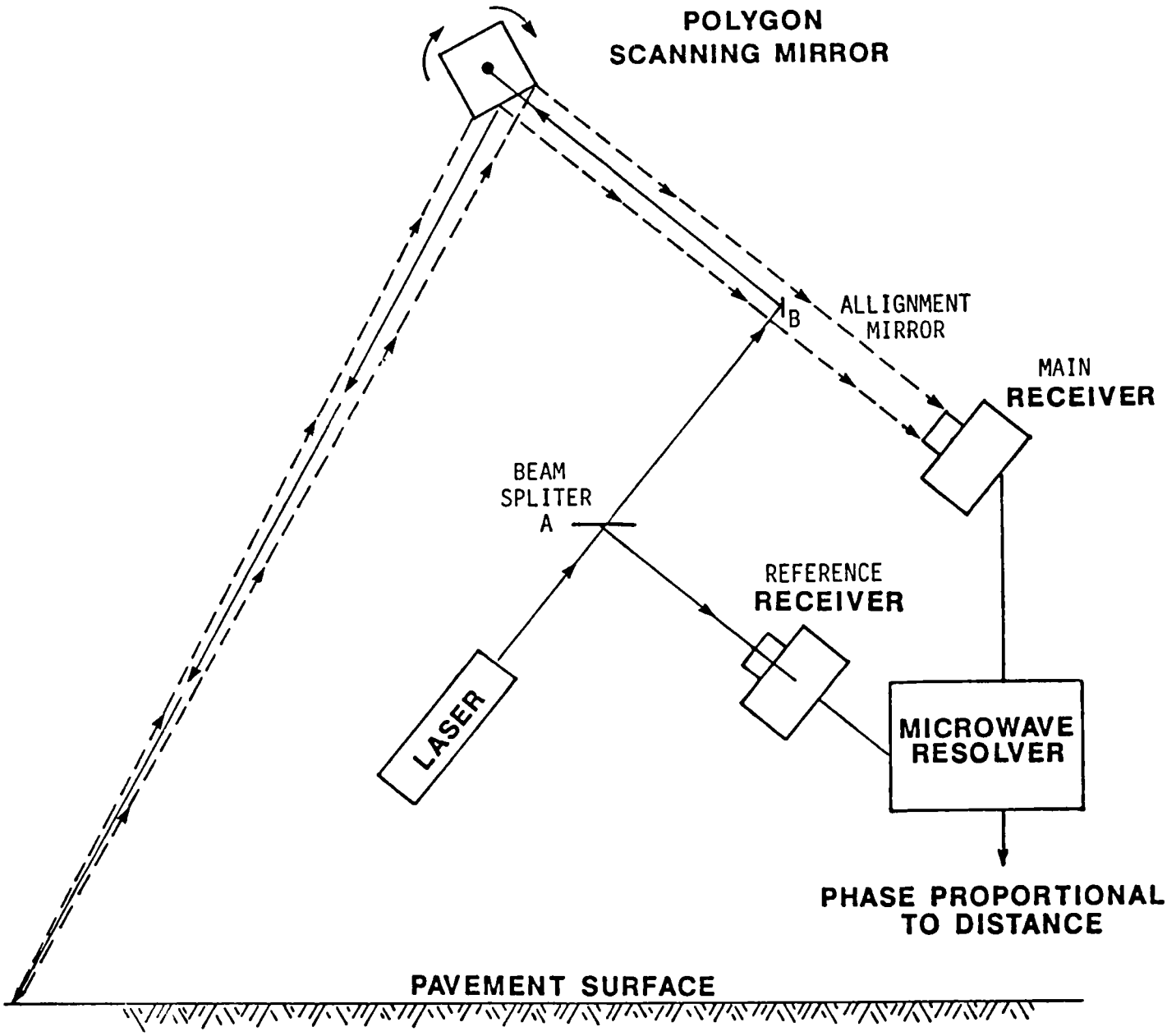

Figure 10. Schematic Diagram of the Laser-Beam-Carried Microwave-Interferometer

This optical path, from the second small mirror to the scanning mirror and then down to the pavement surface, has two-way laser information. First, the main incident laser beam propagates toward the road surface. Second, the diffuse-reflected laser beam also returns from the road surface toward the main receiver over this path.

The main receiver detects the reflected laser beam and converts it to an electrical signal in the 400 MHz range. The outputs of the two receivers are then put into a microwave phase resolver which measures the phase difference between them. This phase difference is proportional to the distance between the scanning mirror and the road surface at each point along the transverse scan. This distance d is a function of the angle θ which is measured between the vertical and the instantaneous direction of the laser beam. The raw signal is a combination of the transverse profile and this trigonometric scanning function.

Project Summary and Progress

A roadway's topography influences motorists' ride and safety. Features considered important for characterizing topography include cross slope variations, longitudinal profile, surface undulations or waves, depressions, holes, ruts, bumps, shoulder/pavement discontinuities, and dropoffs. A mobile and automated system capable of rapidly surveying a roadway's surface to quantify its topography accurately will be a useful measurement system for evaluating roadway conditions affecting motorist ride and safety.[1,2] Previous transverse profile measurement procedures involved, manual measurements, noncontact sensors, and 35 mm photographs with a "hairline projector" light beam. Manual measurements require people to occupy the pavement surface, and the process is dangerous and slow. [3]

---

[1]Kurt D. Smith, Michael I. Darter, J. Brent Rauhut, and Kathleen T. Hall, Distress Identification Manual For The Long-Term Pavement Performance (LTPP) Studies, FHWA Contract No. DTFH61-85-C-0095, Draft, March, 1987.

[2]J. Brent Rauhut, M.I. Darter, R.L. Lytton, P.R. Jordahl, and M. Gardner, Data Collection Guide for Long-Term Pavement Performance Studies, FHWA Contract No. DTFH61-85-C-0095, Draft Report, June, 1987.

[3]James C. Wambold, Gordon L. Hayhoe, William H. Park and Mac E. Bryan, Survey System for Road Roughness, Rutting, and Topography (SIRST), FHWA Contract No. DTFH61-80-C-00049, Report No. FHWA/RD-86/034, February, 1986.

Of the noncontact systems, three are currently in use: laser; ultrasonic; and infrared. These systems use individual sensors arranged transversely over eight to twelve feet. The smallest number of sensors used is three (wheel path-center lane-wheel path) and the highest number used is 17. The problem attendant with all these systems is that the transverse profile measured is sampled only at discrete intervals.[4]

The LBCMI system provides advantages over all of these current methods.

- It can be operated in daylight at normal highway speeds.
- It produces a smooth transverse profile of the roadway.
- The instantaneous-field of view of the laser determines the minimum horizontal resolution, and is adjustable.
- The LBCMI output can be directly digitized and stored by an on-board computer in the survey vehicle.
- The amount of data stored for analysis is under software control.
- Partial data analysis and reduction can be accomplished in real time.

Because the depth measurement is obtained from the microwave modulation of the laser beam, low-power lasers can be employed and a smaller signal-to-noise ratio can be tolerated than with existing laser techniques.

The laboratory scanning experiments were performed at a scanning distance of approximately 1.5 m with white posterboard as the target surface. With this configuration, the LBCMI system produced sufficient reflected light to measure a full 90° scan. Also, the signal-to-noise ratio was sufficient to produce a properly decoded surface profile. However, when the system was tested while scanning pavement surfaces in the field at its design height of 2.0 m, the reflected signal was only strong enough to produce reliable results for the center 2 m of the 4-m scan path. Because of the reduced signal-to-noise ratio the decoding algorithm did not perform properly and the apparent surface profile tends to be curved rather than flat. However, even with the overall surface distortion, specific surface perturbations are still visible and measurable

---

[4]Ronald W. Carmichael, Automated Pavement Data Collection Equipment Roughness and Profile Measurement: Equipment Report, FHWA Demonstration Project No. 72, Report No. FHWA-DP-72-1, September, 1986.

on the decoded scans. The results of this research have proven that the laser-beam-carried microwave-interferometer theory will work and a highway profiler using it is practical.

The output of the LBCMI in the laboratory matches very closely the theoretical predictions. When the laboratory prototype LBCMI was transferred to the moving platform for field tests the signal-to-noise ratio which had produced smooth results in the laboratory tests at 1.5 m from a white target, became marginal for actual road surfaces at the operational height of 2 m. In spite of this problem, the results do demonstrate the potential capabilities of the LBCMI technology.

Due to the fall-off in returned signal at large angles, the decoding algorithm could not normalize the raw data sufficiently to produce a reasonably flat profile over the entire 4-m path. Rather, the scans all show a curved nature. However, the details of the target surfaces in the center portion of the scan clearly show that the system is accurately measuring the surface profile. The scans can be found in the transverse profiler final research report.[5]

Several different types of target surfaces were scanned to test different capabilities of the system. Likewise, in order to simulate the results which could be expected from a system with a higher signal-to-noise ratio, several scans from the same surface were averaged together. The averaging process could not correct for the overall curve seen in the data. It can only correct for the high frequency noise which obscures the profile details.

Technical Issues for Further Consideration

The conclusion drawn from preliminary tests is that the fundamental limitation of the laboratory prototype LBCMI was the lack of a commercially available light detector with a combination of high speed and high sensitivity. For the laboratory prototype system, the highest performance tube that was found to be commercially available, a Hamamatsu R1547 photomultiplier tube, has a rise time of 1.4 nanoseconds. The lack of a higher-speed detector forced the user to a maximum microwave modulation frequency of 300 MHz. This limitation has reduced the accuracy of the LBCMI.

---

[5]Dwight D. Egbert and M.S. Fadali, A Transverse Profiler Using Laser-Beam-Carried Microwave-Interferometry, (SHRP-ID/UFR-90-003), December, 1991.

If the capabilities of the newly announced Hamamatsu photomultiplier tube are available for a future version of the LBCMI system, these averaged scans should be representative of the expected results.

Freeze Coring of Fresh Concrete and Air Void Measurement

IDEA 007 - Quantitative and Rapid Measurement of Air Void Systems in Fresh Concrete

Investigator: Will Hansen, The University of Michigan, Ann Arbor, Michigan

IDEA Product

A technique was developed to core a sample of fresh concrete. This contractor also developed a laser device for rapidly measuring the air void distribution at the surface of the core.

Innovation

This new technique for coring fresh concrete consists of freezing the core length with liquid nitrogen and extracting the frozen core for sampling. The coring device consists of a 35-mm-inner-diameter steel drilling bit with a diamond cutting surface. It is thin-walled with a thickness of about 0.4 mm for smooth drilling. Pressured air is used for removing the dust produced by drilling. The steel mold used to facilitate rapid freezing, consists of an inner cylinder into which fresh concrete is cast, and an outer cylinder with a top flange for attachment of the drilling device. The outer cylinder is closed at the base and has a ring with two pins for attachment of the inner cylinder. The pins prevent the inner cylinder from rotating during coring. The inner cylinder is also open at both ends. Liquid nitrogen is poured between these two cylinders. Figure 11 illustrates the mold design.

The laser instrument consists of a specimen lathe bench, laser detector with electronics, and a microcomputer for data storage and analysis. A 10 mW laser diode beam about 2.5 μm in diameter scans the concrete surface from a distance of about 20 mm. The laser scans the specimen surface in a number of prescribed concentric circles for obtaining air-void measurements.

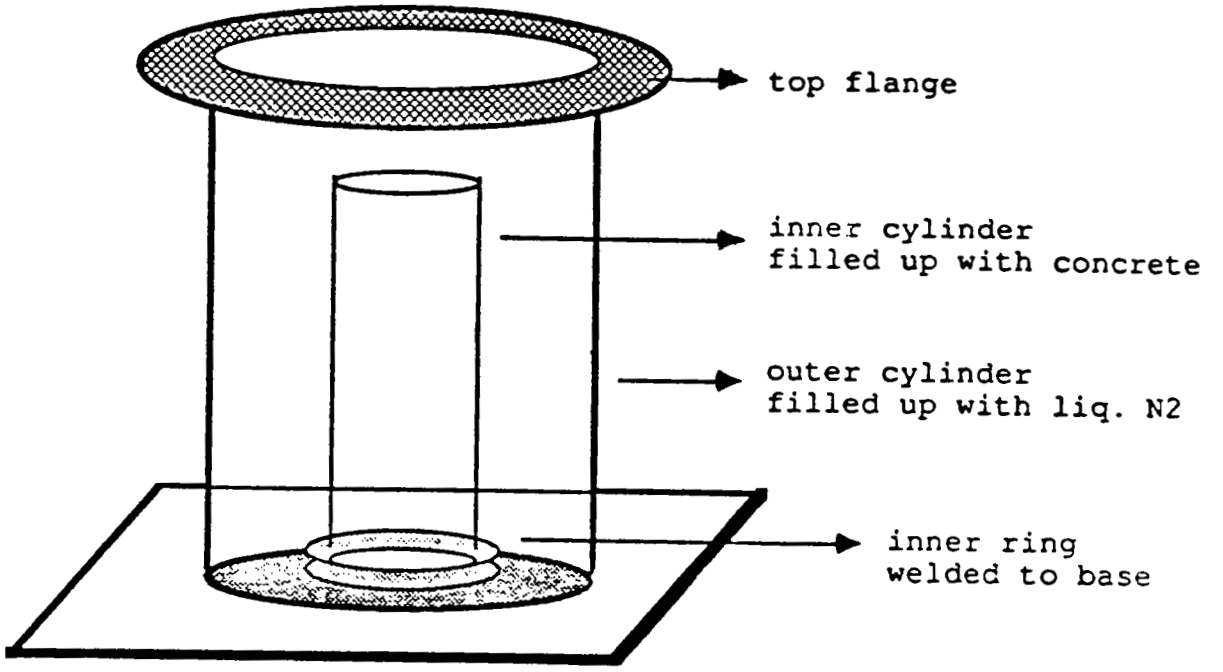

Figure 11. Specimen Mold for Freezing Fresh Concrete

Project Summary and Progress

Entrained air greatly improves the resistance of concrete to freezing and thawing cycles. The microscopic air bubbles produced by the air entrainer relieve pressures caused by water freezing in the capillary pores in the hydrated cement paste. Without these air bubbles, the concrete may scale and disintegrate.

Total air content is often used as a measure of frost resistance of fresh and hardened concrete, although the major parameter controlling frost resistance is the spacing of these air voids. The ASTM method for obtaining the spacing factor of the air-void system is only applicable to hardened concrete and is costly and time-consuming.

Results from coring in fresh concrete were encouraging. Fresh concrete was frozen hard within about five minutes after pouring liquid nitrogen into the specimen mold. However the specimens were not long enough for measurement by the laser. They broke off at a length of about 50 mm. A minimum length of 100 mm is required for measurement. The problem was in the removal of dust from drilling. The air pressure was not sufficient to remove the particles at greater depths.

The laser detector consists of a photodiode, lenses and a beam splitter. The detector has four light sensitive photodiodes arranged in a quadrant. At a given distance to the specimen surface, the incoming and reflected beam in the detector plane will determine a circular light spot in the x-y plane. If the distance between the laser and the surface changes, either due to an air void or movement of the surface in excess of about 10 μm, the detected signal will form an ellipsoid with the minor axis in the direction of the surface scanned. Assuming that changes in distance of the laser beam are due only to air voids, the total number of times (N) the laser signal is ellipsoid, multiplied by the beam diameter (about 2.5 μm) determines the total chord length for all the air voids. The signal processing unit keeps track of the individual chord length for all air voids since it knows when a given air-void starts and ends. Figure 12 shows how total air-content is calculated together with the specific surface area which is needed for estimating the spacing factor. In the present version the relative paste volume fraction must be known for the analysis.

Sample specimens were used to evaluate the laser technique. These were air-entrained concretes with 4% and 5.5% total air content as measured by the image analyzer. Data was obtained with the image analyzer and the laser instrument. The data show that for optimum laser setting the total air contents are in good agreement.

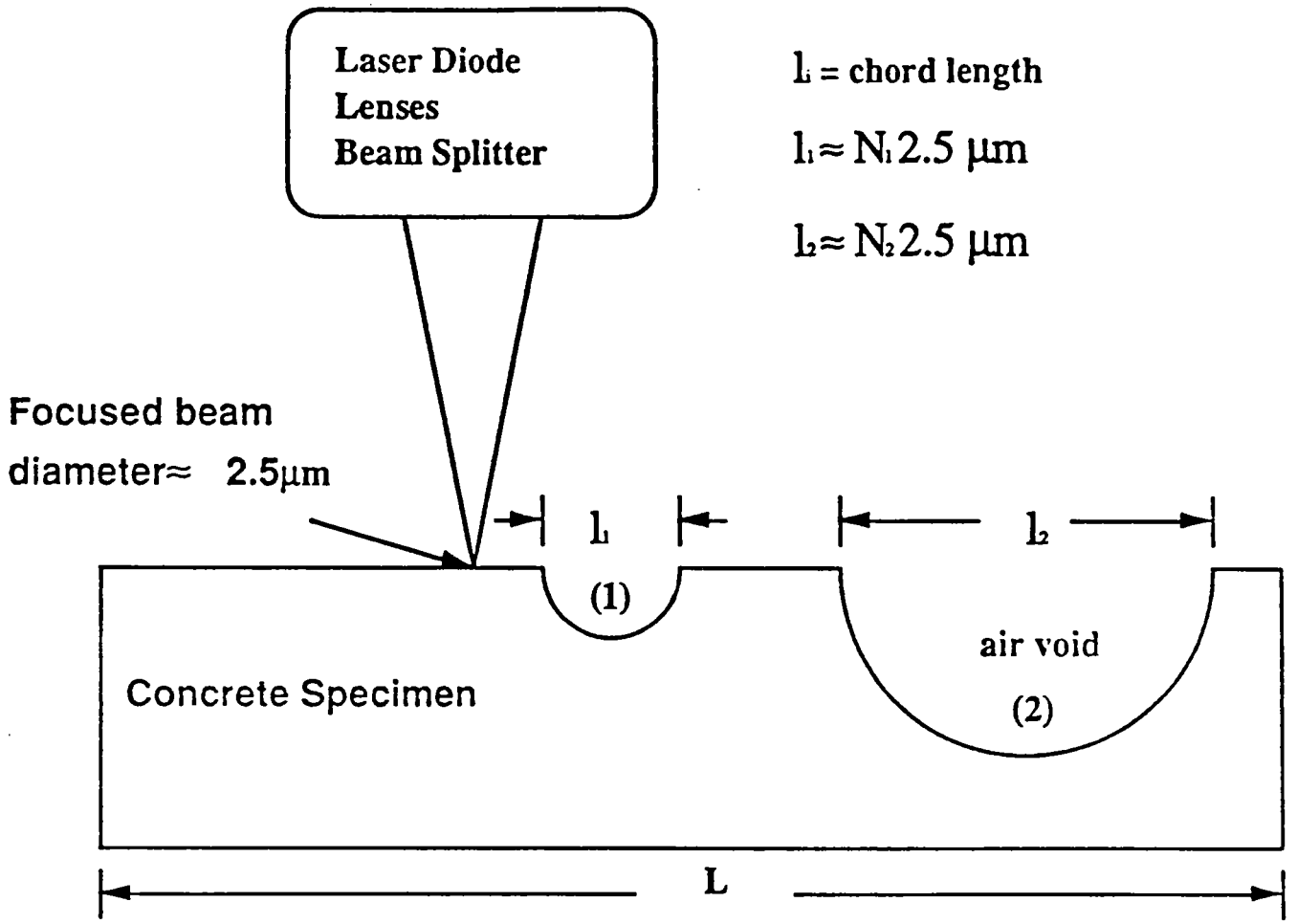

where

$$A = \frac{\sum l_i}{L}$$

A= air content and L= traversed length

$$\alpha = \frac{4n}{A}$$

n = bubble frequency (# of bubbles / in)

Figure 12. Schematic of Air Void Measurement by Laser Instrument

Technical Issues for Further Consideration

A coring technique for fresh concrete has been developed. Minor refinements are needed.

Reproducibility is one of the major problems experienced with the laser. This was due to the effect of focal distance between the laser and the specimen surface on the results. Total air content of a given specimen varies between 100% and 0% for a distance of 16 mm and 17.5 mm respectively. The reason for this is not clear. Clearly a much better control is needed. With the current method a variability in measurement distance of about 0.2 mm produces a 10% variation in total air content of a given specimen.

As a result of these findings, modifications are being made to the laser instrument. They include: (1) introducing an electronic autofocusing system for applying the laser head to the specimen surface to make the laser much more accurate and stable; and (2) redesigning the specimen turning bench so that it becomes more stable when the specimen rotates.

Additional work on this product is not planned under the IDEA program. However, further work would be necessary to develop a commercial semi-automatic linear transverse system. The rapid freezing technique must be upgraded in order to obtain a frozen, fresh concrete sample with a plain and smooth surface for measuring air voids.

Portable Corrosion Rate Monitor

IDEA 008 - Evaluation of Electrochemical Impedance Techniques for Detecting Corrosion on Rebar in Reinforced Concrete

Investigator: D.D. MacDonald, SRI International, Menlo Park, California

IDEA Product

An electrochemical technique to detect corrosion on reinforcing bar (rebar) in concrete is being developed.

Electrochemical techniques have unique abilities to detect metal oxidation processes remotely by using relatively simple equipment and analytical techniques. This ability arises from the fact that corrosion is an electrochemical oxidation process in which iron metal is converted into corrosion products (rust). The method can measure corrosion rates on bridge decks, and will aid engineers in choosing the most cost effective repair methods.

Innovation

A conceptual study indicated that corrosion may be located by imposing a sinusoidal current at a monitoring point on the surface to measure the rebar/concrete impedance (ratio of voltage to current) as a function of frequency (typically from 10^{4} to 10^{-3} Hz). The corrosion rate is measured on the basis that the distance traveled by the alternating current (ac) wave down the rebar increases as the frequency is lowered. At some characteristic frequency, the ac wave intersects the corroding region, resulting in a sudden but perceptible change in the measured impedance (Figure 13). The technique proves to be a powerful in situ technique for rapidly surveying concrete structures to detect corrosion and to assess the extent of damage before the structural integrity is compromised.

Project Summary and Progress

The project evaluated the applicability of ultralow frequency ac impedance spectroscopy (ULFACIS) for characterizing the corrosion of rebar in concrete. The project provided definitive answers to the following questions:

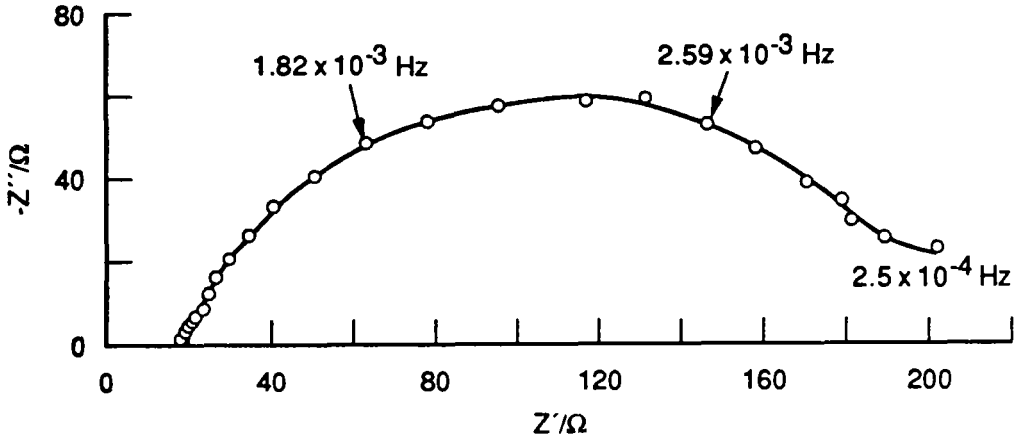

Figure 13. Typical Impedance Spectrum of Corroding Rebar in Concrete

$[CaCl_2]$ = 0 wt%; imposed current = 50μA (peak to peak)

1. Can ULFACIS be used to locate and characterize corrosion nondestructively in reinforced concrete structures?

2. Can impedance spectroscopy be used to measure the polarization resistance of steel embedded in concrete and hence to calculate the steel corrosion rate?

The importance of the first question is due to the fact that by the time corrosion becomes apparent as rust stains on the concrete surface, extensive damage has already occurred, frequently requiring the complete removal of the concrete, cleaning and repassivation of the rebar, and replacement of the concrete cover. However, this procedure does not guarantee that corrosion will not occur at some other location at a later time. The importance of the second question results from the fact that rebar represents a distributed impedance system that can be modeled as an electrical transmission line. As noted above, one characteristic of a transmission line is that the length of the rebar sampled in any electrochemical test is a function of time or frequency. As the time of sampling increases or the frequency decreases, the imposed signal travels farther down the line. Thus, the area being sampled is not well defined, and the sampled area at any given frequency depends on the concrete resistivity and the impedance of the rebar/concrete interface. The goal then is to develop a technique for extracting the polarization resistance from the impedance data.

The results of bench scale laboratory tests showed the following:

1. The electrical impedance of the rebar/concrete system is sensitive to the presence and extent of corrosion on rebar in reinforced concrete structures.

2. The electrical properties of rebar in concrete may be accurately modeled using transmission line electrical equivalent circuits consisting of passive elements (resistors and capacitors). This finding is extremely important because it provides a readily manipulated model that can be used to calculate the distance of corroding regions from the monitoring point from the frequency of the applied ac and the properties of the concrete.

3. Confirmed the theoretical prediction that the phase angle at low frequencies (.0 to 0.01 Hz) is the most sensitive indicator of the presence of corrosion.

4. Demonstrated that, by scanning the reference electrode (which is used to detect the alternating voltage) across the surface, ULFACIS can be used to spatially resolve areas of corrosion activity and hence can form the basis of a practical method for surveying corrosion damage to concrete structures.

5. Established a new procedure for extracting the corrosion rate of the rebar from measured impedance data. This procedure eliminates the complexities of measuring corrosion rates based on electrochemical techniques.

Although the project was exploratory in nature, it has demonstrated the feasibility of practical techniques for the in situ location and characterization of corrosion on rebar (ULFACIS) and for estimating rebar corrosion rate in concrete structures before damage becomes evident to an external observer. The development and field testing of practical corrosion surveying instruments based on the exploratory work described here will be carried out in a future program.

Technical Issues for Further Consideration

The refinements of the concept and the project results provides adequate basis to develop and test portable corrosion rate monitor in active field operations.

A SHRP-IDEA Phase II contract has recently been awarded to perform prototyping and field testing of the corrosion rate monitor system. The Phase II project is cost-shared with CALTRANS.

Biological Material for Ice Control

IDEA 009 - Snow and Ice Control on America's Highways

Investigators: Thomas Caceci and Thomas E. Toth, Virginia Polytechnic Institute and State University, Blacksburg, Virginia

IDEA Product

Prototypes of biologically based materials can suppress the formation of ice. The project will produce a novel biologically based antifreeze peptide with the capacity to suppress the freezing point of water to the region of 15°F. Tests of this material will be conducted to examine the effectiveness, optimal concentration, and stability in the open environment. The material would have application in the control of ice and snow in specialized situations, such as bridge decks. This anti-icing material will be biodegrdable and nontoxic, and can be applied before icing begins.

Innovation

Using the antifreeze peptide (AFP) of the winter flounder (Pseudopleuronectes americanus) as a model, the project employs genetic engineering as a means to design and product artificial AFPs that mimic the structure and function of these natural materials. In natural AFPs, ice-suppression activity is related to molecular size. Based on what is known of natural AFPs, this molecule will have an ice-suppression capability below that of natural ones.

Natural materials capable of suppressing ice formation are present in a number of animals, principally certain Arctic fish species. These materials typically depress the freezing point of water to about 12.0°C (28°F) by a noncolligative mechanism approximately 500 times more effective than would be predicted from concentration relationships.

Project Summary and Progress

For many years it has been known that several species of fish in the polar oceans spend much of their lives in waters well below the freezing point of their body tissues. These fish do not freeze, however, due to circulating peptide or glycopeptide antifreezes

synthesized in the liver and present in body fluids. All of the antifreeze molecules typically depress the freezing point of the tissues to roughly -2.0°C. Fish antifreeze materials do not simply depress the freezing point of the tissues by colligative action. They interfere actively with ice crystal formation. On a molal basis the various antifreeze molecules produce a freezing-point depression up to 500 times that which would be predicted from colligative relationships. The protein antifreezes from the winter flounder are among the best known, and are called "alanine-rich" AFPs because of the high proportion of alanine ($\geq$ 60%) in their composition. Flounder AFPs are composed of a series of repeating 11-amino-acid units, of the form:

$$\text{THR-}(X)_2\text{-polar amino acid-}(X)_7$$

in which *X* is usually alanine (Figure 14). The smallest flounder AFP has three such repeats (the minimum required for activity) and the longest for which DNA has been identified has five. Alanine residues appear to function as "spacers" to locate the active groups (i.e., the polar side chains) properly. The secondary structure is an alpha-helix stabilized by charged group and hydrophobic interactions; there are no intramolecular covalent bonds (such as disulfide bridges). Studies of circular dichroism and viscosity indicate that alanine-rich AFPs have a tertiary conformation in the form of a rod-shaped molecule. The peculiar repeating pattern of the amino acid sequence and the rod-shaped structure are necessary for ice suppression activity. The polar side chains of the molecule are all located along one side, rather like teeth on a comb. They are spaced to coincide with the oxygen molecules in the basal plane of a forming ice crystal lattice. The AFPs are thought to preferentially adsorb to the forming face, directed and oriented to it by the dipole moment of the molecule. The congruent spacing of oxygens and active groups facilitates hydrogen bonding. Adsorption of the AFP at steps in this plane is thought to block crystal growth where the molecule covers the step because it alters the surface area: volume ratio of the forming crystal, increasing the free energy barrier to the formation of new steps (Figure 15). It also ties up sites for incorporation of new water, and hence freezing requires a lower temperature to take place. Adsorption of two or more molecules in tandem, or adsorption of a longer molecule, would block more of the step, and would allow crystal formation to occur only in an even smaller unblocked region. The mechanism by which AFPs are thought to work can be thought of as a special case of a well-known phenomenon: the "poisoning" of crystal growth by impurities. The AFP molecules can be conceptualized as "deliberately designed" impurities which the fish uses to protect itself against ice formation.

There is a relationship between AFP size and activity. The adsorption-inhibition model argues that there should be a minimum effective size for AFPs, since if too small a region of the face is blocked, the increase in the free-energy barrier would be insignificant. A minimum of three repeats of the basic sequence is required for

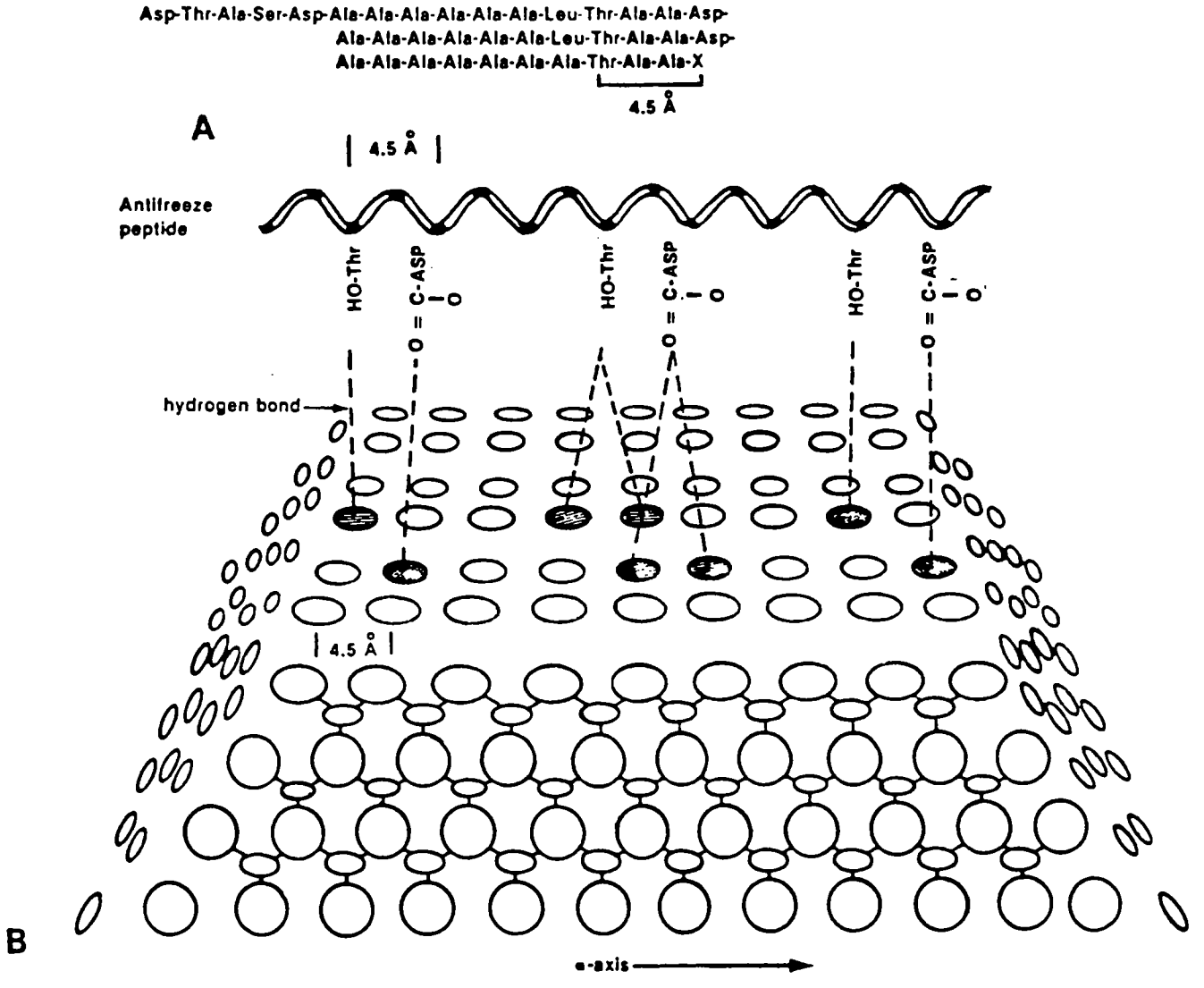

This figure is redrawn from DeVries, 1984.

Figure 14. Schematic of AFP Binding to Ice

The primary amino acid sequence of one of the peptide antifreezes from the winter flounder (*Pseudopleuronectes americanus*) is shown in the upper illustration (A). It consists of a straight-chain peptide, most of which is alanine, with 4.5 angstrom spacing between threonine and the adjacentpolar amino acid. This basic structure is found in all the different peptides, which vary mostly in length and not in composition. The lower illustration (B) shows how the spacing allows hydrogen bonding to the face of a forming ice crystal.

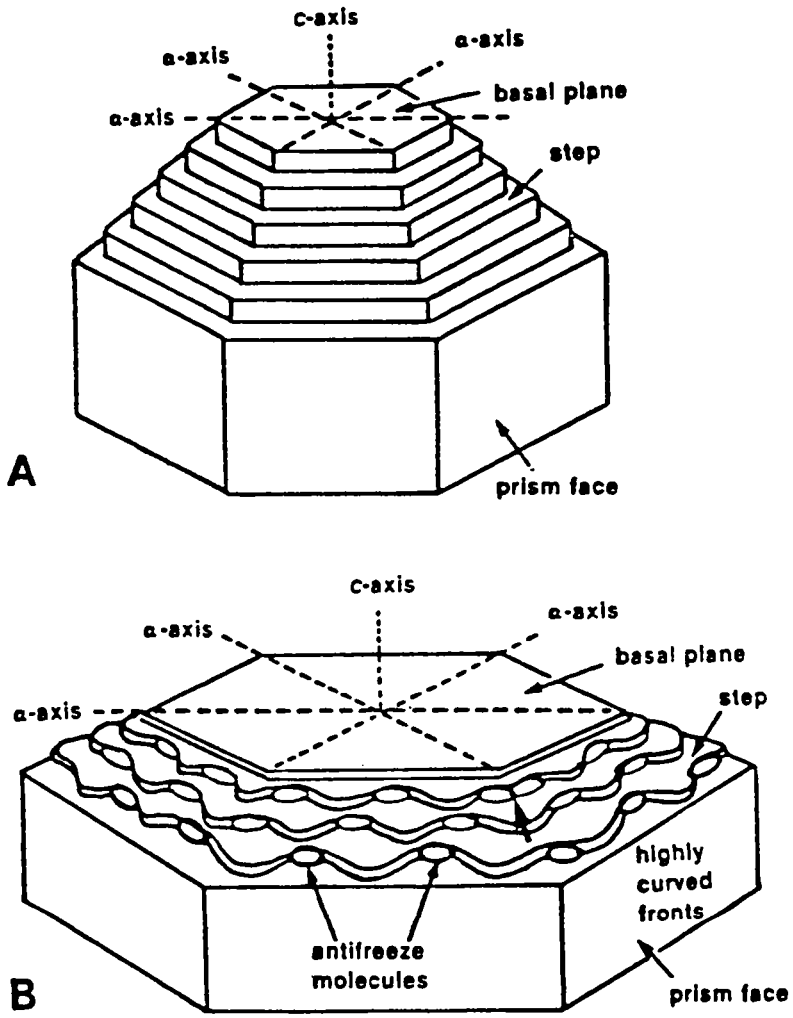

This figure is redrawn from DeVries, 1984.

Figure 15. Blocking of Crystal Growth by AFPs

Ice crystals form in two directions, as depicted in the upper illustration (A). The crystal grows outward along the α-axis, and at right angles to this plane along the *c*-axis. By binding to the forming prism faces in the α-axis, the antifreeze molecules disrupt the formation of the step, preventing smooth formation of the face, and resulting in curved fronts. Where the molecules happen to bind closely (arrow) the front is even more effectively blocked. The same effects occur with longer molecules, which block more of the step.

ice-suppression activity. Smaller molecules are inactive because of few potential ice-interaction sites. If crystal growth can occur only in regions which are not blocked, then it follows that above the minimum size limit larger AFP molecules should be more effective than small ones in preventing crystal growth. This is observed in natural systems, and on a molar basis, the larger molecules are more active in ice suppression than the smaller ones. Increasing the number of potential ice-interaction sites should increase the effectiveness of AFPs whether natural or artificial.

AFPs longer than five repeats apparently do not exist in nature. Within the class of alanine-rich AFPs there is a strong correlation between molecular weight and activity. When comparing natural alanine-rich AFPs, one of MW 4000 has an observed activity higher than one of MW 3300. Furthermore, reduction of the chain length and molecular weight reduces activity. Specifically, the differences lie in the number of repeats of the basic sequence, and in overall molecular weight. The conclusion to be drawn is that, within this class of antifreeze peptides, molecular weight and antifreeze activity are directly related to each other. The artificial forms made and planned are also of the "alanine-rich" type. Size is the principal difference among the natural forms and between those natural forms and our synthetic form(s).

One can construct a synthetic gene to code for the synthesis of any desired sequence of amino acids, and the bacteria commonly used as hosts can be made to express virtually any protein, even one which does not exist in nature. The current approach is based on the following hypothesis.

Increasing the size of synthetic AFPs beyond that of the largest known native AFP should produce a freezing-point depression greater than that of any known native one, because the number of available ice-binding sites will be greater and the coverage of the forming crystal face more complete. In order to test this hypothesis, the contractors are engaged in the synthesis of wholly new molecules, having no counterparts in actual animals, as prototypes for further developmental work on practical forms.

The first step in this program was to synthesize an 8-repeat synthetic analog of one of the flounder AFPs, containing the 11-amino-acid sequence described above. This was named "WF8R," an abbreviation for "Winter Flounder, 8 Repeats." The synthetic gene coding was deliberately designed to allow easy incorporation of more DNA coding for additional repeats. In this way it is possible to continue increasing the number of repeats and ice-binding sites in the molecule. The contractor is now producing WF8R in small amounts and beginning initial tests of ice-suppression activity.

Technical Issues for Further Consideration

The principal issues to be settled with respect to artificial AFPs are: 1) how low a freezing point can be reached; and 2) whether they can be made in sufficient quantities to become economically competitive with other forms of ice control. The first question can only be settled by constructing and testing new variant forms. It seems likely that the strategy of extending the molecule has some limit to its effectiveness, but only direct manipulation of new forms can answer this.

The second question--which the biotechnology community calls "scale-up"--is another matter. At the present time, biotechnology products are limited to materials with high unit value and low levels of production demand. Examples include some therapeutic agents and pharmaceutical products. This situation is the exact opposite from the requirements for large-scale application of material to roadways. However, it should be noted that scale-up presents technical difficulties to solve which will require substantial investment in plant and equipment. It is possible that the current situation reflects industry's collective opinion that the returns are already sufficient, and that corporations are reluctant to engage in expensive efforts to overcome obstacles to mass-scale production. Previously there has not been much incentive for private enterprise firms to overcome such obstacles. It is possible that the commercial value of artificial AFPs will prove attractive enough to convince someone to tackle the problem of making them cheaply.

The potential of bacterial systems to product artificial AFPs on a large scale is limited, and suggest that other organisms (such as yeasts) might be more suitable hosts. Other mass-use materials are produced in this way for industrial purposes. In the interim, bacterial production can provide AFPs on a scale sufficient for testing of new forms, and for experimenting with the best means of application.

Chemical Agents to Control Alkali-Silica Reaction

IDEA 010 - Development of Chemical Agents for the Control of Alkali-Aggregate Reaction in Concrete

Investigators: Kumar Natesaiyer and Kenneth C. Hover, Cornell University, Ithaca, New York

IDEA Product

Aluminum sulfate (an aggregate pretreatment) and zinc sulfate (used as a traditional admixture), can control alkali-silica reactivity (ASR) damage in fresh concrete. Zinc sulfate is also a promising chemical agent for the control of alkali-silica damage in hardened concrete already suffering from ASR.

The chemicals used as aggregate pretreatments and admixtures would allow current restrictions on cement alkali contents and aggregate sources to be relaxed, resulting in an overall reduction of initial cost. The use of zinc sulfate or other zinc salts as a penetrant to control further damage in existing structures will provide a rehabilitation option which does not now exist.

Innovation

ASR occurs when silica substances in the aggregate react with alkalis in the cement to form a gel-like reaction product. The gel absorbs water and expands, cracking the concrete. This process, although slow, is presently irreversible and can cause structural failure. This project is testing chemical agents to reduce the solubility of silica in medium- and high-alkali solutions to slow down the generation of the gel reaction product.

Project Summary and Progress

Ten chemicals were tested to determine their effectiveness in reducing the dissolution of silica in 1N sodium hydroxide solutions in Stage I of this project. Two types of reactive aggregates were used in the project: Opal and Spratts. Opal is a highly reactive form of amorphous silica and is occasionally found in small amounts in aggregates used for concrete. Spratts aggregate is a slowly reactive natural aggregate which has caused

damage to concrete structures in Canada. Of the ten chemicals tested, three chemicals--aluminum sulfate, zinc sulfate, and pyrogallol--proved to be effective. Aluminum sulfate reduced the solubility of silica in 1N sodium hydroxide by more than 98%, zinc sulfate reduced the solubility of silica by about 75%, and pyrogallol reduced the solubility of silica by about 50% (Figure 16). The concentration of chemicals needed to reduce the dissolution of silica was found to be proportional to the reactivity of the aggregate. The highly reactive Opal, when compared with the slowly reactive Spratts, required a larger concentration of chemical to reduce its solubility in sodium hydroxide solutions.

The three chemicals selected (aluminum sulfate, zinc sulfate, and pyrogallol) were tested as admixtures in Stage I of the project to determine their effectiveness in reducing expansion of mortar bars made with reactive aggregates. Due to instability in high pH solutions, aluminum sulfate had to be used as an aggregate pretreatment rather than as an admixture.

The aluminum sulfate pretreatment and the zinc sulfate admixture seemed to reduce the net expansion of mortar bars made with Spratts aggregate. The pyrogallol admixture did not significantly alter the expansion of mortar bars made with Spratts aggregate. All bars, however, experienced a large shrinkage during the first week. The bars with admixtures had shrinkage strains greater than the bars without admixtures. There was no significant difference in the post-shrinkage expansion of bars made with and without chemical admixtures.

The gel fluorescence test for the amount of reaction product revealed no significant difference between bars containing Spratts aggregate made with and without admixtures.

The required concentration of all chemical agents was increased in experiments with Opal as the reactive aggregate. At the high concentrations required, pyrogallol and zinc sulfate admixtures dramatically altered the setting properties of mortar mixes (pyrogallol was a strong retarder, zinc sulfate was a strong accelerator). Therefore, all three chemicals were used as aggregate pretreatments for mortar mixes made with Opal replacements. Zinc sulfate pre-treatment at 240 mM concentrations and aluminum sulfate pretreatment decreased the expansions of mortar bars made with 3% Opal replacement, while pyrogallol pretreatments increased the expansion of mortar bars made with 3% Opal replacement (Figure 17). For mortar bars made with 1% Opal replacement, pyrogallol pretreatment increased the expansions while zinc sulfate and aluminum sulfate pretreatment did not decrease the expansions.

For bars made with 3% Opal replacements, there was no significant differences in the amount of reaction product with and without admixtures. However, for bars made with 1% Opal replacement, zinc sulfate and pyrogallol pretreatments markedly reduced the

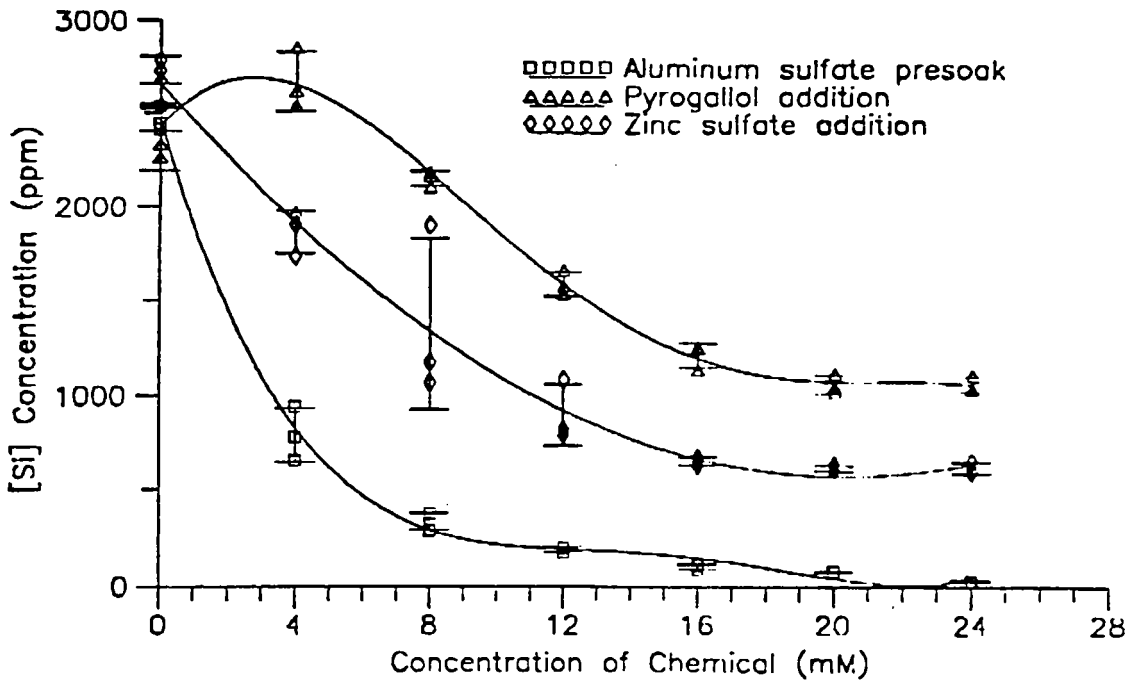

Figure 16. Effect of Chemicals on Solubility of Spratts Aggregate

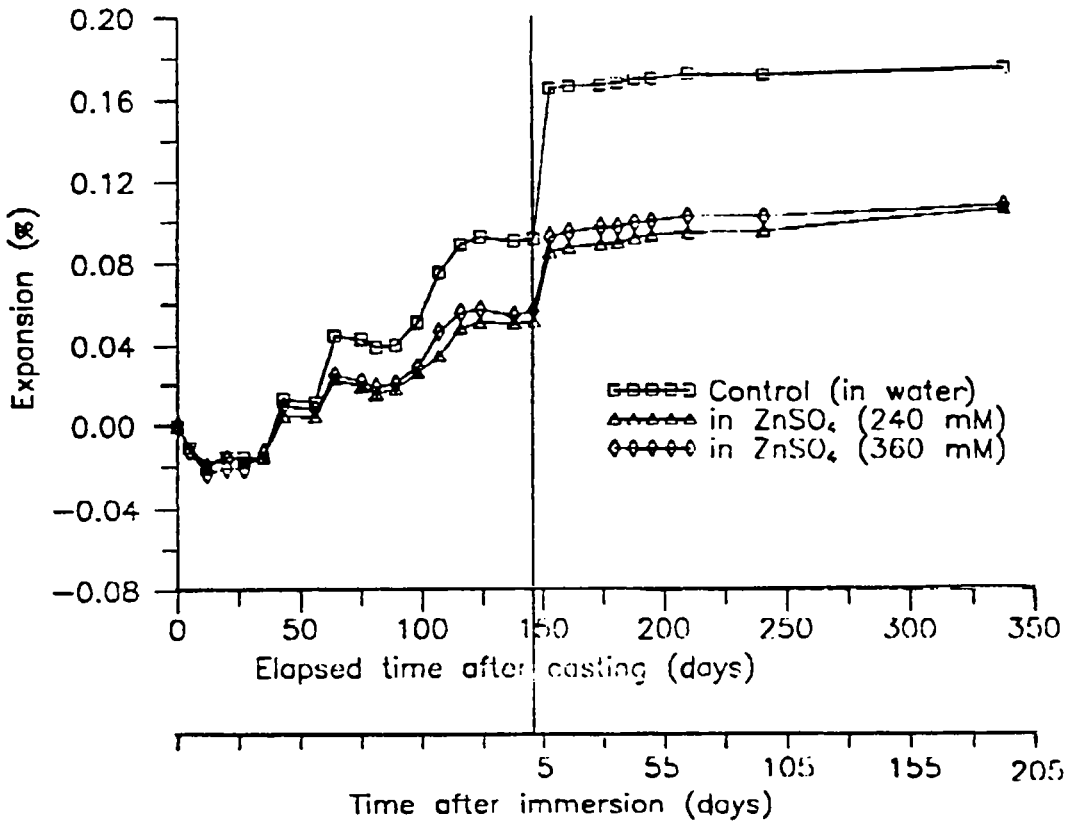

Figure 17. Expansion of Mortar Bars Made with 3% Opal Replacement: Stage III, Penetrant Tests

gel product as observed using the ultraviolet test. Ultimate expansions, however, were not similarly affected.

The admixtures did not cause any significant reduction of the compressive strength of mortar cubes made with either Spratts aggregate or with Opal replacements.

Zinc sulfate and pyrogallol were tested as penetrants to determine their effectiveness in reducing expansions due to ASR already in progress in hardened mortar. Initial tests with mortar cubes in pyrogallol solutions showed that the pyrogallol solutions coagulated and discolored the surface of the cubes. It was decided, therefore, that pyrogallol solutions would not be used for soaking mortar bars.

Immersion in zinc sulfate solutions did not have any significant effect on the subsequent expansions of mortar bars made with Spratts aggregate. All mortar bars made with Opal replacements expanded upon immersion, and the final expansions of bars made with 1% Opal replacement were not significantly different from the expansions of bars immersed in water. At 3% replacement, however, immersion in zinc sulfate solutions significantly reduced the subsequent expansions. While none of the bars immersed in zinc sulfate solutions cracked, all the bars immersed in water cracked,. Zinc sulfate immersion, thus, seemed to inhibit both expansion and cracking of bars made with 3% Opal replacement.

There were no significant differences in the amount of reaction product between bars immersed in water and bars immersed in chemical solutions. This conclusion held both mortar cubes made with Spratts aggregate and for mortar cubes made with Opal replacements.

In summary, zinc sulfate and aluminum sulfate have been tentatively identified as promising chemical agents for the control of alkali-silica reaction in fresh concrete. Since pyrogallol did not have any significant effect on the expansion of mortar bars made with Spratts aggregate and seemed to increase the expansions of mortar bars made with Opal replacements, it has not been recommended. Zinc sulfate is tentatively recommended for use as a penetrant to retard the progress of alkali-silica reaction in hardened concrete.

Technical Issues for Further Consideration

The efficacy of ten chemicals in retarding the dissolution of silica in a model high-alkali solution, namely 1N sodium hydroxide, was evaluated in Stage I of this project. The results obtained clearly show that pyrogallol, zinc sulfate, and aluminum sulfate

dramatically reduced the dissolution of silica in 1N sodium hydroxide. It was also found that Spratts aggregate (a naturally reactive aggregate from Ontario) required chemical concentrations of less than 24 mm, while highly reactive Opal required a much larger concentration (360 mm) of chemicals for similar reductions in solubility. This result suggests that to obtain similar reductions in silica dissolution in concrete, the concentration of chemical agents in the final pore solution in concrete must be similar to the concentrations proven effective with 1N sodium hydroxide.

While the initial chemical concentration represented by the admixture dosage in Stage II matched those determined in Stage I, the fraction of dissolved species which may have been incorporated into the products of hydration or otherwise reacted with the portland cement is not known. As a result, the final or effective concentration of the chemical agents at the aggregate surface is not known. One can only estimate that the final concentration of the chemical agents in the pore solution probably would have been lower than the initial concentration. Pore solution extraction techniques can determine the concentration of the chemicals in the pore solution or at the aggregate surface. Subsequent tests with the correct dosage should then provide conclusive evidence of the efficacy of the chemicals in preventing damage due to ASR in concrete.

An alternative approach to determine the effectiveness of the chemicals in cement-water systems would be to conduct a modified Quick chemical test with cement-water crushed aggregate systems and added alkalis. Since the mixture has to be filtered to determine the silica concentration in solution, a high water to cement ratio (2:3) should be used.

The significant reduction in the subsequent expansion of mortar bars made with 3% Opal replacements and immersed in zinc sulfate can be interpreted to mean that if the chemical concentration in the pore solution is similar to that used in Stage I, zinc sulfate may retard the expansions due to ASR. The delivery of the desired chemical agent to the reaction site may be the biggest practical problem in the use of penetrates to retard ASR.

Fiber-Optic Air-Void Meter

IDEA 011 - In Situ Determination of Entrained Air in Freshly Mixed Concrete Using Fiber Optics

Investigator: Farhad Ansari, New Jersey Institute of Technology, Newark, New Jersey

IDEA Product

A hand-held portable device was developed for rapid, in situ monitoring of the entrained air content in concrete during mixing, transporting, and placement. The device currently is undergoing field testing for potential application to practice.

The new fiber-optic apparatus monitors entrained air bubble content in freshly mixed concrete for quality control of concrete in the field.

Innovation

Air bubbles in fresh concrete are detected by changes in the intensity of reflected light transmission through a thin optical fiber. Intensity changes occur due to the differences in the index of refraction between an air bubble and concrete. A small laser diode provides the light source for transmission through the fiber optics, and a photodetector is employed for measurement of the reflected light intensity. An electronic amplifier is designed for conditioning the raw output of the photodetector. A signal processing algorithm is developed for conversion of light intensity data to air content (Figure 18).

The new device is rapid, accurate, and easy to use. Therefore, it can be continuously employed during construction for proper quality assurance. Accurate determination of air content in fresh concrete is especially important during construction of highways, where improper amounts of air may lead to miles of cracked pavement.

Project Summary and Progress

Accuracy, reliability, and speed of the new fiber optic air meter was examined through repeated experiments against conventional techniques.

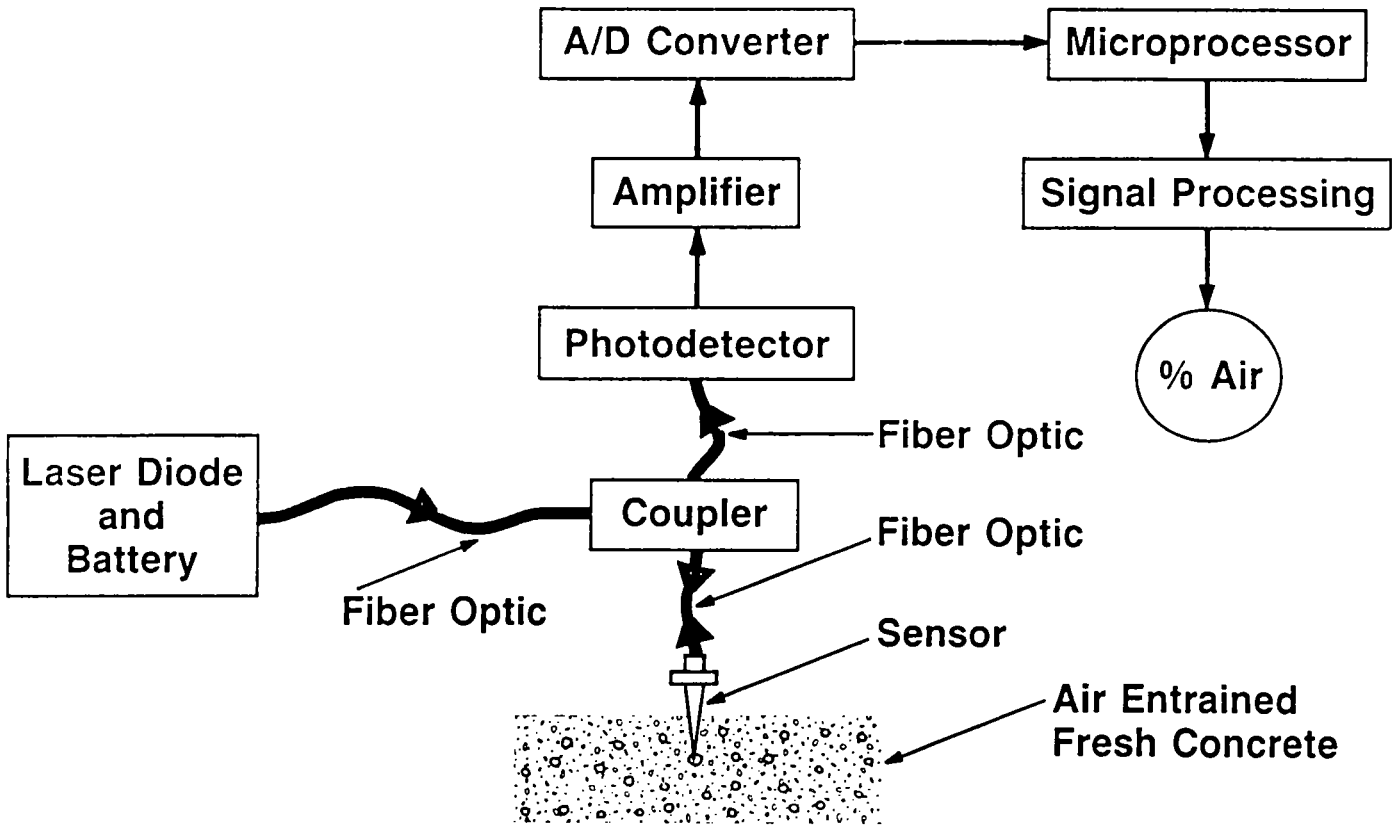

Figure 18. Components of the Fiber-Optic Air Meter

Throughout the entire period of the research, efforts were focused on designing the device so that the highway construction crew would be able to use it as a hand-held instrument during mixing and placing of the air-entrained concrete (Figure 19, 20). Accordingly, all the electric power requirements to the laser, electronics, and the photodetector in the air meter are delivered through rechargeable batteries.

When a light wave travels from one medium into another, the indices of refraction in the two mediums determines the ratio between the amount of refraction and reflection. If the light wave travels from a material with higher refractive index into a material with lower index, depending on the angle of incidence, most of the light reflects back. If the refractive indices are the same or almost the same, most of the light will enter the new medium. The simple concept of refraction and reflection when combined with fiber optics results in a powerful measurement instrument for air-entrained concrete. If the light exiting the end of a glass optical fiber (refractive index N=1.4) meets an air bubble (N=1.003), most of the light will reflect back due to a large difference between the indices in the two mediums. Immersion of the same fiber tip in fresh concrete, however, brings about a large decrease in the intensity of the reflected light, owing to the refraction of light into the concrete. In concrete, the glass/air interface at which total internal reflection occurs is eliminated and index of the glass is nearly matched by the concrete (N=1.25). When this happens, the light will no longer totally reflect and most of the optical power is transmitted from the fiber end into the concrete.

Various optical and electronic components of the fiber optic device were connected together in a compact manner so that the system could be employed as a hand-held device during concrete mixing and placement. A diode laser emitting visible light at a 670 nm wavelength is employed in transmitting optical signals. A silica glass multimode optical fiber delivers the light to a coupler. The coupler directs the signal to the exit end of the fiber. Depending on the amount and number of air bubbles in the fresh concrete, light will reflect back into the fiber. The coupler separates the reflected and transmitted signals, and directs the reflected signal to a photodetector. The reflected light intensity signal is changed to an electrical current in the photodetector and amplified through an amplifier. At this stage, the voltage output of the amplifier is converted to a digital signal via an analog-to-digital converter. Real-time data is then transferred to a laptop computer for data processing and air content determinations.

During the Phase II part of the project, two additional prototypes of the fiber-optic air meter were constructed. Most of the field trials were performed in cooperation with the New York, Pennsylvania, and Minnesota state department of transportation authorities. Earlier experiments in Pennsylvania and New York indicated that the sensor tip could be damaged easily by the stiff highway concrete mix. Several attempts were then made for designing a suitable protective head to repel the large aggregate particles that come

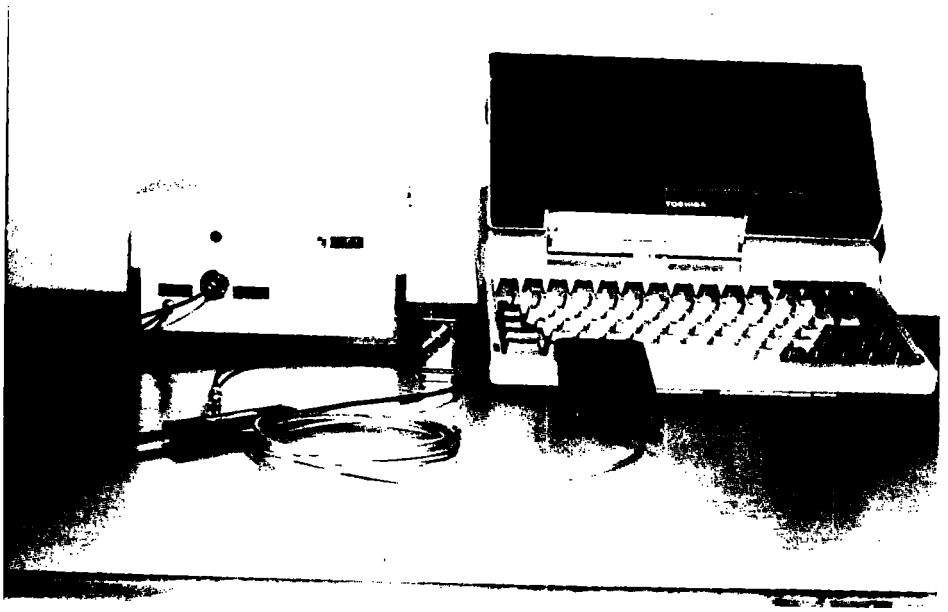

Figure 19. Fiber-Optic Air Meter with Laptop Computer

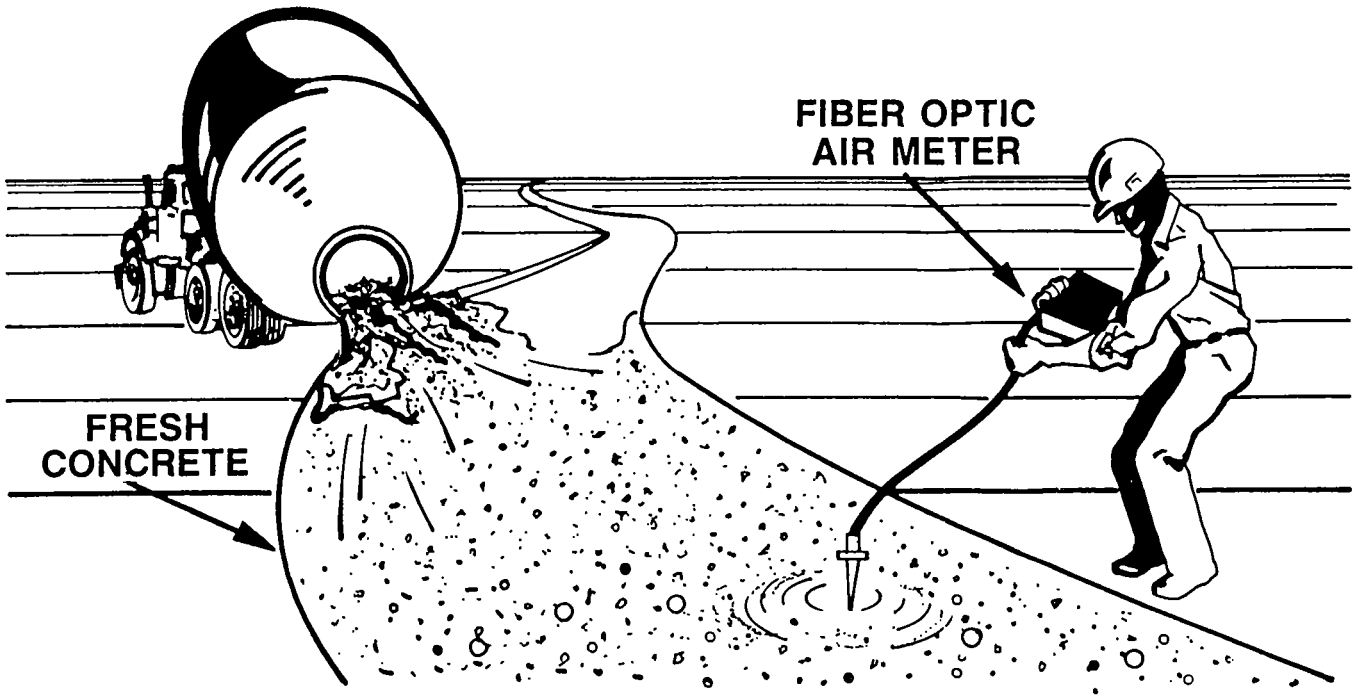

Figure 20. Fiber-Optic Air Meter in the Field

in contact with the sensor. The final design consists of a U-shaped aluminum head to repel the large aggregates that come in contact with the sensor. Laboratory trials were performed using the aggregate repelling head on highway concrete mixes. The new head yielded satisfactory results, and it was employed in all the subsequent experiments.

Technical Issues for Further Consideration

The following improvements to the current system could enhance the capabilities of the fiber optic air meter under field conditions:

1. Amplitude of the reflected light intensity output (measured in volts) is directly related to the air bubble size distribution (measured in micros). Air bubble size distribution is an important factor which is directly related to the durability of concrete. A quantitative understanding of the principles require more extensive investigations than carried out for the SHRP-IDEA project.

2. The fiber optic sensor tip loses its optical properties after few experiments. The tip of the fiber optic has to be treated with a special coating in order to create a shield for the tip while preserving the original refractive index of the fiber.

A SHRP-IDEA Phase II project is currently under way to assess the applicability of the device to field practice.

Low-Cost Carbon-Fiber Concrete

IDEA 012 - Carbon-Fiber-Reinforced Concrete for Bridge Decks

Investigator: D.D.L. Chung, State University of New York, Buffalo, New York

IDEA Product

Carbon-fiber-reinforced concrete with high flexural strength and toughness is under development. This concrete contains short carbon fibers in the amount of 0.5 or 1.0 percent by weight of cement, and appropriate chemical additives. This concrete may improve the durability and service life of highway pavements and bridges.

Innovation

Carbon-fiber-reinforced concretes show significantly higher tensile strength than ordinary plain concretes. However, the amount of carbon fibers currently needed to double the tensile strength makes the concrete almost four times as expensive. Additives enable the carbon fibers to be more effective as a reinforcement in concrete. A low carbon-fiber mix would improve the cost-effectiveness of carbon-fiber-reinforced concrete technology for highways.

Project Summary and Progress

Concrete is strong under compression and weak under tension or flexure. This problem may be alleviated by the addition of short carbon fibers (typically ~10 μm in diameter). Japanese research on carbon-fiber-reinforced concrete showed that using 2 vol.% 1 carbon fibers approximately doubled the flexural strength. Short carbon fibers in the amount of 0.5% by weight of cement were found to be effective in increasing the flexural strength of concrete by 85% and increasing the flexural toughness by 1600% at 28 days of curing, provided that a dispersant, microsilica and other chemical agents are also used. The project results show approximate doubling of flexural strength with only 0.3 vol.% carbon fibers--an improvement resulting from the use of chemical agents.

All previous work on short-carbon-fiber reinforced concrete used isotropic pitch-based carbon fibers, which are the least expensive form of commercially available carbon fibers. Their tensile strength and modulus are much lower than those of continuous

pitch-based carbon fibers that are used for aircraft. The price of short pitch-based carbon fibers has been steadily decreasing. In the U.S., the price was $12/lb in 1985, $9/lb in 1990, and is expected to drop to below $5/lb. This price decrease is giving much impetus to the use of carbon fibers in concrete. Nevertheless, it is desirable for economic reasons to keep the amount of carbon fibers in concrete to a minimum. Therefore, this project is focused on concrete containing carbon fibers in amounts approximating 0.2 vol.%.

Almost all of the previous work in both Japan and the U.S. on carbon-fiber-reinforced concrete used only fine aggregate (mortar material rather than concrete). Japanese researchers have used both fine and coarse aggregates, but the weight ratio of fine aggregate to coarse aggregate used was 1.3:1--a proportion that is not common for concrete. Concrete used in practice has a larger weight proportion of coarse aggregate than fine aggregate. Therefore, an objective of this project is to extend the technology of carbon-fiber-reinforced concrete to concrete of common mix proportions, (i.e., concrete containing more coarse aggregate). Since the effectiveness of the carbon fibers in improving the flexural strength of concrete may decrease as the aggregate size increases, this area deserves further investigation. The project results show that the aggregate size effect is quite minor, so that the technology of carbon-fiber-reinforced concrete is indeed viable for concrete with coarse aggregates, such as concrete that is typically used for highway pavements.

The technique of dispersing carbon fibers randomly in the concrete mix is critical to the success of the carbon-fiber-reinforced concrete technology. Two options are possible. One is to mix the fibers with cement and fine aggregate in the dry state (referred to as "dry mix"). The other option is to first disperse the fibers in water and then pour the dispersion into the slurry with cement and fine aggregate (referred to as "wet mix"). The second option is much more practical. The project results also show that wet mix is an effective method only if a dispersant and a defoamer are used.

Technical Issues for Further Consideration

The project results show promise for significantly reducing the cost and enhancing the practical use of carbon-fiber-reinforced concrete technology. The following additional investigations may be required for effective use of this technology:

1. Development of carbon-fiber-reinforced concrete with air entrainment.

2. Development of carbon-fiber-reinforced concrete of different water/cement ratios.

3. Measurement of the drying shrinkage.

4. Measurement of the freeze-thaw durability and compressive strength.

Based on these investigations, large-scale laboratory tests and field trial testing are necessary for examining the efficacy of carbon-fiber-concrete technology for pavement use.

Fiber-Optic Weigh-In-Motion Sensor

IDEA 013 - A Low-Cost Fiber-Optic Weigh-In-Motion Sensor Application

Investigators: A. Safaai-Jazi and S.A. Ardekani, Virginia Polytechnic Institute and State University, Blacksburg, Virginia

IDEA Product

A prototype of a fiber-optic weigh-in-motion (WIM) sensor was designed and the performance was tested in the laboratory. The sensor system gives more reliable responses to varying pavement loading conditions than the piezoelectric WIM system.

Innovation

The fiber-optic sensor mechanism operates in an extrusic mode where the modulation of light takes place outside the fiber. The pressure generated by the weight of a vehicle passing over a fluid-filled pneumatic tube is converted to displacement by means of a diaphragm. The deflection of the diaphragm modulates the light (Figure 21). In the absence of any external disturbance, the properties of light remain unchanged. If an external disturbance such as pressure, stress, strain, temperature, or an electric field perturbs the transmission medium in some way, one or more properties of the light will change. The amount of change is a measure of the external disturbance.

Pressure can perturb the transmission medium in many different ways. If the transmission medium in contact with the pressure region is an optical fiber, perturbations would commonly include bends, microbends, refractive index change, induced anisotropy, and dimensional changes, all of which affect the transmission properties of the light propagating in the fiber.

Project Summary and Progress

The feasibility of a fiber-optic WIM sensor was tested. The project work involved the development of a prototype optical pressure sensor and performed laboratory tests with a Material Test Systems (MTS) machine to study the sensor response under different loads at different frequencies, analysis and test of significance of data, and comparison with the piezoelectric sensor.

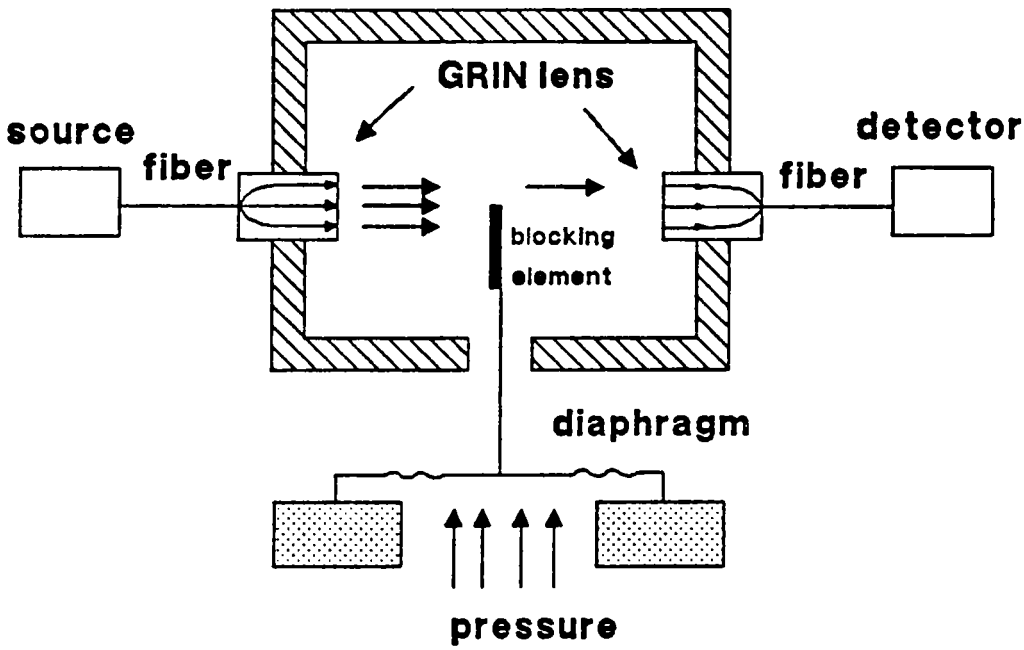

Figure 21. Schematic Diagram of a Transmission-Based Pressure Sensor

Design and Manufacturing of the Sensor

The essential elements of the proposed fiber-optic WIM sensor are a pneumatic tube filled with an incompressible fluid, a diaphragm to convert pressure into displacement, and an optical displacement sensor (Figure 22).

The tube is an expandable hose with an inner diameter of 0.25 inches. It is housed in a rubber pad which serves as a mechanical support. The tube is connected at both ends to flexible but nonexpandable stainless steel hoses and is filled with an incompressible fluid.

The diaphragm is made of stainless steel and is placed between the optical displacement sensor and the flexible steel hose at one end of the pneumatic tube. The applied pressure causes the diaphragm to deflect. One side of the diaphragm is attached to a light-blocking element which serves as a spatial light modulator. Pressure changes experienced by the pneumatic tube are converted into variations in light intensity.

Two fiber-optic displacement sensors based on intensity modulation of light were designed and evaluated. Both sensors were studied in the laboratory using a micropositioner to simulate the deflection of the diaphragm. The use of gratings to increase the sensitivity was also investigated.

The rubber pad is used primarily for mechanical support and to evenly transmit the applied pressure to the encased expandable tube. The material composition of the pad is resin, softening agent, and curing agent. The hardness of the pad plays an important role in transmitting the pressure from a vehicle to the expandable tube, thus affecting the magnitude of the sensor output signal and requiring calibration.

Two steel hoses, one 6 ft long and another 1 ft long, were used. The function of the longer steel hose is to transmit the pressure with minimal loss from the load region to the diaphragm. The short steel hose is to facilitate the removal of trapped air bubbles. Two air-bleed valves, one at each end of the sensor assembly, are used to remove trapped air in the fluid-filled part of the system.

Laboratory Tests and Performance Evaluation of the Sensor

The sensor was fabricated and tested using a 20-Kip MTS machine to stimulate different vehicle weights and speeds. The rubber pad was mounted onto the stationary upper plate of the MTS machine. Load was applied from below through a metallic support plate. Ten levels of loads, from 1 Kip to 5.5 Kips in 0.5 Kip increments, were applied.

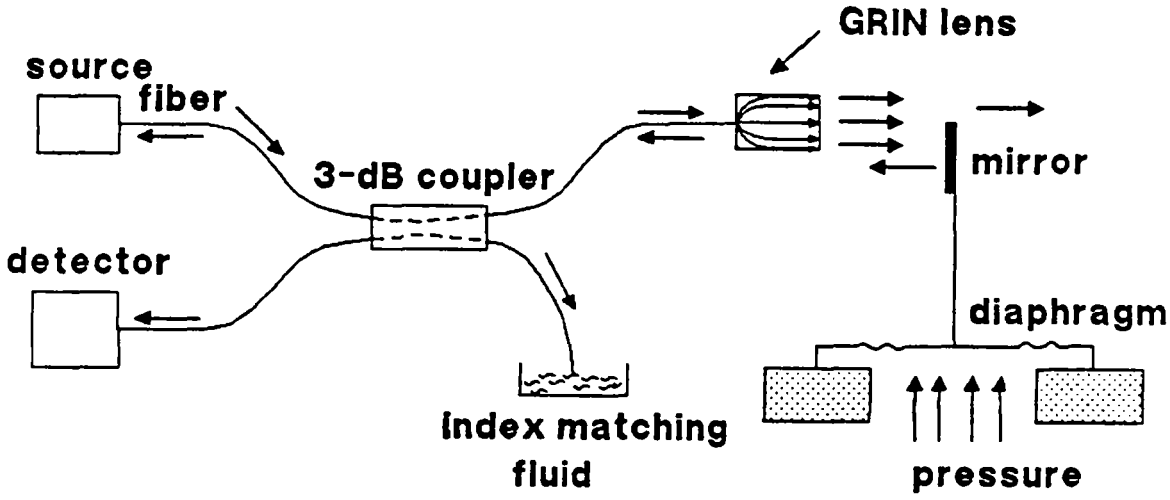

Figure 22. Schematic Diagram of a Reflection-Based Pressure Sensor

Each load was applied at frequencies of 0.25, 0.5, 1.0, 2.0, 5.0 and 10.0 Hz. Several cycles of a square wave were applied for each load-frequency combination. The input and output waveforms were monitored simultaneously using a dual channel oscilloscope and photographed following each load application. Examination of the output waveforms revealed an interesting feature: for square wave input waveforms, the output waveforms were also square. This property of the optical sensor is a major advantage over the piezoelectric sensor and will be very useful in processing the output signal and correlating it to the weight of the vehicle.

The measured output signal voltages suggest that in the frequency range 0.25 Hz through 10.0 Hz, the sensor response is largely frequency independent. To assess the behavior of the sensor response quantitatively, the output voltage versus the applied load was plotted for six different frequencies. Furthermore, statistical tests were performed on the data to determine the level of significance (p-values) and the coefficient of determination (R^2) as measures of frequency independence and linearity of the sensor response, respectively. The independence of the sensor output signal from frequency implies accurate measurement of weights at different vehicle speeds.

An important attribute of the sensor response is the correlation between the applied load and the output signal voltage. The best fit regression line through the data points was obtained. The coefficient of determination, R^2, is 99.5%, indicating a practically linear relation between the applied load and the output signal.

Similar laboratory tests and data analyses were performed on a piezoelectric sensor for the purpose of comparison with the proposed optical sensor.

Significance of Results and Comparison with Piezoelectric Cable

Shape, linearity, and variations with frequency of the output signal have a direct bearing on the accuracy of a WIM sensor. In terms of the shape of the output signal, the piezoelectric cable generated exponentially decaying output waveforms for square wave inputs. The optical sensor, on the other hand, produces square wave outputs for square wave inputs. In other words, the optical sensor was reporting a constant voltage reading as long as the MTS loading cell was in contact with the sensor. On the contrary, the piezoelectric sensor output signal peaks to a maximum value upon the application of the load and decreases exponentially with time. In processing the WIM sensor output signals, the area underneath the output signal is an important factor in determining the axle weights. Therefore, the square wave output signals of the fiber optic sensor offer a major advantage over the exponentially decaying output signals of the piezoelectric cable.

Another advantage of the fiber optic sensor is in output signal variations with load frequency. Comparison of output waveforms as well as the output voltage-load curves for the optical and piezoelectric sensors indicate that the signal outputs vary considerably less with load frequency in the case of the fiber-optic sensor. Ideally, the response of a WIM sensor should be entirely frequency independent. The stronger frequency dependence of the piezoelectric output signal in both the shape of the waveform and the peak voltage implies that the speed and axle spacing of vehicles could be a serious source of error in piezoelectric WIM sensors but not in the proposed fiber-optic WIM sensors. The linearity of the output voltage with load for both optical and piezoelectric sensors is satisfactory.

In short, both the output waveform and the lack of strong frequency dependence in the fiber-optic sensor output signals greatly contribute to higher accuracies. In addition, the fiber-optic signal can be made immune to electromagnetic interference. Unlike the piezoelectric case, the electronic components in the optical sensor are not in direct contact with the wheel. Finally, the optical sensors can be made temperature insensitive. The bending characteristics of the piezoelectric sensors, however, have been shown to change at high temperatures experienced in the roadway environment.

The electronic components of the optical sensor are cheaper and readily available since they are mass-produced for a variety of other applications in the fiber-topics and communications fields. The electronic and optical components of the sensor, which comprise a major fraction of the total sensor cost (over 60 percent), cost under $600 per sensor unit at the time of writing this report. Furthermore, the electronic and optical components are installed on the side of the road or even housed in a remote location and would never be in contact with the traffic, thus lasting longer. The abovementioned attributes contribute to a lower life cycle cost of the optical sensor as compared with other conventional WIM sensors in use today.

Technical Issues for Further Consideration

The operational feasibility of the fiber-optic WIM sensor needs to be tested in actual field conditions to compare its performance with other conventional WIM systems currently used.

Conducting Polymer Anode for Cathodic Protection

IDEA 014 - Feasibility Studies on Nondestructive Incorporation of a Conducting Polymer Anode Bed into Bridge Deck Concrete

Investigators: S. Hettiarachchi and M.F. Asaro, SRI International, Menlo Park, California

IDEA Product

This project is developing a technique for nondestructively incorporating a conducting polymer anode into bridge deck concrete for cathodic protection (CP).

The proof-of-concept of monomer incorporation by electrochemical injection was achieved, and its polymerization inside the concrete matrix to form a conducting polymer was accomplished. During proof-of-concept, it was shown that the applied voltage necessary to polarize the rebar to a potential of -0.85 V was lower for the concrete block with the conducting polymer, confirming the presence of conducting polymer inside the concrete matrix.

Innovation

Conventional cathodic protection of a bridge deck requires laying a conducting anode on the deck surface, covering it with an overlay of concrete, and polarizing the reinforcement steel to a cathodic protection potential. The technology tested involves an innovative approach of forming a conducting polymer in situ inside the concrete and using it as the impressed current anode for cathodic protection of the rebar steel. This is an attractive alternative to the conventional CP technology system.

If the conducting polymer incorporation into concrete can be performed effectively, it would greatly simplify the currently practiced cathodic protection technology. For example, the anode can be incorporated by an in situ technique, and would not require a concrete overlay that is necessary when metal mesh anodes are used.

Project Summary and Progress

The project has proved that incorporating conducting polymers into concrete by both chemical and electrochemical approaches is feasible. The conducting polymer formed was approximately 8000 Å to 1 μm thick as determined by scanning electron microscopy (SEM), and hence is not visible to the naked eye. A pulse polymerization technique was devised to allow sufficient time for monomer diffusion to occur between electrooxidation pulses. The applied voltage required for polarizing the rebar potential to -0.85 V was 42 percent lower for the block containing conducting polymer.

The project's approach to study the feasibility of the nondestructive incorporation of a conducting polymer anode bed into bridge deck concrete involved the in situ incorporation of an extended conducting polymer anode network inside the concrete. In this study, both electrically charged and uncharged monomers were used as precursors for the conducting polymer. If completely successful, the anticipated advantages of this technique are that it is less costly to implement, can be used for protection of substructures and columns, can provide uniform anode distribution, and can be improved to remain stable under heavy traffic loads because the anode is embedded in concrete.

Chemical polymerization was also performed in a few experiments to prove that polymerization of the monomer within the concrete matrix is feasible. SEM examination of fractured concrete, as shown in Figure 23, showed the presence and the morphology of the conducting polymer formed inside. Both chemical and electrochemical polymerization formed the polymer inside the concrete. However, the polymer formed within the matrix was approximately 8000 Å to 1 μm thick as determined by SEM.

Monomer mapping experiments were performed to determine the rate of movement of the monomer into concrete. The results of these experiments, illustrated in Figure 24, showed that the rate of monomer ingress into concrete varied from 0.024 in/min at a depth of 0.2 in to 0.008 in/min at a depth of 0.6 in. This decrease in rate is due to the gradual lowering of monomer concentration at greater depths.

The concept was tested by determining the externally applied voltage (between the rebar and the platinum wire in contact with polypyrrole) needed for polarizing the rebar potential to -0.85 V with respect to the $Cu/CuSO_4$ reference electrode. The applied voltage needed to achieve this polarization was 42 percent lower for the block containing polypyrrole. The conductivity measured across two platinum wires embedded in the concrete containing the conducting polymer was higher ($3.7 \times 10^{-3} \Omega^{-1} cm^{-1}$) than that for the block without the polymer ($5.3 \times 10^{-4} \Omega^{-1} cm^{-1}$).

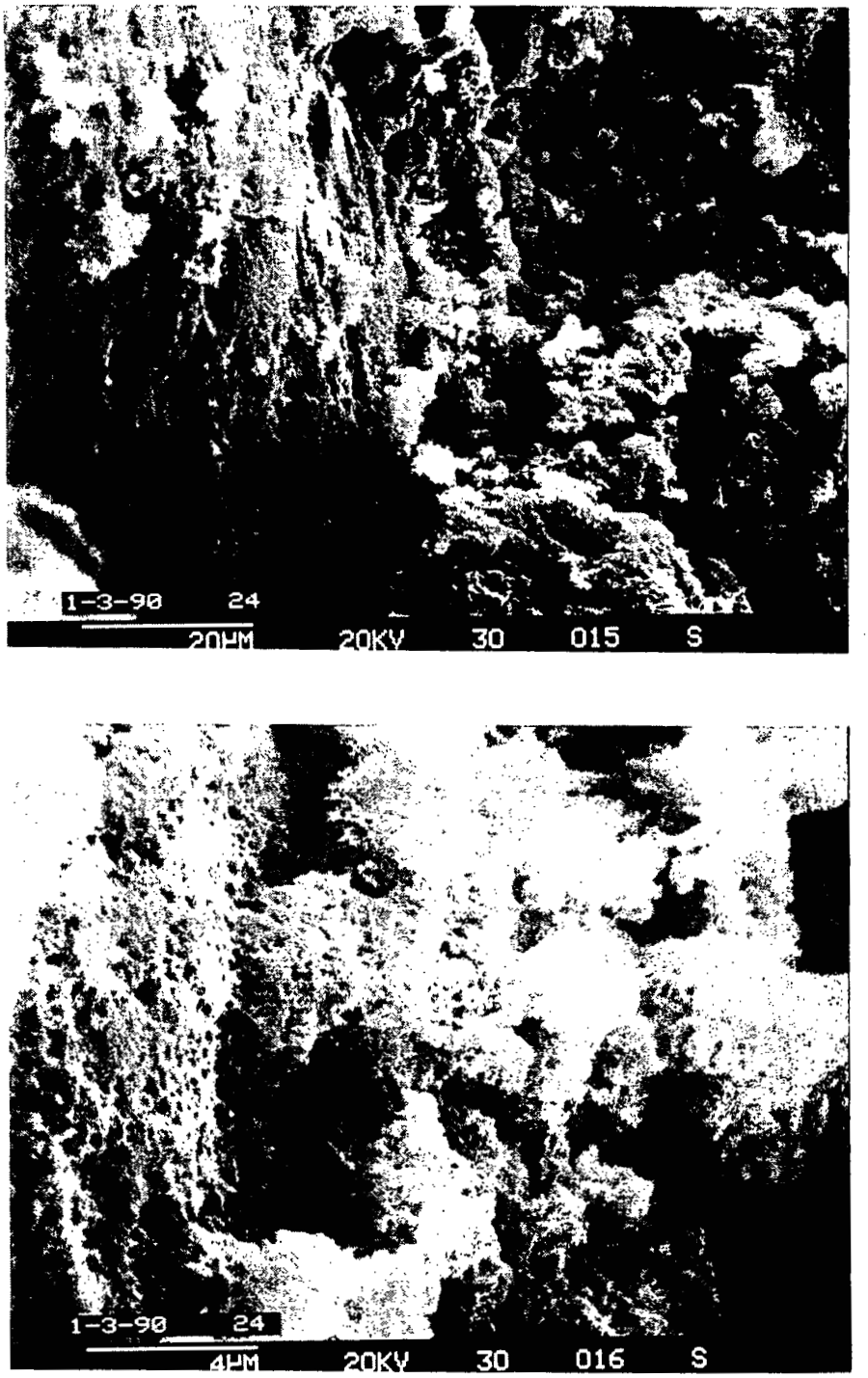

Figure 23. Polypyrrole in a Concrete Specimen

Morphology of the fractured surface of a concrete specimen in which polypyrrole is formed electrochemically inside the cured concrete matrix.

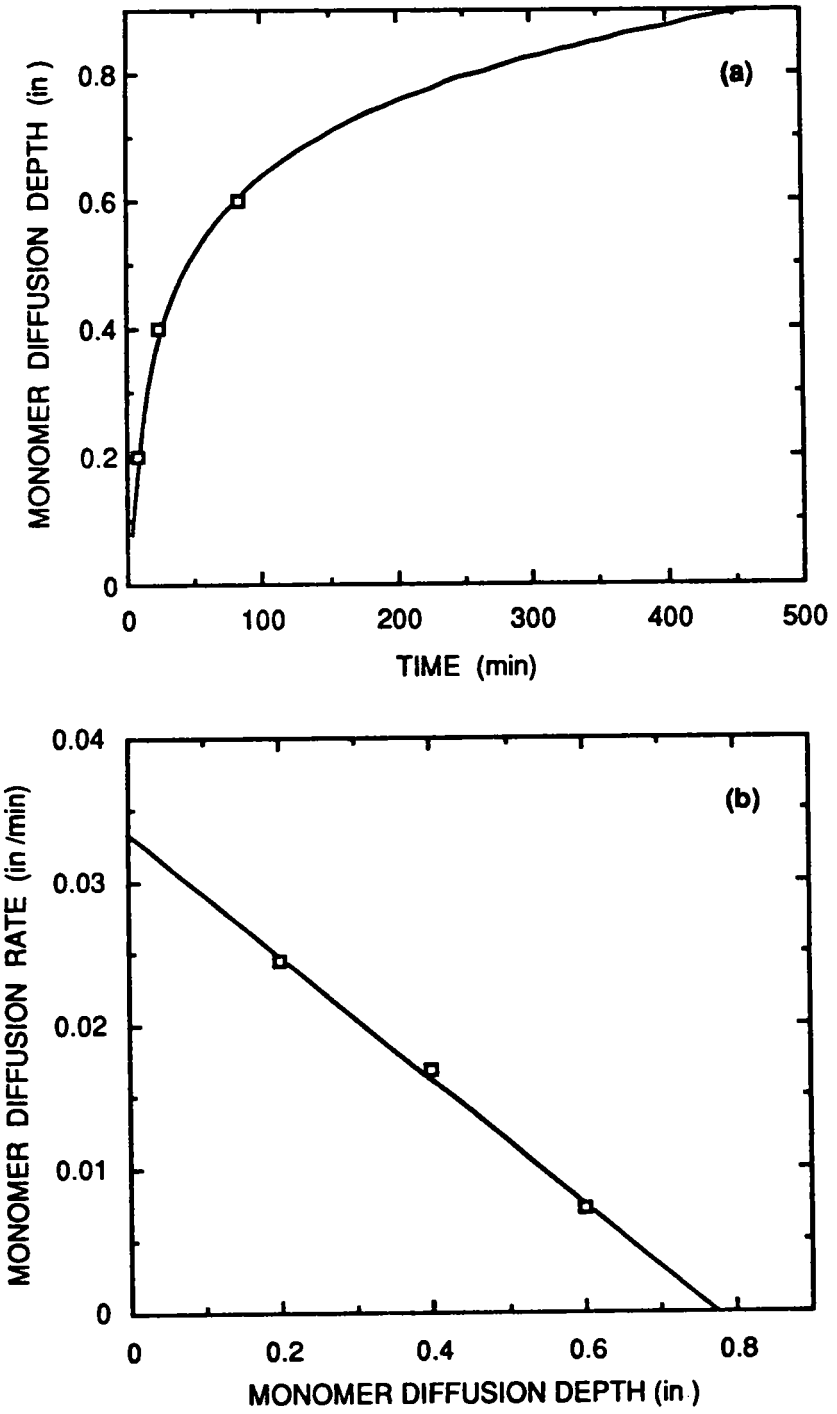

Figure 24. Diffusion of Monomer through Concrete

Technical Issues for Further Consideration

The research conducted so far indicates that conducting polymers can be formed inside concrete matrices. The conductive nature of the polymers can be exploited to use them as in situ anodes for cathodic protection of rebars imbedded in concrete. However, it is imperative that the conductivities be increased by at least three orders of magnitude before this technology is employed in the field. The conductivities can be increased by numerous approaches such as employing better-conducting polymers and using improved methods for incorporating the conducting polymer in the concrete matrix, so that interlinking of the conducting polymer is enhanced.

The biggest drawback to this concept is the instant polymerization of the monomer on platinum lead electrodes, which causes a depletion of the monomer in its immediate vicinity. Thus, sufficient time must be allowed for the monomer to diffuse into the depleted zone. In our most recent studies, we devised a pulse electropolymerization approach that allows sufficient time for monomer diffusion to occur between oxidation pulses. Pulse polymerization provided the highest conductivity of $3.7 \times 10^{-1} \Omega^{-1} cm^{-1}$. Higher conductivities can be achieved by optimizing the conditions needed for pulse polymerization.

Load Measuring Mat

IDEA 015 - Load Measuring Mat for Dynamic Wheel Loads

Investigators: David Cebon and Christopher B. Winkler; University of Cambridge, Cambridge, United Kingdom, and University of Michigan Transportation Institute, Ann Arbor, Michigan

IDEA Product

The narrow capacitative strip transducer (known as a WIMstrip) is relatively inexpensive, reliable and potentially more accurate than other existing low-cost WIM sensors.

The load measuring mat used in this project is a thin polymer carpet 1.2 m (4 ft) wide, 38.4 m (128 ft) long, and 13 mm (0.5 in) thick that contains a capacitative strip transducer every 0.4 m (16 in) along the wheel path. The mat is attached to a road surface and it measures the wheel forces of heavy vehicles that are driven over it.

Innovation

A WIM sensor measures the instantaneous dynamic force generated by an axle. This force can be considerably different from the static axle load which would be measured on a conventional static weighbridge (typically ±20 to ±50 percent). Thus, the accuracy of a single-sensor WIM system is limited fundamentally by the dynamics of the vehicles being measured. WIM sensors developed in the IDEA project provide the possibility of using two or more sensors along the road in order to compensate for the effects of dynamic forces in the determination of static loads.

The load measuring mat utilized WIMstrip wheel force sensors with an approximate cross section 9 mm x 30 mm (0.35 x 1.2 in) and 1.2 m (4 ft) long. The sensors were encapsulated in stiff polyurethane tiles 1.2 m x 1.2 m x 13 mm (4 ft x 4 ft x 0.5 in) in dimension, with three sensors per tile, laid transverse to the wheel path at a spacing of 400 mm (16 in) between strips. Thirty-two tiles, containing a total of 96 sensors were obtained for the project. These were mounted end-to-end on the test track, to provide an instrumented test section 38.4 m (128 ft) long. Note that a load measuring mat of practically any length can be constructed simply by adding more tiles and data loggers.

Project Summary and Progress

A schematic cross section of a capacitative strip sensor is shown in Figure 25. Tire contact pressure applied to the top surface of the strip causes the top "plate" of the aluminum extrusion to deflect, reducing the air gap between the top plate and the inner conductor is reduced. This results in an increase in the capacitance of the device, which, with appropriate processing, can be related directly to the contact pressure change. In order to determine the instantaneous wheel load it is necessary to integrate the transducer output with respect to time for the duration of the tire contact.

Figure 26 shows a view of the load-measuring mat system during testing. The mat installation utilized six Golden River "Marksman 600" data loggers. Each sensor was attached to a data logger by a 5-m-long, three-core cable. Each data logger processed the outputs of 16 sensors, performed the integration described above, and stored the results. The data loggers were connected into a network in a daisy-chain configuration by RS232 serial data cables. An IBM PC/AT micro computer was connected to the network and used to download the raw axle load information from the data loggers after each vehicle test run.

A theory was developed for the design of evenly spaced, multiple-sensor WIM arrays. The theory yielded a simple design formula, by which the optimum sensor spacing can be calculated, providing the average traffic speed is known. The theory was found to agree quite closely with the experimental results. Both theory and experiment indicated that a very good WIM array design is to use three sensors, evenly spaced along the wheel path. Such a system is accurate for a wide range of vehicle types and speeds. The root mean square (RMS) static load estimation error of a three-sensor system is likely to be only 30-50 percent of the RMS error of a single-sensor WIM system. In the near future, it should be possible to measure routinely the static axle loads of vehicles travelling at highway speeds with RMS errors of approximately 5-8 percent. This is a considerable improvement over the 12-20 percent for existing single-sensor WIM systems.

A prototype mat 10 m long was installed on the test track of the Transport and Road Research Laboratory during 1988. The 96-sensor mat installation for the SHRP/IDEA project was the first use of the load measuring mat technology for a major research project.

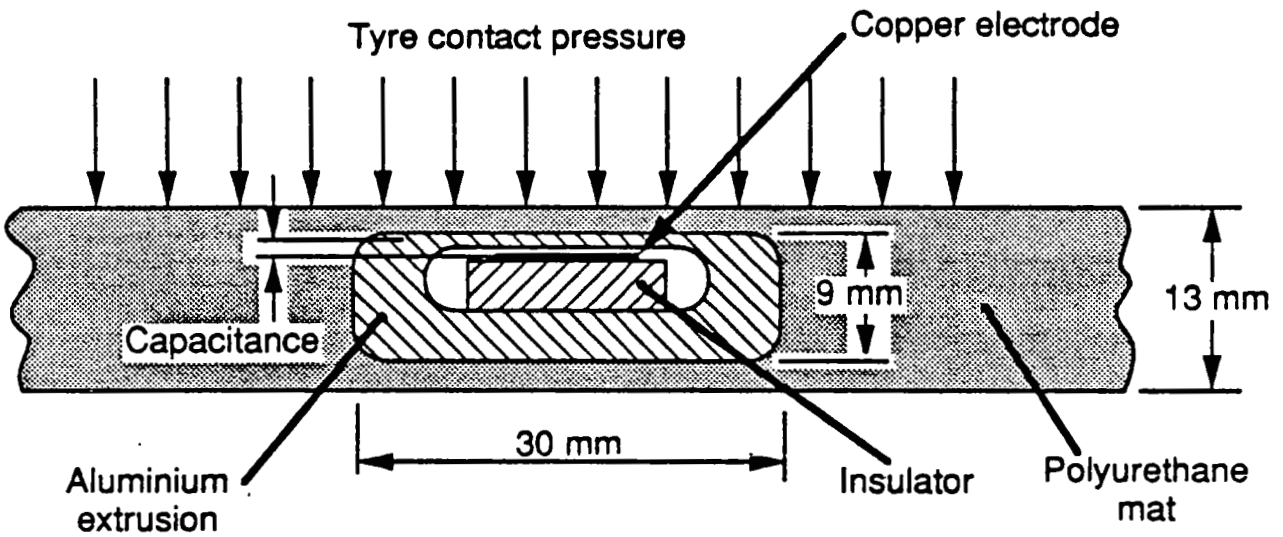

Figure 25. Schematic Cross Section of a Capacitative Strip Wheel Force Sensor Incapsulated in a Polyurethane Tile

Figure 26. Photograph of WIMstrip Prototype

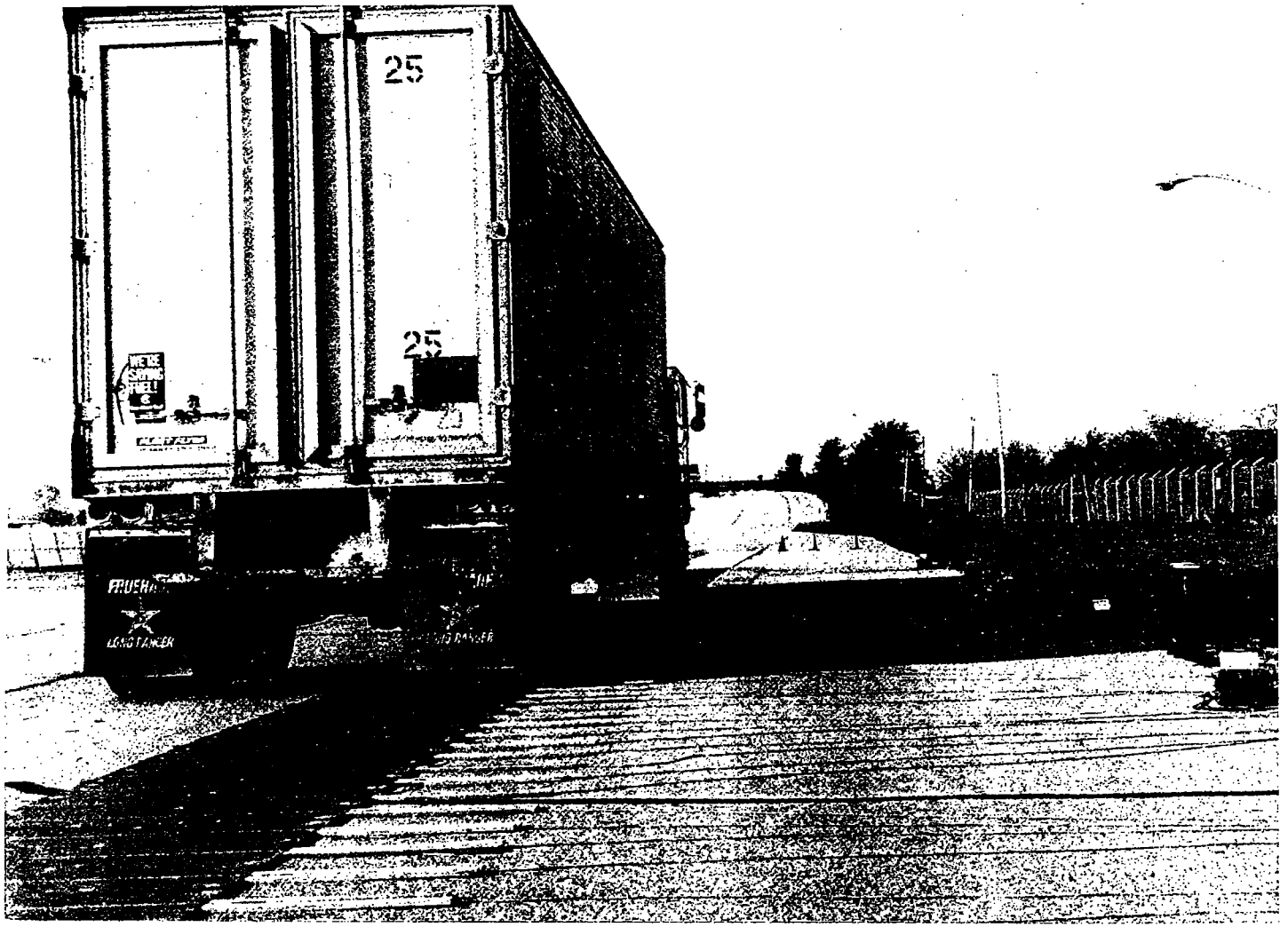

The project accomplishments are the following:

- Tested the performance and accuracy of the load measuring mat for measuring the dynamic wheel loads generated by heavy commercial vehicles and to assess the suitability and accuracy of the WIMstrip transducers for weigh-in-motion.

- Developed a workable design of multiple-sensor weigh-in-motion systems for determining loads at actual highway speeds.

The results show that a good design for multiple-sensor WIM systems is to use three sensors, spaced evenly along the road. The sensors should be spaced according to a simple formula which depends only on the average traffic speed. The expected static axle load estimation errors for such a system are likely to be 30 to 50 percent of the errors of a single-sensor WIM system.

This is a collaborative project, funded jointly by six organizations: SHRP, Golden River (UK) Ltd., Michigan DOT, University of Michigan, Navistar Technical Center and Cambridge University, United Kingdom.

The WIM system developed under this project is currently marketed by Golden River (UK) Ltd. in Europe and in the United States.

Smart Structure Technology

IDEA 016 - Smart Structure Technology for Nondestructive Evaluation of Concrete and Asphalt

Investigator: Robert E. Shannon, Westinghouse Electric Corporation, Pittsburgh, Pennsylvania

IDEA Product

This project is designed to establish, demonstrate, and qualify the Westinghouse patented tagging technology as a nondestructive inspection concept for the quality control and long-term assessment of the condition of highways. Tiny sensor particles in the material can be used by an eddy current tester to passively measure critical mixture proportions, such as:

- water-to-cement ratio in Portland cement concrete;
- bulk density of compacted asphalt;
- thickness of asphalt pavement layer.

Magneto-acoustic signatures obtained from activating the tagging particles can further be used to interrogate the material's mechanical properties.

Innovation

Tagging involves adding a small amount of tiny sensor particles directly to the material during manufacture. Specifically, ferrite particles distributed throughout a composite material can be subsequently sensed or activated using penetrating electromagnetic fields.

The tagging technique can provide an alternative to current nondestructive methods, such as nuclear gaging, pulse velocity, and others. The incorporation of "smart" sensors into concrete will eventually allow direct measurement of important material properties over the entire structure, obviating the need for destructive sampling.

Project Summary and Progress

The project developed and tested a new technology called "tagging for improved inspection," or simply "tagging", for nondestructive assessment of highway pavement. Phase I addressed three principal issues: (1) to establish tagging/sensor strategy; (2) to formulate tagged structural materials; and (3) to demonstrate potential applications for highway paving materials. Two interrelated methods of tagging under development at Westinghouse, called passive tagging and active tagging, provided the focus for the investigations.

In passive tagging applications, a small amount of tiny ferromagnetic particles is added to an otherwise nonmagnetic, nonconducting material and a simple electromagnetic device is used to measure variations in magnetic properties. Experiments show that eddy current testing provides a simple, economical technique for quantitative tagging measurements. As practical demonstrations, tagging was applied to two problems: (1) measuring the water-to-cement ratio in Portland cement concrete and (2) monitoring asphalt concrete compaction density.

In the first demonstration, tagged cement was prepared with varying amounts of water tagged with an aqueous colloidal suspension of ferrolignosulfonate, which has a number of unique properties that are advantageous to uniformly distributing tagging particles. It is a stable dispersion of ferrite with a particle size range of 50 to 200 angstroms, so there is virtually no settling. The results from measuring tagged fresh concrete, plotted in Figure 27, show a direct correlation between the eddy current reading and water-to-cement ratio. Subsequent measurements of the hardened cement during the curing period show the readings remain unchanged. A unique eddy current probe also has been designed to allow coil insertion into fresh concrete, giving an instantaneous measurement of the water-to-cement ratio in any size or shape container.

In the second demonstration, tagging was shown to provide a technique for measuring asphalt concrete compaction as illustrated in Figure 28. Asphalt cement was tagged with a uniform distribution of ferromagnetic particles. Upon compaction, changes in asphalt density cause a corresponding change in the tagging particle spacing, which, in turn, is easily measured by an eddy current instrument. Experiments have shown that the asphalt concrete may be formulated by tagging either the asphalt cement or one of the aggregate gradations before mixing.

Recent developments involving tagging combined with the utilization of electromagnetic field probe and an acoustic sensor have led to a potentially unique nondestructive approach to assessment of material integrity. In active tagging, the underlying principle involves the electromagnetic activation of the implanted ferromagnetic particles and the

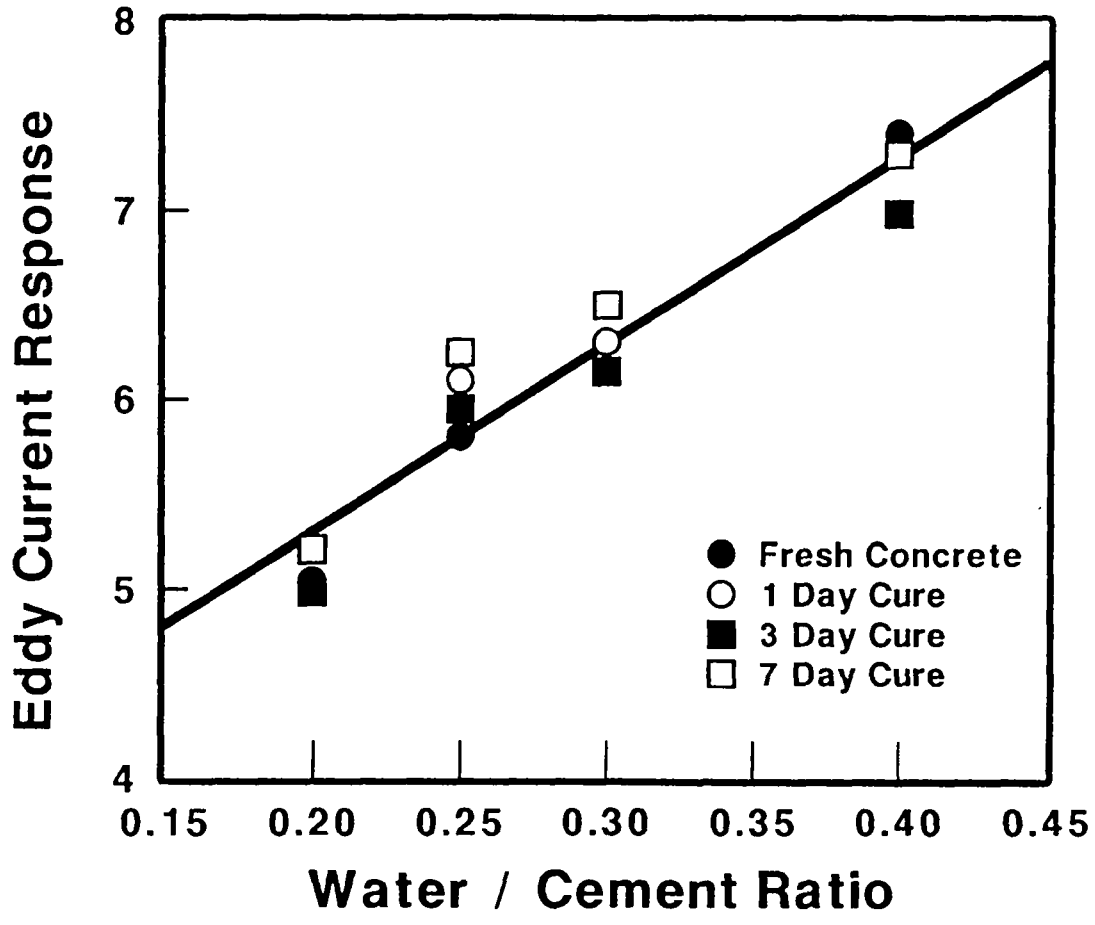

Figure 27. Eddy Current Assessment of Ferrite Tagged Cement

Measurements of Portland cement containing tagging material were made during the cure cycle. A direct correlation was shown between the eddy current reading and the water-to-cement ratio in this passive tagging demonstration.

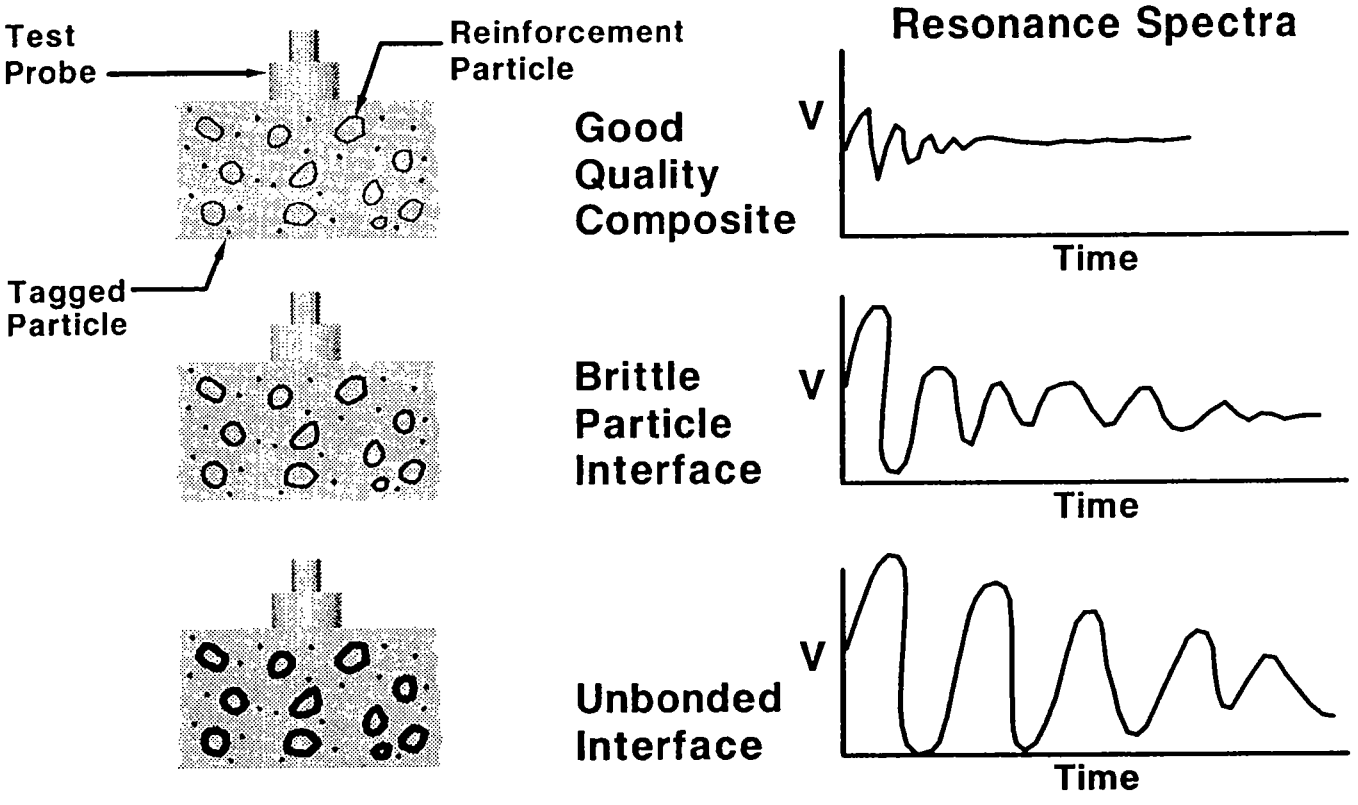

Figure 28. Schematic of the Active Tagging Concept

The volume of material beneath the probe can be tested or inspected by analyzing the vibration signature from different quality conditions.

subsequent analysis of the particle vibration signatures corresponding to variations in material conditions. Figure 29 presents a schematic illustration of this innovative test methods as it might be applied to the assessment of a composite material, such as concrete or asphalt. Note that variations in the matrix modulus alter the restriction of motion between the particles and matrix, resulting in a significant change in the vibration signature (resonance). An advantage of the tagged particle concept will be the ability to focus the test on the volume of material directly beneath the sensing probe. The tagged particle approach offers an assessment technique that is applicable to a wide range of material combinations and many inspection options.

Technical Issues for Further Consideration

Further development of the tagging concept as applied to asphalt concrete pavements will require a follow-up project (Phase II) addressing the following issues:

1. Demonstration of the manufacture of tagged asphalt on a pilot scale to evaluate tagged asphalt design and economic impact;

2. Development of a prototype sensor/instrument compatible with highway construction and maintenance equipment; and

3. Conducting field trials with a realistic test parameter matrix, including follow-up sample extraction for comparison.

Water-to-cement ratio measurement using tagging technology has been shown on a proof-of-principle basis. A feasibility study and prototype demonstration program is required to further develop the application details.

The tagging concept also can be developed to address the problem of measuring asphalt pavement thickness in applications where a tack coat, or some other substrate, is applied below the pavement layer. By tagging the underlying layer, it is a simple matter of monitoring the eddy current probe "liftoff" signal to measure the intervening pavement layer thickness.

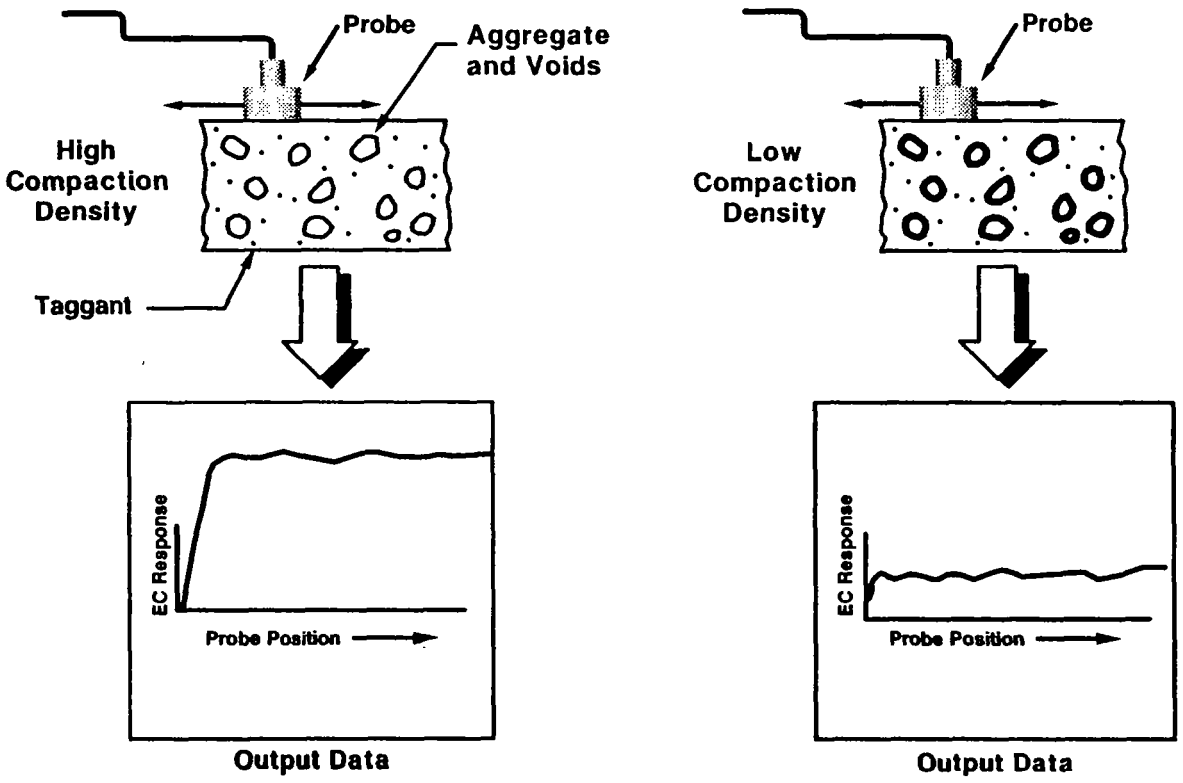

Figure 29. Eddy Current Measurement of Asphalt Concrete Compaction

Density measurements of tagged asphalt by an eddy current technique showed the effects of compaction.

Automated Crack Repair System

IDEA 017 - Automated Crack Sealing and Repair

Investigators: Chris Hendrickson and Sue McNeil, Carnegie Mellon University, Pittsburgh, Pennsylvania

IDEA Product

The product of this project is the design, construction, and feasibility assessment of automated crack sealing equipment for roadway maintenance. The primary benefits of such equipment are to reduce worker exposure to traffic hazards and to reduce labor costs.

Innovation

A combination of video imaging and electronic range scanning is used to identify, locate and map routed cracks of 2 cm (0.9 in) with an accuracy of better than 1 cm (0.5 in). A unique representation of the data in a two-and-a-half-dimensional quadtree facilitates the fusion of the data from two sensor sources, and simplifies the perception and modeling operations for crack routing and repair. Cracks are then traversed automatically for cleaning and sealing.

Project Summary and Progress

The benefits of a robotic crack sealing system include reduced labor costs and improved quality and safety. Assuming a four-year system life, system acquisition costs of $100,000, annual operating and maintenance cost of $25,000 per year, a 10 percent discount rate, productivity rates comparable to existing approaches, and the elimination of two laborers, the net savings realized using the automated crack filler may be as high as $60,000 per unit per year or 19 percent of costs on a national basis. This is equal to $24 million per year in national savings due to labor costs alone.

A prototype laboratory system was constructed and demonstrated as part of the project. Possible designs for field systems were investigated, and the economic feasibility of automation for this application was analyzed. A second phase of research will extend perception to unrouted cracks and undertake field trials.

The proposed field system for an automated crack filling system consists of a lead vehicle towing an x-y table or robot arm as shown in Figure 30. The lead vehicle would transport generators, computers, sensor processing hardware, and controllers. Mounted on the rear of the vehicle would be a video camera, used for identifying routed cracks. The x-y table is similar to a pen plotter moving within a rectangular frame mounted on a cart. Tools mounted on the x-y table would be: a depth sensor for verifying cracks; a hot air lance for cleaning cracks; and a sealant wand for filling cracks. Bulk supplies of sealant material and propane would trail behind the x-y table.

The laboratory prototype, shown in Figure 31, emulated the proposed system in a stationary environment and demonstrated the following steps:

1. The vision system identified potential cracks and generated a traversal plan for the depth sensor to collect range data.

2. The range data was fused with the video data into a unified map. Potential cracks identified by the vision system, but not corroborated by range data, were dismissed as filled cracks, shadows or oil spots.

3. The center lines for the corroborated cracks were identified and a trajectory minimizing the motion of the tools was generated. The cracks were traversed first with the hot air lance, cleaning the crack with compressed air. After the crack was prepared, the system again traversed the crack and filled the crack.

Sensing Pavement Cracks

A commercial VHS camera was used to generate the video signal required by the image processing board. An image processing board, commonly referred to as a frame grabber, was used to convert the analog video image signal to a digital matrix of numbers representing the gray scale. In the laboratory prototype, individual raster cells in the digital image were approximately 4 x 4 mm (0.2 x 0.2 in). An infrared laser range sensor was used to develop three-dimensional profiles of the roadway surface. The range sensor had a "footprint" of 15 mm (0.6 in) in the configuration used in the laboratory prototype and range readings were taken every 2 cm (0.9 in) across the pavement surface.

Other sensors were considered for the system, including sonar as an alternative for range sensing. However, sonar systems were susceptible to environmental noise from wind and

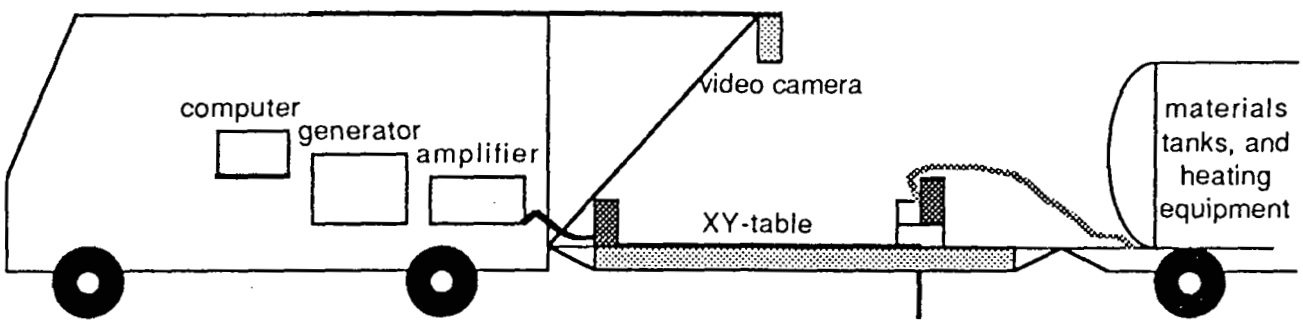

Figure 30. Illustration of a Possible Field System for Filling Cracks

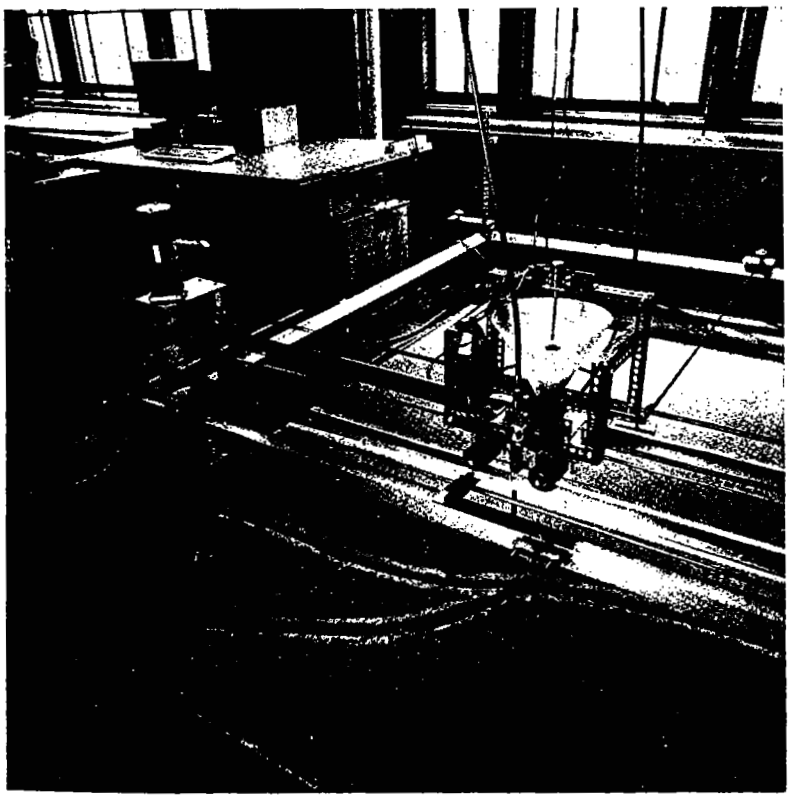

Figure 31. Photograph of the Laboratory Demonstration System

precipitation. The infrared laser range sensor, therefore, was selected for testing the laboratory system.

A dual sensor system was selected because exclusive use of video or range sensing was not adequate. Surface dark spots or lines could be easily mistaken for cracks in the video image. Range sensing was relatively slow since the sensor had to be moved above each spot being mapped. Range sensing from a single point would be expensive to achieve the required accuracy, and a linear array of multiple sensors would likewise be expensive. Thus, video imaging was used to identify area of potential cracks, and range sensing was used to confirm the location and identity of pavement cracks.

Filling Pavement Cracks

Once pavement cracks were identified and mapped, specialized control software was used to traverse cracks on the pavement surface for cleaning and filling. The motor controls and related software in the laboratory system proved to be quite accurate for single and repeated movements, with an accuracy over a 3 x 3 m (10 x 10 ft) area of 5 mm (0.2 in). However, the x-y frame was insufficiently rigid to permit rapid movement of the blower and filler. As a result, the filling operations for cracks on pavement scenes required several minutes. A more rigid frame would alleviate this problem.

Alternative System Designs

Several alternative system designs were considered for commercial and field systems. These options included:

1. Continuous movement systems with a set of linear nozzles. Unfortunately, controlling the application of the sealant would be difficult since instant on-off is required, and the cost of crack perception would be high with such systems.

2. Small, mobile, highly maneuverable robots tethered to a field vehicle were considered as an alternative to the x-y table. This approach could provide continuous filling but might increase costs and control problems.

3. Alternative sensing systems, such as single-point laser range sensors, were examined. These types of sensors have the potential of dramatically reducing the time required for range scanning, but the existing technology could not provide fine-enough resolution.

4. Alternative systems, such as robot arms, could replace the x-y table system. However, these pose difficulty in terms of load-bearing capacity, controlling contact forces, spatial constraints and computational intensity.

Technical Issues for Further Consideration

Field trials will address several technical issues that require further consideration. These include:

1. Expected productivity rates will be quantified. System productivity was assumed to be equal to that of manual crack filling.

2. The level of supervision and manual intervention will be determined. Unexpected obstacles and breakdowns should have little impact on a robust system.

3. Setup time and effort will be determined. The proposed system is intended to be transportable and require little on-site assembly.

4. Investigating the effect of real artifacts on crack perception. In the field, unrouted cracks may be filled with dirt and obscured by oil, debris and vegetation.

5. Evaluating the impact of variable environment such as changing ambient lighting. Crack perception under variable lighting conditions may be more difficult.

6. Evaluating the quality and consistency of the material delivery.

Because many states do not rout cracks, better sensors and modified software must be developed to improve the capability to perceive and trace unrouted cracks. Experiments are required to determine the requisite resolution and accuracy. A new system frame is also required to enable greater mobility and provide enhanced structural stability. More detailed economic analysis needs to take into account the variability in crack-filling practice.

This project is in its second phase and is developing prototypes for field testing. The project is cost-shared with CALTRANS.

Intelligent and Localized Weather Prediction

IDEA 018 - Localized and Intelligent Weather Prediction for Snow Control

Investigators: Elmar R. Reiter and Luiz Teixeira, Wels Research Corporation, Boulder, Colorado

IDEA Product

The product is a prototype software package which will deliver real-time, 24-hour, localized snow and ice forecasts on a statewide basis in computer-generated, graphical displays. These forecasts will exhibit, on a three-hourly or hourly time-lapsed basis, anticipated road conditions for the statewide road network.

Innovation

Instead of relying on television weather forecasts, the method generates numerical weather prediction results on a desktop computer (hardware cost: approximately $10,000), using the same data as the National Weather Service. Prediction results can be displayed at hourly intervals and can be input directly to software that provides graphic exhibits of predicted road conditions. Observations by human observers or automatically reporting sensors can be used to correct these forecasts, if discrepancies between expected and actually encountered weather conditions begin to appear.

Project Summary and Progress

The ongoing research program is aimed at developing an objective prediction method for snow and ice accumulation on highways which takes into account local conditions of topography and can assimilate user-supplied observational data for the purpose of forecast corrections.

Because of the much greater detail in predicted timing (onset and cessation) and in the local impact of snowstorms, decision makers will be able to allocate their resources more efficiently. Greatest savings are anticipated from optimizing plowing and sanding operations by directing them to start when and where needed, and canceling them as soon as appropriate. Such optimization could result in 5 percent budget savings, to be allocated for other maintenance operations.

Highway maintenance operations, such as snow and ice control, are currently guided by weather forecasts disseminated by the news media. Although the quality of these forecasts has improved steadily over the years, they still leave much to be desired for operational decision making. There are at present no facilities available to upgrade a forecast if timing or intensity of a predicted snow or ice event does not agree with reality. Therefore, operators often must assume worst-case scenarios. This means that equipment and personnel are deployed longer than necessary, at great cost to the state highway department. Frequently more chemicals are used than is warranted by actual weather conditions. Better weather information is needed to optimize such operations and to save money.

Weather information provided by the news media and even by direct access to National Weather Service data does not provide sufficient detail about time and space resolution of inclement weather essential for tactical planning. To provide such resolution, the project has developed a numerical weather prediction model which provides 24-hour forecasts of near-surface and upper-air weather conditions over a statewide region. Particular emphasis is given to precipitation, temperature and wind conditions. Forecast output is generated at three-minute intervals at grid points 96 km apart, covering the region of interest. A "zoom" version of the model can produce weather forecast output at a grid mesh width of 24 km. For practical purposes, these forecast outputs can be stored in computer memory at hourly or three-hourly intervals. From these data the user can see the cumulative effects of a predicted snowstorm event. To generate a 24-hour forecast in this fashion requires approximately 24 to 45 minutes of computer time, depending on the desired space resolution--96 or 24 km. The computer system used is a 486/33 mHz personal computer costing approximately $10,000. Output from these predictions comes in the form of weather data (precipitation, temperature, wind speed and direction) at equidistant grid points arranged in a mesh that covers the area of interest (up to 1000 x 1000 km).

Even a horizontal grid resolution of 24 km does not meet the requirements of highway maintenance operations in mountainous terrain. Within such a distance, a road can climb from valley elevations to high mountain passes and down into a valley again. Road conditions can change from wet to icy to snow-covered. To cope with such local effects of terrain, the project has developed computer methods (used with the aforementioned hardware) that can access large geographic data bases containing terrain elevation and road network data. The data base presently used in Colorado applications can offer a resolution as fine as 900 m between elevation data points. For practical applications, such as displaying a state map, a resolution of about 4 to 5 km is sufficient. A zoom capability to higher resolution can be put in place for areas that might need frequent and detailed scrutiny.

The weather forecast information, developed by the numerical prediction model described above, will be generated to match the resolution of the terrain and road data base chosen for display. In this merger of data, the project has used an approach that treats each 5 x 5 km area of terrain as an object with certain attributes, such as location, elevation, and anticipated precipitation. Depending on the values given to such attributes, display colors and shading patterns are assigned to each of these squares. Thus, terrain maps can be painted on the computer screen.

In the very likely event that actual snow observations of highway patrol officers or equipment operators do not match the predicted conditions, Wels has developed a prototype capable of adjusting the forecast for the remainder of the prediction period. At present, the user must decide why the forecast is inadequate: (1) mistaken estimation of the snow storm's time of arrival; (2) errors in forecasting the storm's intensity; (3) both of the above; and (4) localized weather that does not represent a larger area. The user may then choose to adjust predicted snow cover amounts for the remainder of the forecast period. Facilities to allow user input to adjust forecasts will become more sophisticated as these weather prediction applications are used more.

Verification of the software system will be completed with Phase II of the SHRP-IDEA project. Meteorological data needed to run the numerical model will be received from a satellite communications link from the Zephyr Weather Information Service. Hardware and software for such a data link can be acquired by any user at very reasonable installation and monthly subscription costs. The project is currently developing data quality control procedures to be imposed on data stream received through the aforementioned communication facilities. Figure 32 shows the modules of current system designs.

The numerical model will undergo extensive in-house testing with a variety of weather scenarios. Operational testing will be done by the Colorado Department of Highways. This testing phase will provide us with valuable experience on personnel training. It also will be of important to assure software robustness.

A number of improvements are planned during Phase II which will help in the adjustment of forecasts by user input. These improvements will take advantage of tools developed within the field of artificial intelligence. A major concern to be addressed is the mapping of surface temperature and snow predictions to terrain details provided by the geographic data base.

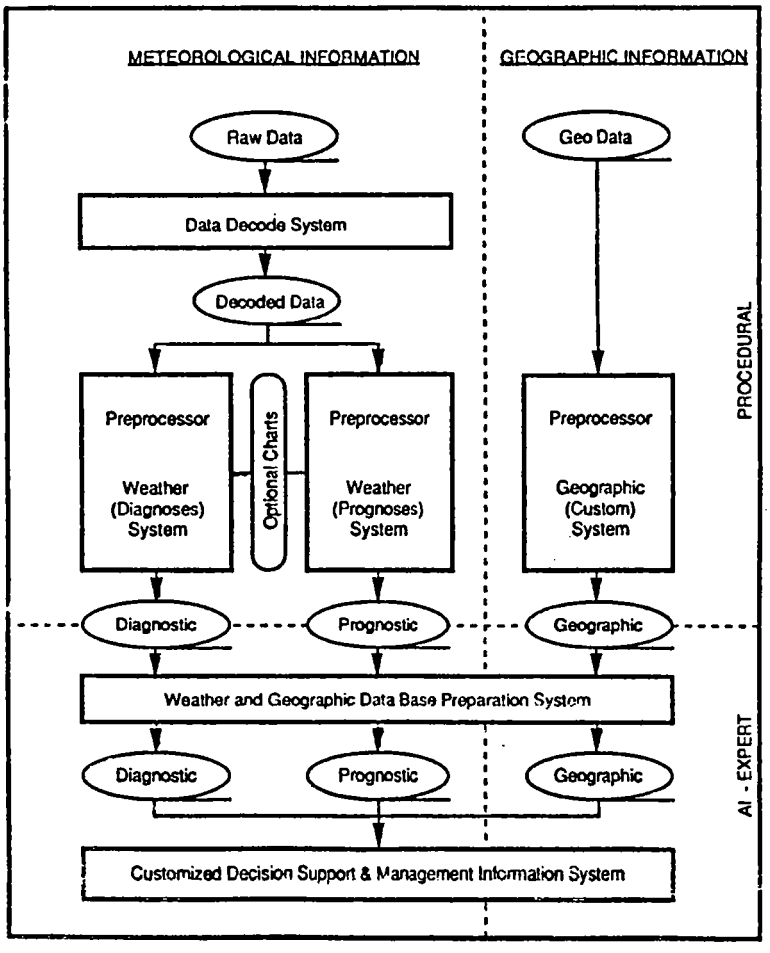

Figure 32. Modules of Current System Design

Technical Issues for Further Consideration

After completing operational tests in Colorado, the system can be used in other states and Canada. There are, however, certain preconditions that have to be met for successful operation in other environments:

1. A high-resolution geographic data base of terrain elevations, slope, and azimuth angles must be developed and structured to the exact specifications of the project model.

2. Purchasers of the system will require a geographic data base of their road network. This data base must be made available. Again, this data base must be formatted to the exact specifications of the project model.

3. A satellite communications link, providing access to the required weather observation data (radiosonde and surface data, collected twice daily from North American stations) must be put in place. Zephyr Weather Information Service, in cooperation with Wels, will provide the necessary reception hardware and data decoding software.

This project is in its second phase and is creating prototypes and field-testing them in Colorado. Phase II of the project is cost-shared with the Colorado Department of Highways.

Electro-Acoustic Modification of Concrete

IDEA 019 - Electro-Acoustic Technology as a Means to Modify the Properties of Concrete: A Feasibility Study

Investigators: Eric W. Brooman and Han Wu, Battelle Memorial Institute, Columbus, Ohio

IDEA Product

This project is determining the efficacy of applying electro-acoustic technology to improve and modify concrete properties during curing. The method has potential for application in the following:

1. The time required for electro-osmotic chloride removal in concrete may be cut in half because of facilitated mass transfer. This will reduce operating costs and the disruption of the roadways.

2. When the method is applied to monomer impregnation in polymer impregnated-concrete (PIC), the costly drying process prior to impregnation may be eliminated. Under proper conditions, the polymerization also may be induced by ultrasound waves and further eliminate the heating step generally adopted for polymerization. This will result in a significant saving in operating costs.

3. When the method is applied during concrete curing, the distribution of the hydrates and water inside the concrete may become more uniform. This would improve the properties of the concrete, thus improving performance.

Innovation

The method was originally developed as a simple, efficient, and cost-effective method of dewatering sludges, mineral slimes, food, and pharmaceutical products. The technique uses an electrical (voltage) gradient to move charged species through the medium, coupled with acoustic energy to free the more tightly bound water molecules or perhaps destabilize colloidal phases.

By analogy, concrete can be viewed as an inorganic medium containing free water, trapped (pore or gel) water, bound water, and ionic species with varying degrees of

mobility. Electro-acoustic technology, therefore, could: (1) affect the distribution of water during and after curing; (2) affect the distribution of detrimental ions, such as chlorides; (3) affect the distribution of beneficial ions, such as chloride ion scavengers or corrosion inhibitors; (4) affect the distribution and extent of in situ electro-polymerization; and, (5) facilitate the cathodic protection of reinforced structures, and perhaps lower the energy requirements.

Project Summary and Progress

Acoustic (ultrasonic) energy has been combined with an electric field in various electrochemical methods that have been applied to improve the properties of concrete, or as a remedy for rebar corrosion inside concrete. A synergistic effect has been observed by the combination of an electric voltage gradient and the periodic, mechanical force from ultrasonic waves. The result was enhanced mass transfer of, for example, organic monomers into concrete specimen even without drying prior to the impregnation. A schematic representation of the experimental electro-acoustic equipment setup is shown in Figure 33.

Electrochemical impedance change of the concrete, and thus the migration of water across the concrete/solution boundary, indicated that a 50 percent savings in time may result with the application of this method, as shown in Figure 34. Without drying, methyl methacrylate (MMA) has been impregnated into concrete specimens to a depth of 0.8 inch in two hours compared to a depth of 1 inch with prior drying. Ultrasound power and process time are the most important factors in a polymer impregnation process. The optimal conditions are being investigated.

The literature search indicated that this method has been applied to the dewatering of materials such as coal and sewage sludges, but no efforts were described of using this method in highway and concrete applications. It was shown, however, that acoustic energy was useful to a certain extent in the absorption of water into concrete. The overall objective of this project is to determine if Battelle's novel electro-acoustic technology can be used to minimize the degradation of existing reinforced concrete structures.

Preliminary experiments on applying this method to chloride removal and monomer impregnation showed:

- The impedance of a concrete specimen, using this method, changed twice as fast as that of a specimen with an electric field applied only. This result indicates that a faster mass transfer occurred when this method was applied.

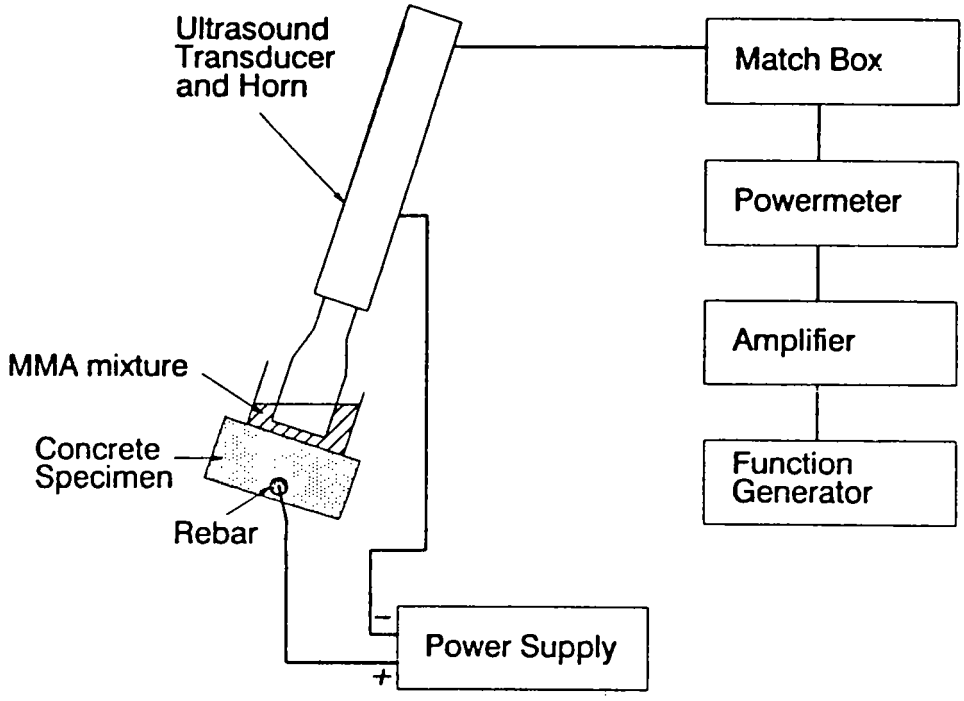

Figure 33. Schematic of the Experimental Setup of the Electro-Acoustic Technology

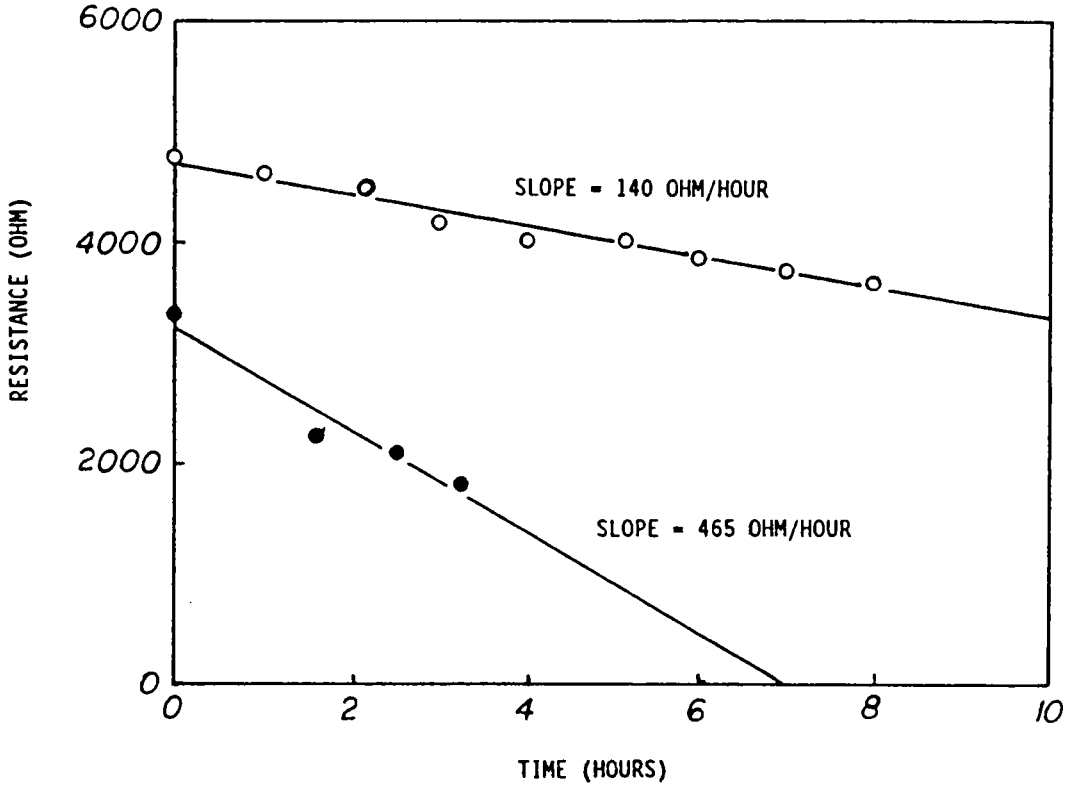

o Control specimen with electric field only
• Specimen with the addition of acoustic energy

Figure 34. Effect of Electro-Acoustic Technology on the Electrochemical Impedance of a Concrete Specimen

- When impregnating MMA into concrete, this method gave a small enhancement of the penetration depth of MMA. The effect of acoustic energy was more important than the effect of electric energy.

During the experiments on polymer impregnation, bubbles were observed to escape from the concrete specimen and were trapped under the acoustic horn. It was also found that the frequency at which ultrasonic waves were produced was an important factor. Therefore, improvements were made to avoid collecting bubbles underneath the horn for better ultrasound transmission, and to tune the ultrasound generating device so that a global maximum rather than a local maximum of ultrasonic transmission was used.

The penetration of MMA into concrete after these improvements showed that the monomer could infiltrate about 0.8 in into a concrete specimen without drying in two hours and fifteen minutes compared to 1 in penetration of a previously dried specimen in two hours. The experimental work is still continuing at this time.

Technical Issues for Further Consideration

This approach seems to significantly enhance mass transfer in concrete. In order to apply this technology to the field, certain issues have to be considered.

The material of the ultrasound horn has to be carefully chosen. An insulating coating should be applied to reduce the current leakage when the horn is present in an electric field. In preliminary experiments, the ultrasound horn was connected to an electric ground to protect the horn, and there was a current leakage detected during the chloride migration experiments.

The position and dimensions of the ultrasound horn, the power of the acoustic energy applied, and the voltage gradient of the electric field all have to be considered when scaling up this method for highway practice. For example, in experiments on a laboratory scale, the temperature of the monomer increases as a result of the acoustic energy application. The process time and the power levels of the ultrasound have been restricted by the polymerization temperature of the monomer system. In the field, the process time may be increased because the mass of the monomer systems will be increased and the power will remain at the same order of magnitude as in the laboratory tests.

Another issue is the method of applying this method to impregnating polymers. Ultrasound transmits much more efficiently in pure liquids than in liquid/solid mixtures. The usual practice of using sand as a retaining matrix for organic monomers will

decrease the process efficiency greatly. Therefore, a batch-type holding reservoir will have to be used. Issues such as safety, leaking, and evaporation must be resolved before the process can be applied to the field.

Conversion Residue Binder for Asphalt

IDEA 020 - The Use of Conversion Residue as a Component to Reduce Moisture Induced Damage in Asphalt

Investigators: Richard E. Root and Richard B. Moore, Chicago Testing Laboratory, Northbrook, Illinois, and Shell Development Co., Houston, Texas

IDEA Product

This project is developing a low-percentage blend of conversion residue with a vacuum-distilled asphalt to produce an acceptable asphalt binder for enhancing asphalt pavements' resistance to moisture damage.

Innovation

The use of conversion residue will reduce the effect of moisture damage without using expensive anti-stripping additives. It will lower the cost of binder and extending the service life of the pavement.

Project Summary and Progress

The work thus far indicates that blending the conversion residue with vacuum-distilled asphalts can produce binders with equal quality to our present specification. Initial testing indicates that the value as an aid to reduce moisture damage will require testing of each binder/aggregate combination.

Two samples of conversion residue were blended with two sources of asphalt cement to prepare samples of asphalt cement (AC-20). The asphalt cement was blended using conversion residue in concentrations of 0%, 5%, 10%, 20% and 40%.

Each of these blends was tested for comparison with common specifications for AC-20 with additional penetrations at 4°C. Temperature susceptibility, Fraass brittle point and thermal cracking temperature were calculated on the original and thin film residues.

Three sources of aggregate were obtained from the SHRP Library. These were Georgia granite, Maryland limestone and Texas chert. Marshall mixture designs were prepared

using each of these aggregates in order to obtain the optimum asphalt content.

Each of the asphalt cement blends was then tested with each of the three aggregates in order to evaluate the potential for moisture-induced damage. The procedure used was ASTM D-4867, which was developed in NCHRP-274. Figure 35 shows typical test results.

The blends of the AC-20 all complied with common specifications for AC-20. The spot test using 65% heptane and 35% xylene tended to be positive at the 20% and 40% concentrations of the conversion residue. The conversion residue serves to enhance the temperature susceptibility of the blends, especially with the higher concentrations.

While the effect of the conversion residue on the moisture induced damage was not pronounced with all combinations of vacuum distilled asphalts and aggregates, there is a trend toward a higher percentage of retained tensile strength as the concentration of conversion residue increases.

Technical Issues for Further Consideration

The use of conversion residue in asphalt shows that it enhances the mechanical properties and resistance to moisture-induced damage. Additional tests are necessary to determine the efficacy of using conversion residue for enhancing the performance of asphalt pavements.

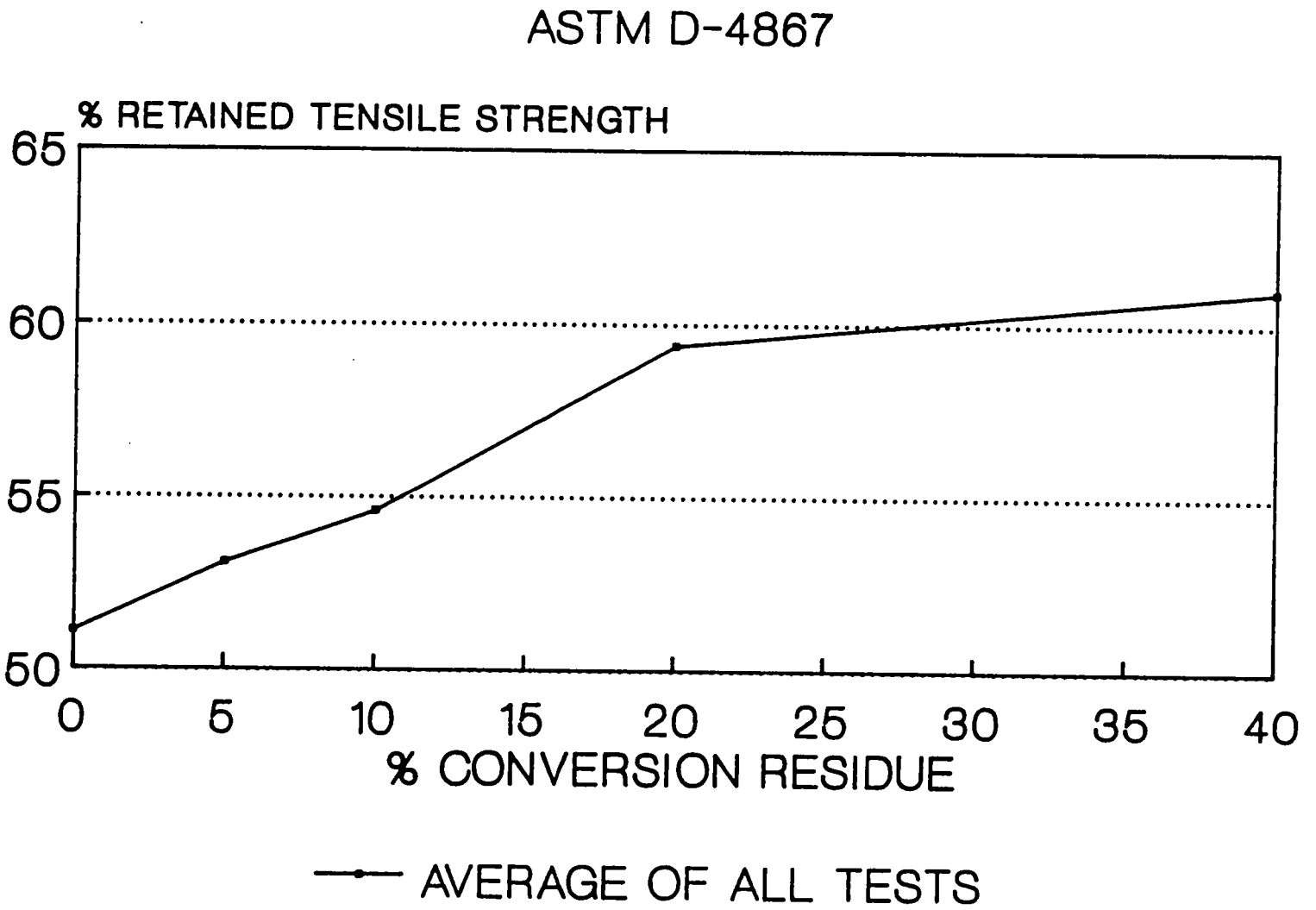

Figure 35. Moisture-Induced Damage

Automated Asphalt Process Analyzer Using Nuclear Magnetic Resonance

IDEA 021 - The Application of Small Nuclear Magnetic Resonance Spectrometers to Quality Control Measurements of Asphalt and Asphalt/Aggregate Mixtures

Investigator: Robert M. Pearson, Tri-Valley Research, Pleasanton, California

IDEA Product

This project is designing and testing a small nuclear magnetic resonance (NMR) spectrometer system to measure the amount of asphalt in a hot mix as it is being prepared in a hot mix plant. The application was shown feasible in Phase I. Phase II work for building and testing a full-sized prototype spectrometer in a hot mix plant, and for the study of core physical properties in the laboratory, is being evaluated by SHRP.

Innovation

This project is an innovative application of a well-established form of molecular spectroscopy to plant process control. NMR can be applied to measure physical properties of asphalt and asphalt content during processing.

This method could quantitatively measure the amount of asphalt in an asphalt/aggregate mixture, and also could determine the physical condition of the asphalt in a core. This technology may have an important affect on methods used to determine asphalt content in asphalt/aggregate composites as they are processed for pavement construction.

Project Summary and Progress

This project has produced a NMR technique capable of qualitatively measuring the amount of asphalt in an asphalt/aggregate composite or a highway core. It has also been shown how these techniques can be used to study the physical properties of both the neat asphalt and asphalt/aggregate composite samples. Detailed correlations between asphalt physical properties and NMR spectra were obtained.

The feasibility of using small NMR spectrometers for these purposes is a straightforward application of the known principles of magnetic resonance. A design of the instrumentation was developed.

Simple free induction decays could not be used to determine the amount of asphalt in samples mixed with aggregate. Although free induction decays work well for neat asphalt samples, the presence of the aggregate creates a high magnetic susceptibility in the sample which broadens the NMR line and creates a very fast-decaying signal. This was overcome by adopting a Carr-Purcell-Meiboom-Gill (CPMG) pulse sequence as our standard method for composite samples. This is an echo-producing sequence which averages out the effects of the magnetic inhomogeneities caused by the high susceptibility of the aggregate.

Figure 36A shows CPMG data for an asphalt/aggregate mixture. The intensity of the first echo is used to relate NMR intensities to the known concentration of asphalt in the mix. Figure 36B illustrates this correlation. The scatter in this calibration curve is caused by the mixtures prepared at this low asphalt concentration. This problem will be overcome by fabricating an instrument suitable for measuring full-sized highway cores of known asphalt concentration. Figures 36C and 36D show CPMG data on a neat asphalt sample. The plot in Figure 36D can be divided into three straight line portions which represents three hydrogen populations of different mobility.

The spectrometer includes several state-of-the-art innovations in NMR instrumentation. These innovations include installing, whenever possible, commercially available components into a personal computer. Appropriate electronics and a high-power transmitter (Figure 37) allows inexpensive spectrometer design while maximizing the ease of system maintenance.

The operating software for the spectrometer is based on a commercially available software package. This, combined with a standard personal computer outfitted with the aforementioned commercial components, insures prospective purchasers that both hardware and software updates will always be available for this system.

Technical Issues for Further Consideration

The measurement of the amount of asphalt in hot mix is a straightforward application of the CPMG method to this problem. The calibration curve shown in Figure 36B is not accurate enough for good quantitative work. This problem is not with our present instrumentation, but is caused by the sample preparation techniques used to prepared

Figure A

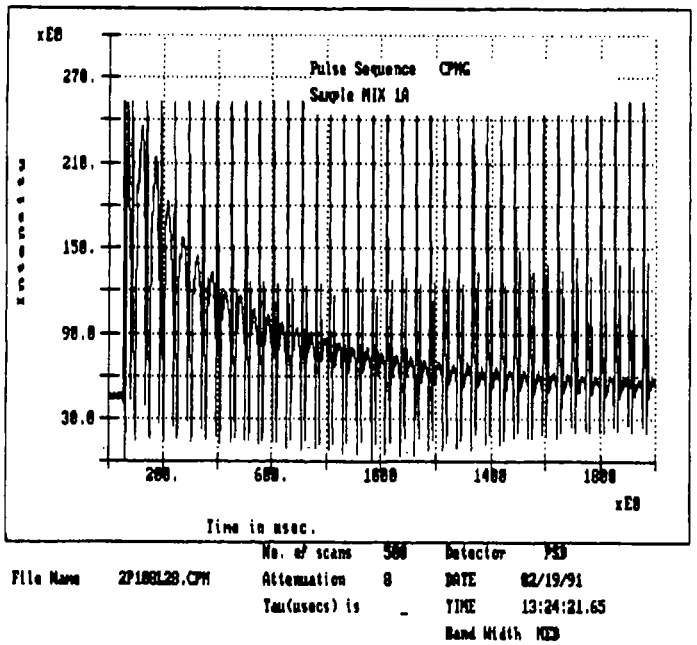

Figure B

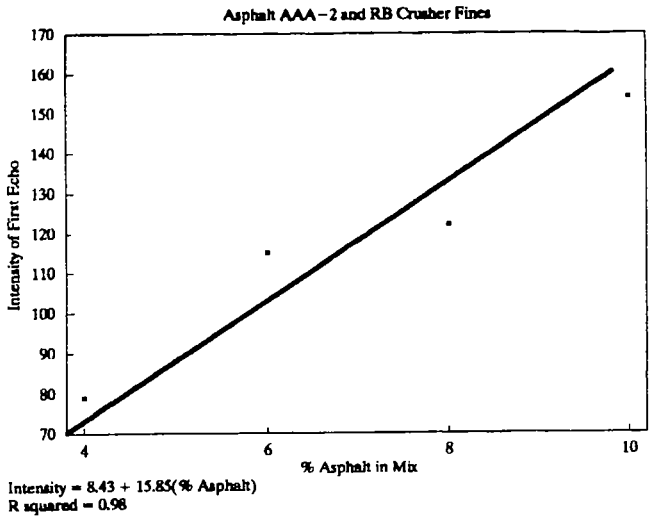

Figure C

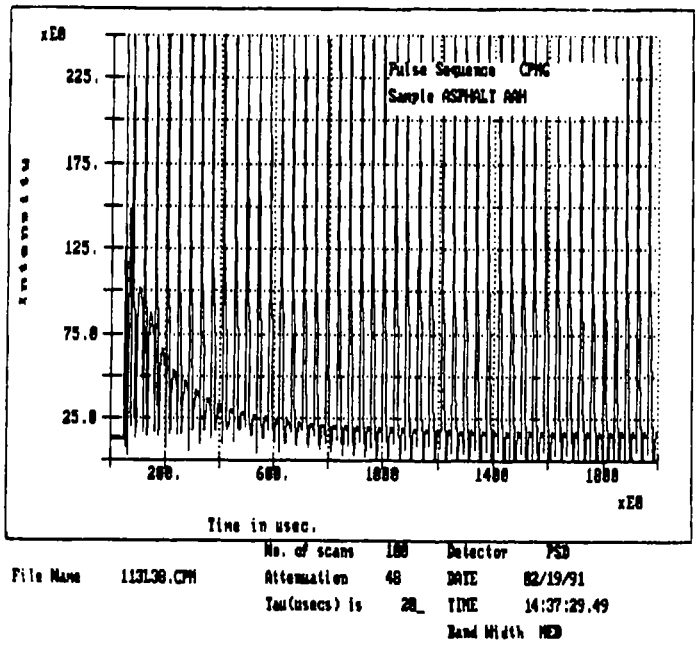

Figure D

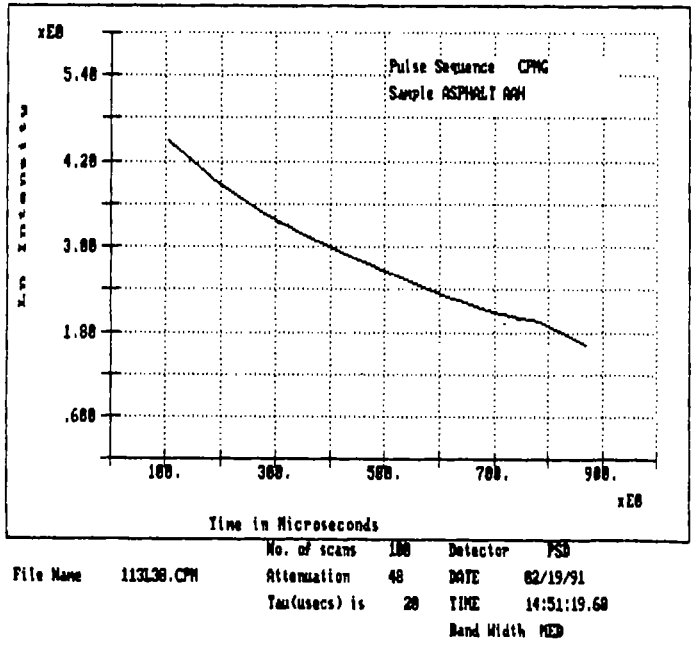

Figure 36. Pulse Sequences in Asphalt Samples

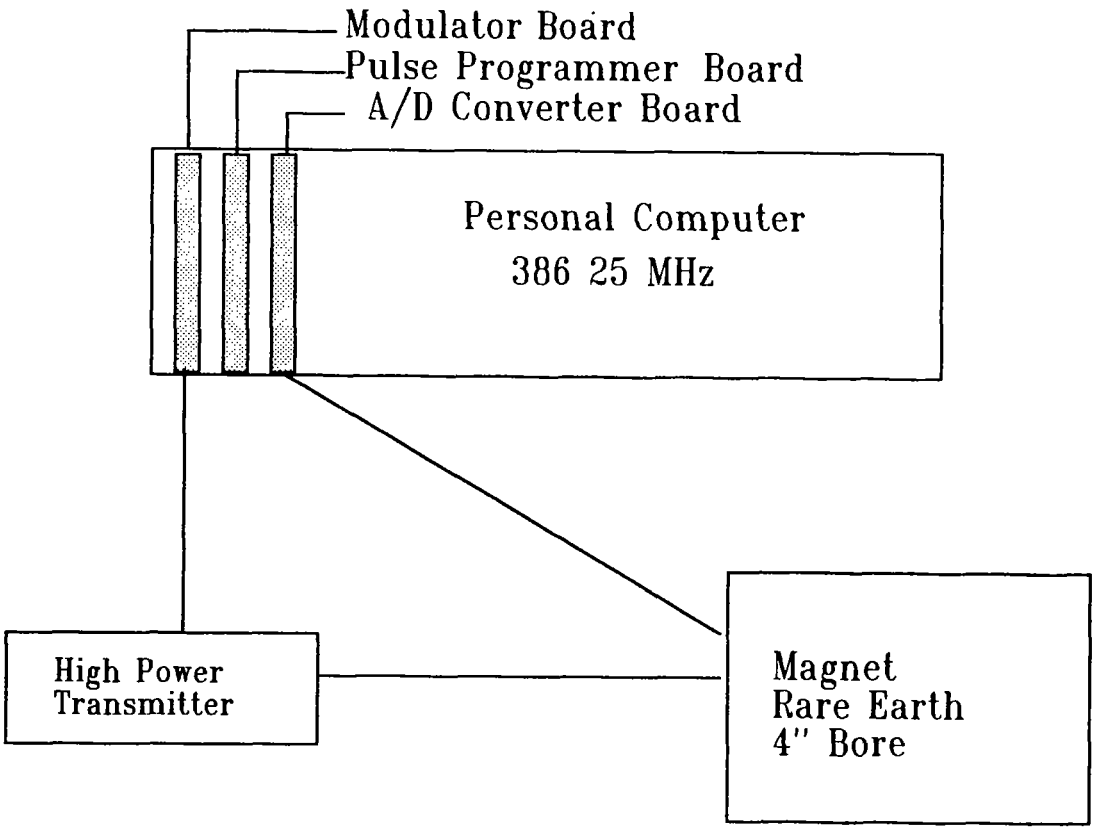

Figure 37. Block Design of the Proposed Spectrometer

the mixes of varying composition. This problem will be overcome by using full-sized highway cores of known composition to calibrate the full-sized prototype instrument.

A full-sized prototype instrument is required to study relationships between NMR spectra of highway cores and their physical properties. The project results indicate that the presence of the aggregate changes the mobility of the hydrogen atoms in the asphalt, and therefore alters the asphalt's physical properties.

If the above is true, then the physical properties of the asphalt/aggregate mix depend on both the properties of the neat asphalt and the changes that occur when the neat asphalt is mixed with the aggregate. Thus, the physical properties of mixtures prepared from the same asphalt but with different aggregates can be very different, and these differences can only be measured in the mix.

Once this initial application has been proven it should be possible to adapt flat magnet technology to the measurement of the physical properties of an asphalt roadbed without removing a core. Flat magnet technology has been used in other applications with some success and it should be possible to develop and apply flat magnet technology for the NMR process.

Flexible Stress Cell

IDEA 022 - Development and Verification of a Flexible Stress Cell

Investigators: Steven L. Kramer and Rubens Sigelmann, University of Washington, Seattle, Washington

IDEA Product

A prototype flexible stress cell will be constructed and tested under controlled laboratory conditions for verification of its ability to measure stress in pavements. Algorithms and software for interpretation of the stress cell output will be developed.

Innovation

The flexible stress cell will consist of a compliant plate embedded with ultrasonic transducers. The travel time of ultrasonic stress pulses propagated through the plate from one transducer to another will be used to measure the deformed shape of the plat. The stresses acting on the boundary of the plate can be calculated from the deformed shape of the plate and the constitutive properties of the material from which it is constructed. With this system, both normal stresses and shear stresses can be calculated.

Conventional stress cells attempt to measure a single component of stress. In order to isolate the stress-sensing element from other components of stress, they are typically fabricated from very stiff metallic elements. The incompatibility of stiffness between conventional stress cells and the soil in which they are embedded causes significant stress redistribution so that the measured stress is not the free-field stress of interest. Consequently, conventional stress cells are very limited in accuracy and reliability. The flexible stress cell, by virtue of its compliance, causes much less stress redistribution than conventional stress cells. Consequently, the flexible stress cell can measure free-field stresses much more accurately than conventional stress cells. Additionally, the flexible stress cell can measure multiple components of stress, thereby providing a much more complete evaluation of the stress conditions in a geotechnical or pavement structure.

Project Summary and Progress

The specific goal of this project is to verify the stress cell's ability to accurately measure normal stresses and shear stresses under static and dynamic loading conditions.

Development of the flexible stress cell requires innovative, interdisciplinary research in the areas of acoustics, electronics, and mechanics. The project team has evaluated the stress cell shape and transducer geometry, identified the materials for the compliant plate and ultrasonic transducers, designed a prototype travel time measurement circuit, and performed preliminary testing of the materials. Further testing and refinement of the prototype design will continue in the coming months.

The proposed stress cell relies on the use of ultrasonic pulse travel time measurements to reconstruct an image of the deformed shape of the cell. Once the deformed shape is known, calculation of the boundary stresses is a relatively straightforward matter. Measurement of the deformed shape, however, is a difficult problem.

The deformation of the stress cell will be very small at low stresses. Hence, the displacement resolution of the ultrasonic pulse travel time measurement system must be very small. The actual travel time resolution will be so small as to be unmeasurable by commonly available timer circuits. For this reason, the use of a travel time "loop" procedure, in which a pulse detected at the receiver triggers a new pulse at the transmitter, is required. By measuring the time required for a known number of loops and knowing the time delay of the associated circuitry, the travel time for each loop can be measured with great accuracy. Figure 38 shows a schematic of the flexible stress cell system.

Achieving the project's goals requires a detailed, multidisciplinary investigation of the mechanical, acoustical, and electronic aspects of the flexible stress cell and its components. Each of these aspects is coupled with, and consequently influences, the others. The mechanical properties will influence the degree and nature of stress redistribution in the vicinity of the stress cell. They also influence the nature of the materials from which the flexible stress cell will be constructed and the resolution with which ultrasonic measurements must be made. The acoustical properties will influence the choice of materials, the electronic circuitry requirements and also the potential for making dynamic measurements. The electronic properties of the cell and associated instrumentation must be selected to make the required measurements as quickly and reliably as possible, given the constraints imposed by the mechanical and acoustical properties. The technical issues involved in these investigations are very complex, particularly with respect to the acoustical and electronic aspects of the stress cell.

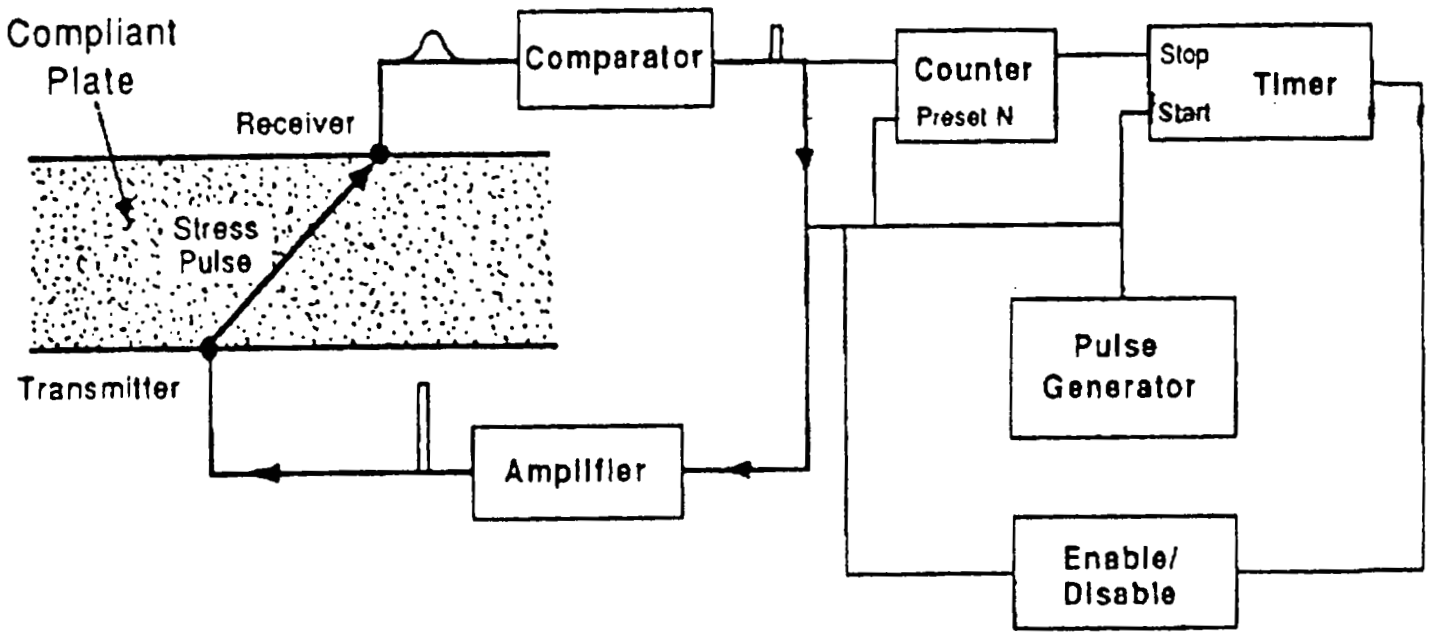

Figure 38. Diagram of Flexible Stress Cell

The first phase of the research has involved detailed analytical investigation of the mechanics, acoustics, and electronics of the system. The mechanical investigation has been directed toward optimization of the compliant plate geometry and identification of the desired piezoelectric sensor locations. The acoustical investigation has been concerned with the modelling of the propagation of ultrasonic pulses from transmitters to receivers, emphasizing material and geometric effects on the amplitude and frequency content of the received signal. The electronic investigation has concentrated on the accuracy with which travel time measurements can be made by the multiple loop process.

A key to the performance of the flexible stress cell will be its ability, by virtue of geometry and material properties, to minimize stress redistribution in its vicinity. The optimum size, shape, and material properties of the compliant plate have been investigated by analytical methods. Two-dimensional finite element analyses have been performed to evaluate the influence of a number of variables including: the size, shape, and material properties of the compliant plate; and loading conditions on the accuracy of the flexible stress cell. The finite element analyses have shown that the effects of stress redistribution are greatly reduced when a flexible stress cell is used in place of a rigid stress cell. Some redistribution of stresses is inevitable and the amount that occurs depends on the relative stiffness and relative compressibility of the cell and the surrounding soil.

The results of the finite element analyses have been used to determine optimum sensor locations and for the development of a boundary stress model for interpretation of the results of the ultrasonic measurements. The analytical results indicate that the aspect ratio of 10:1 is appropriate for measurement of normal and shear stresses. A smaller aspect ratio would allow uniform stress conditions over only a small area near the center of the cell. The boundary stress model is being developed to allow calculation of stresses on the boundaries of the compliant plate from the results of travel time measurements.

A critical element of the success of the flexible stress cell is the resolution of the measurement of the travel time by propagation properties of the ultrasonic wave through compliant materials. A typical pulse will include components at many different frequencies. Both geometric and material attenuation will influence the characteristics of the pulse--both in terms of amplitude and frequency content--as it propagates through the cell. Thus the pulse detected at the receiver will be of a different form than that of the pulse generated at the transmitter. In order to design electronic circuitry to measure the time accurately, it is extremely important to understand the effects of propagation on waveform characteristics such as pulse duration and band width. Two major factors which will affect the waveform characteristics have been investigated: one is the

aforementioned attenuation, and the other is the integrated signal received at the cylindrical receiver/transducer. The effects of these factors on the waveform characteristics will influence the requirements of the comparator which must detect each pulse that passes through the receiver.

Attenuation has been studied to evaluate its effect on the amplitude and frequency content on a pulse propagating through a compliant material. A particular Gaussian pulse has been investigated in both the time and frequency domains using fast Fourier transfer (FFT) and propagation theory. It was observed that the attenuated wave had the same waveform but an expanded pulse width.

The second factor affecting the waveform is the geometry of the receiving transducer, which must be considered since the transducer is large compared to the very small deformation of the stress cell. The transducers will be cylindrical so that stress waves will propagate radially. The effects of receiver geometry on Gaussian pulses with different widths have been investigated by integrating the received signal through the transducer region, accounting for the electro-mechanical characteristics of the transducer. These analyses indicate that these geometric effects will cause waveform distortion and a time delay.

Technical Issues for Further Consideration

It is anticipated that the stress cell will be required to measure deformations as small as 0.001 mm. This distance will correspond to a travel time delay on an order of 10^{-12} seconds, which is about one million times less than the time for the acoustic wave to propagate through the cell. In order to achieve such resolution of travel times, a positive feedback loop approach will be used. Because the accuracy of travel time measurement will be dependent on the probability of the rise time of the comparator, the derivative of the time determination will increase for the feedback and reconstructed signals. This theoretical model is still under investigation.

The research will continue the mechanical, acoustical, and electrical investigations begun in the first phase. The second phase activities will concentrate on nonlinear, elastoplastic analyses of soil/cell interaction and on final preparation of the direct simple shear apparatus for prototype testing. The acoustical aspects of the second phase research will be further investigated. The cell materials will be selected as will the ultrasonic transmitter and receiver transducers. The waveform analysis will be refined to include both material and geometric attenuation and the results will be verified by a series of ultrasonic wave propagation experiments. The Phase II investigation of the electrical aspects of the flexible stress cell will be directed toward analysis of the

electronic circuitry requirements and design of a prototype travel time measurement circuit. Both the comparator and the timing circuit will be carefully examined as they represent critical elements in the flexible stress cell system.

Silicon Coating Process for Rebars

IDEA 023 - Coatings for Corrosion Protection of Steel Rebars Used in Reinforced Concrete

Investigators: Angel Sanjurjo, Samson Hettiarachchi, Gilbert Tong, and Bernard Wood, SRI International, Menlo Park, California

IDEA Product

A silicon coating process is being developed for corrosion protection of steel rebars used for reinforcing concrete. The technique produces surface-siliconized steel rebars for use in reinforced concrete at low cost. The siliconized surface will be selectively oxidized to form a protective native silicon oxide layer.

Innovation

SRI has developed a novel chemical-vapor deposition technique that combines the low cost of pack metallization with the high heat and mass transfer of a fluidized bed reactor. The iron-silicide/native-silica coating on the steel rebar is expected to perform dual protective functions. First, it will protect the steel rebar during storage even in open, humid environments such as yards. Second, it will protect the steel after it is embedded in the concrete. This coating is particularly effective in preventing corrosion in chloride environments.

Project Summary and Progress

The project has succeeded in depositing iron silicide coatings on steel rebars using a simple 7.5 x 20-cm-high fluidized bed reactor. Steel samples were immersed in the silicon powder bed and coated at temperatures in the range 400-750°C. Coating rates were relatively fast, reaching 1 μm per minute at the highest temperatures. Thinner coatings (less than 10 μm) were obtained at the lower deposition temperatures ($<$ 550°C) and shorter deposition times ($<$30 minutes). They were compact and adherent and obviously protective, as they did not tarnish when exposed to humid air. The absence of any observed changes in the microstructure of the underlying steel substrates, even at the highest coating temperature, indicated that the coating had no effect on the structural properties of the steel rebars.

Work is in progress for optimizing the coating conditions to obtain a much thinner (<5 micron), adhesive, and compact silicon layer on the steel rebars. Selected coated samples will be tested for corrosion resistance by chemical and electrochemical techniques.

Deposition of Coatings

The steel rebars that were chosen for coating are typical of those used in highway construction. The coatings were applied in a 7.5-cm-internal-diameter fluidized bed reactor (FBR) filled with powdered silicon that can hold up to four steel samples for coating at the same time. The coating system consists of the FBR, a gas delivery unit, and an on-line mass spectrometer to determine the composition of the reactor effluent (Figure 39). The reactor is made of quartz, although other inert, heat-resistant materials could be used. Metallurgical-grade silicon powder, with particle sizes ranging from 250 to 500 μm, was mixed with 5 wt% $CuCl_2$ catalyst and loaded into the quartz reactor to form a bed 10 cm high. The bed was fluidized by an inert gas with a linear velocity of 10 cm s^{1}. Argon is used in the laboratory operation, but nitrogen would be equally suitable. The reactor bed is heated to a temperature in the range 450 to 550°C while a mixture of hydrogen and hydrogen chloride (partial pressure of HC1 - 10^{-2} atm) is introduced into the fluidizing gas. These compounds form chlorosilane and silicon subchloride species in the bed, and they react or disproportionate on the steel samples to deposit silicon. The steel rebar samples immersed in the silicon bed were heated to a higher temperature than the surrounding powder by means of a r.f. induction furnace. The coating procedure lasts from 5 to 60 minutes. The ability to control the bed and substrate temperatures independently provides a way to control the driving force for the coating process. The conditions and results of the coating experiments are summarized in Figure 40.

Characterization of Silicon Coatings

Scanning electron microscope (SEM), EDAX and X-ray diffraction (XRD) analyses were performed on the coated surfaces as well as on the cross sections of the samples to determine the morphology, thickness, and composition of the coatings. At temperatures below 550°C, the coatings are adherent, compact and conformal. The main composition is close to Fe_3Si, as determined from EDAX. Some silicon (up to two percent) was observed to have diffused into the underlying substrate.

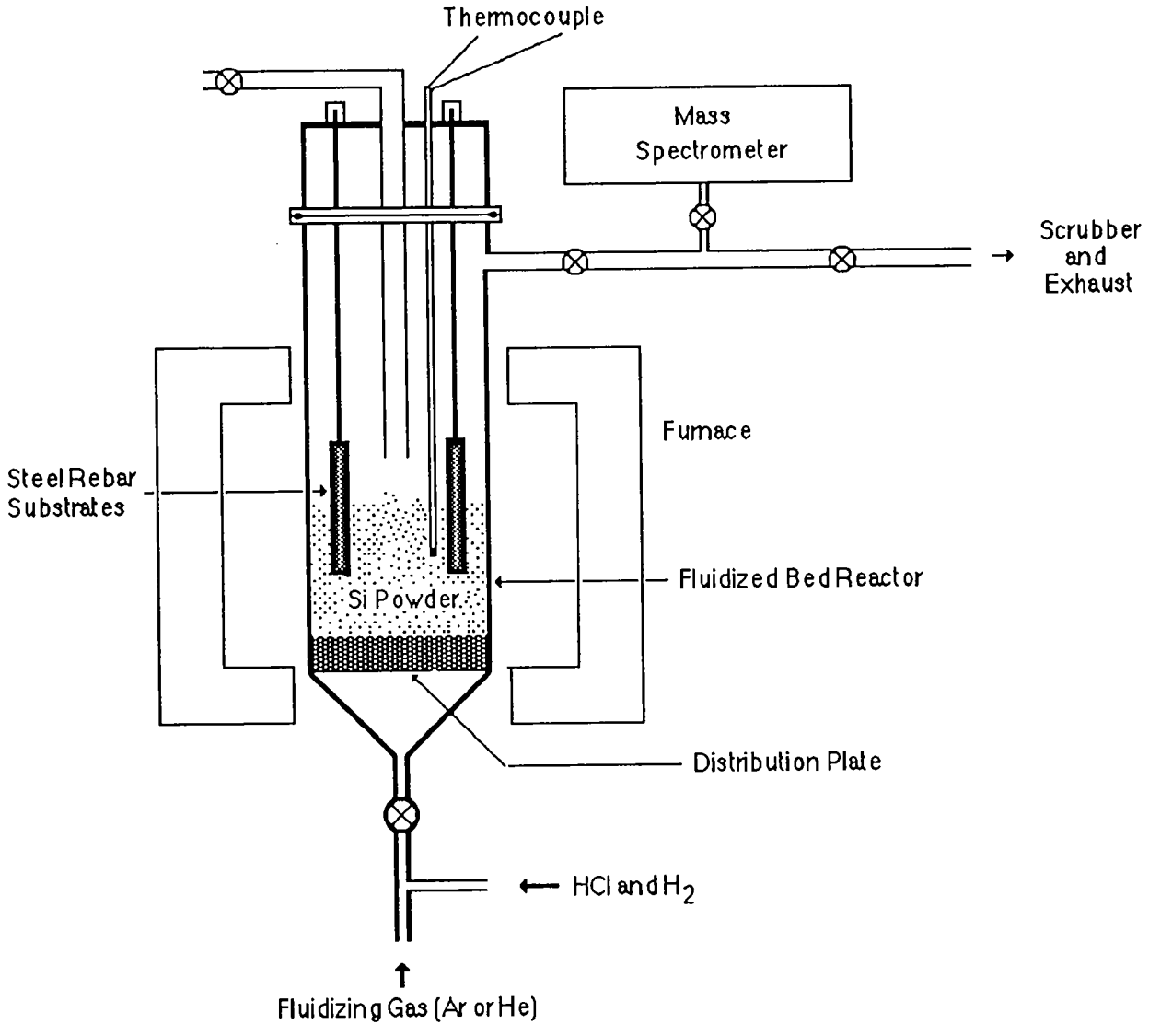

Figure 39. Reactor System for Coating Steel Rebars with Silicon

Run	Reactant	Temperature (°C)	Time (min)	Coating Characteristics
1	HCl	700-750	60	Multilayer Coating Top coating grey corrugated, 100 μm thick, spalls off easily Si crystal deposit adherent Intermediate Coatings FeSi (x-ray diffraction) Fe_3Si, (EDAX)
2	HCl	600-650	60	Multilayer Coating Top coating grey corrugated spalls off Si crystalline deposit, adherent Intermediate Coatings (as above)
3	HCl	550	60	Single Coating Smooth dark grey layer Adherent, No spallation cooling rate 100°C/min.
4	HCl	650	30	Top corrugated layer = FeSi (x-rays) Mid layer = Fe_3Si (EDAX)

Figure 40. Silicide Coatings of Steel Rebars at Different Temperatures

The coatings obtained at temperatures near 650°C consist of two layers of approximately equal thickness: an interdiffusion layer (containing about 15 wt% Si and 76 wt% Fe) on the outside. From these values, the interdiffusion layer appears to be a Fe^3Si phase, but x-ray diffraction shows only a Fe-Si phase. In addition, pure silicon crystal deposits were observed. Coatings at higher temperatures (i.e. 700-750°C), show in addition a very corrugated, easily spalled outer coating of FeSi and also polycrystalline silicon deposits.

Technical Issues for Further Consideration

SRI is presently determining the rate of deposition at relatively low temperatures and very short times in order to identify the conditions in which the coating can be deposited in only a few seconds. The results would lead to simulating conditions similar to those expected in industrial production of steel rebars by hot extrusion. Investigations will also include resistance to bending of rebars before the coating breaks and assess the corrosion resistance in chloride media.

Corrosion Repair Treatment for Marine Structures

IDEA 024 - Low-Cost Corrosive Repair Treatment for Marine Structures

Investigators: Alberto A. Sagues and Rodney G. Powers, University of South Florida, Tampa, Florida

IDEA Product

The project is researching a corrosion control method for marine bridge substructures. The investigation will establish conditions for successful operation, durability and initial field performance of the concept.

Innovation

The method consists of the innovative use of sprayed-zinc anodes for cathodic protection. The in situ application of the anodes is simple and involves low application and maintenance costs when compared with conventional impressed-current systems. The deteriorated components are blasted clean, and arc-sprayed zinc is deposited directly over the exposed, clean rebar and surrounding external concrete surface (Figure 41).

The technique can have be used for repair and corrosion control of a vast number of substructure members (piling, columns, footers, struts) that are currently deteriorating in highway bridges along the U.S. coastline. The concept is expected to be most successful in humid, warm-weather environments, but once the operating limits are determined, the technique may prove applicable in other areas.

Project Summary and Progress

A novel concept using sprayed-zinc galvanic anodes is proposed for testing and development as a low-cost method of controlling reinforcement corrosion in marine substructures. The deteriorated components are blasted clean and arc-sprayed zinc is deposited. The procedure creates reliable electrical contact with the steel, and provides a large area of contact between the anode and the underlying concrete. The appreciable concrete conductivity existing in typically humid marine substructure permits significant current delivery by the action of the unaided galvanic couple. The simple, two-step

Figure 41. Application of Anode on Reinforcing Steel

A zinc sacrificial anode was attached to the Niles Channel Bridge in the Florida Keys. Notice the exposed reinforcing steel at the spall area. After surface blasting, the sprayed zinc is applied over the rebar and the entire portion of the column surrounding the spall.

procedure is applicable to both regular and epoxy-coated rebar, avoiding cumbersome individual electrical connections in the latter case.

The concept represents a new approach in that: (1) it uses a sprayed metal anode and does not require impressed current; (2) it is applied directly to spalled components without requiring a concrete overlay; and (3) the resulting costs are substantially lower than those of alternative repair or protection methods.

This project started in January, 1991. Experiments and procedures for field tests have been initiated. Previous efforts have shown that anode application is straightforward in southern Florida structures, and that the anodes hold well against aggressive weathering conditions. The laboratory experiments will concentrate on determining the extent of protective current delivery and anode durability.

Limited trials of the concept by the Florida Department of Transportation have been highly encouraging. However, accurate information on the capabilities of the method is not available. The objective of this investigation is to obtain quantitative demonstration of the ability of the system to provide adequate protection.

The proposed concept represents a major advance in accomplishing the objectives of the SHRP concrete bridge protection program, especially as it pertains to the cathodic protection contract (C-102) and to the development of the final implementation under contract (C-104).

Three major research tasks will be performed under this project: (1) determining the limits of the ability of deposited zinc anodes to provide the required levels of current protection; (2) determining the effect of service and application parameters on the durability of the sprayed-zinc anodes; and (3) determining the effectiveness of this method under field conditions.

Task 1 will address the limiting conditions of concrete resistivity, anode surface area, effective anode-to-concrete contact, and related parameters within which the method can operate successfully.

For steel in concrete, the ohmic resistance of the concrete is likely to be the most important factor in limiting the performance of a galvanic cathodic protection system. Concrete resistivity varies from essentially infinity for very dry material, to as little as a few hundred ohm-cm for water-saturated, chloride-laden concrete. Marine substructures present a wide range of moisture and chloride content, depending on the evaporation pattern present. At the same time, corrosion (and consequently the demand for protecting current) tends to be more severe in the areas where concrete resistivity is

lower. This task will establish the range of substructure service conditions where the unaided driving potential of the galvanic couple is enough to drive the protective current required by the underlying steel.

Laboratory experiments will be conducted using reinforced concrete prisms containing rebar that has corroded and subsequently applied zinc coatings. The specimens will be exposed to various environmental conditions. In addition, small-scale reinforced concrete columns will be used to determine protective current extent and distribution.

Task 2 will seek to determine which of two zinc spray formulations, and which external coating condition (overlayed or bare) is more desirable to extend the service life of the anode.

As indicated in the previous section, the durability of the anode may be affected by interactions with the external environment and by adverse effects at the concrete-metal interface. The extent of these interactions will depend upon, among other things, the parameters of the coating composition, and on the presence or absence of an external overlay on the zinc. Experiments using a methodology comparable to that in Task 1 will be performed to aid in selecting the most appropriate combination of these parameters.

Task 3, a key task, will implement and supplement the findings of the laboratory work, by subjecting prototype systems to actual service at subtropical test sites in Florida. The field installations will be used to assess the suitability of zinc application methods, measurements of performance of the system as determined by polarization and current measurements, and durability of systems in actual service. Both existing trial installations and new systems will be employed in this task.

Work on all tasks has been initiated and specimen preparation is in progress. Experimental data collection and field measurements are expected to commence in the second quarter.

Technical Issues for Further Consideration

In its first year, this project incorporates a strong component of field testing. For certain conditions (for example, certain marine substructure cases in humid subtropical settings), the method may be very close to implementation at the end of the present effort. Evaluation for wider use is expected to require addition effort. Issues for further consideration include the following:

1. Suitability for use with structures built using epoxy-coated rebar. This effort would supplement investigations initiated by the Florida Department of Transportation to examine applicability of the concept to control corrosion in selected existing structures.

2. Localization of protective current. Shorter electrolytic paths between zinc and rebar are present near the edges of a spall. Adequate protective current may be limited to those areas, especially in cases of relatively high concrete resistivity. Experimental measurements and computer modeling of current distributions in these and similar circumstances are needed to establish operating limits for a wide range of applications.

3. Improved coating performance and application. The present project does not address concrete surface preparation, rate of coating deposition, spray gun parameters and similar factors that may affect long-term durability of the coating. Likewise, only two alternative zinc alloys and one type of topcoat are considered. Optimization of these variables will be required to improve the performance of the concept if large scale application is to be implemented.

Dynamic Analysis Procedure for Falling-Weight Deflectometer Data

IDEA 025 - Pavement Dynamic Analysis Procedure

Investigator: Allen H. Magnuson, Texas Transportation Institute, College Station, Texas

IDEA Product

This contractor is verifying dynamic analysis software for pavement deflection data to estimate the physical properties of pavement layers. The software will be evaluated using falling-weight deflectometer (FWD) data from SHRP's Long-Term Pavement Performance (LTPP) data base.

Innovation

Traditional approaches to deflection data analyses have relied on static models that utilize only peak load and deflection values. This new approach uses the complete load and deflection traces in a dynamic analysis which, in theory, models true pavement behavior more accurately.

Project Summary and Progress

The project work was initiated in January, 1991. The pavement site selection will be made and approved by SHRP. Preliminary back-calculation efforts will be completed on selected SHRP LTPP pavement sites. Pavement layer moduli and viscoelastic parameters will be extracted from full-pulse FWD data.

Dynamic Analysis Methods

1. Scalar potential (SCALPOT) Solution of the forward problem: Given physical properties of the layered halfspace, compute dynamic responses (i.e., displacements, stresses and strains). The SCALPOT uses scalar potentials for representing compressional and shear waves in each layer.

2. Pavement systems identification (PAVE-SID) Solves the inverse problem: given computed responses (SCALPOT, e.g.), extract physical (viscoelastic) properties of pavement layers. The analysis program inverts the direct solutions obtained from SCALPOT to extract physical property data for pavements.

The analysis programs will be used for a full range of frequencies from near-static to true far-field wave regime. The time dependence (convolution integral) will be reduced to an algebraic manipulation in the frequency domain.

Technical Issues for Further Consideration

The initial phase of the project will involve testing the dynamic analysis software using deflection data from LTPP test sections. These test sections will be selected to represent a broad range of conditions. Assuming reasonable results are obtained in that phase, the project will proceed to compare the pavement properties as derived from the deflection data with laboratory test results.

The key issues are: (1) the verification of the method; and (2) the availability of laboratory materials data on which the material properties derived from the analyses. The laboratory materials data is needed to evaluate the reliability of the software's predictions. Based on preliminary investigations, it appears that the required data will be available.